ENERGY MANAGEMENT AND 4E ANALYSIS OF A SOLAR HYBRID GAS TURBINE POWER PLANT IN IRAQ

2024
PhD THESIS
MECHANICAL ENGINEERING

Wadah Talal Taha AL-TEKREETY

Thesis Advisor
Assist. Prof. Dr. Abdulrazzak Ahmed Saleh AKROOT

ENERGY MANAGEMENT AND 4E ANALYSIS OF A SOLAR HYBRID GAS TURBINE POWER PLANT IN IRAQ

Wadah Talal Taha AL-TEKREETY

Thesis Advisor

Assist. Prof. Dr. Abdulrazzak Ahmed Saleh AKROOT

T.C

Karabuk University

Institute of Graduate Programs

Department of Mechanical Engineering

Prepared as

Ph. D. Thesis

KARABUK

May 2024

I certify that in my opinion the presented thesis that has been submitted by Wadah Talal Taha AL-TEKREETY titled “ENERGY MANAGEMENT AND 4E ANALYSIS OF A SOLAR HYBRID GAS TURBINE POWER PLANT IN IRAQ” is fully adequate in scope and quality as a thesis for the degree of Ph. D.

Assist. Prof. Dr. Abdulrazzak Ahmed Saleh AKROOT .....
Thesis Advisor, Department of Mechanical Engineering

This thesis is accepted by the examining committee with a unanimous vote in the Dept. of Mechanical Engineering as a Ph.D. of Science thesis. May 22, 2024.

Examining Committee Members (Institutions)	Signature
Chairman : Prof. Dr. Emrah DENİZ (KBU)	.....
Member : Prof. Dr. Ahmet KABUL (ISUBU)	.....
Member : Assoc. Prof. Dr. Mustafa KARAGÖZ (KBU)	.....
Member : Assist. Prof. Dr. Abdulrazzak AKROOT (KBU)	.....
Member : Assist. Prof. Dr. AEAD M. AHMED (UOM)	.....

The degree of Ph.D. of Science by the thesis that has been submitted was approved by the Administrative Board of the Institute of Graduate Programs, Karabuk University.

Assoc. Prof. Dr. Zeynep ÖZCAN .....
Director of the Institute of Graduate Programs

"I declare that all the information that has been presented in this thesis was gathered and presented by ethical principles and academic regulations and I have according to requirements of those regulations and principles that were cited all those which don't originate in this work too."

Wadah Talal Taha AL-TEKREETY

ABSTRACT

Ph.D. Thesis

ENERGY MANAGEMENT AND 4E ANALYSIS OF A SOLAR HYBRID GAS TURBINE POWER PLANT IN IRAQ

Wadah Talal Taha AL-TEKREETY

Karabuk University
Institute of Graduate Programs
The Department of Mechanical Engineering

Thesis Advisor:
Assist. Prof. Dr. Abdulrazzak Ahmed Saleh AKROOT
May 2024, 128 pages

Improving a polygeneration arrangement and variation of Iraq's electricity system is a strategic goal, with a critical requirement on increasing the use of renewable energy sources. This research focuses on integrating waste heat recovery, solar energy, and an absorption refrigeration cycle for the Al-Qayara gas turbine power plant, offering a novel way to increase efficiency. The current configuration uses the exhaust gases from the Al-Qayyarah gas turbine power plant and the PTC field to generate steam using a high recovery steam generation process and an absorption refrigeration cycle that supplies low-temperature air to the Brayton cycle. A thermoeconomic analysis of the 4E (energy, exergy, exergoeconomic, and environmental studies for the Al Qayyarah power plant configurations) has been conducted. The power produced by the NGCC, ISCC, and ISCC-ARC systems is 489 MW, 554.6MW, and 581.1 MW, respectively; the power generated by the system grows by 34.2 MW when an ARC is added, with overall energy and exergy efficiencies of 44.76% and 43.22% for NGCC,

50.89% and 49.14% for the ISCC, and 51.15% and 49.4% for the ISCC-ARC. The overall specific costs for the ISCC-ARC system range from 62.33 $/MWh in June to 72.18 $/MWh in December, with similar fluctuations observed for the ISCC system, ranging from 70.08 $/MWh in June to 76.79 $/MWh in December. Also, for the NGCC, ranging from 79.4 $/MWh in June to 80.05 $/MWh in December. The environmental analysis depends on the release of carbon dioxide in the system during the year. Emissions have been declining with infrequent fluctuations compared to the emission for CO_2 through the year of ISCC-ARC, which changed from 405.3 $kgCO_2$/MWh in December and 373.5 $kgCO_2$/MWh in June and changed from 439.7 $kgCO_2$/MWh in December and 447.4 $kgCO_2$/MWh in June for the NGCC.

Key Words: Al-Qayara gas turbine, solar energy, waste heat recovery, absorption refrigeration cycle, polygeneration, exergy, exergoeconomic, and environmental

Science Code: 91408

ÖZET

DoktoraTezi

IRAK'TA BİR GÜNEŞ HİBRİT GAZ TÜRBİNİ ENERJİ SANTRALİ İÇİN ENERJİ YÖNETİMİ VE 4E ANALİZİ

Wadah Talal Taha AL-TEKREETY

Karabük Üniversitesi
Lisansüstü Eğitim Enstitüsü
Makine Mühendisliği Anabilim Dalı

Tez Danışmanı:
Dr. Öğr. Üyesi Abdulrazzak Ahmed Saleh AKROOT

Mayıs 2024, 128 sayfa

Irak'ın elektrik sisteminin çoklu üretim düzenlemesi ve çeşitlendirilmesinin iyileştirilmesi, yenilenebilir enerji kaynaklarının kullanımının arttırılması konusunda kritik bir gereklilik içeren stratejik bir hedeftir. Bu araştırma, verimliliği artırmak için yeni bir yol sunan Al-Qayara gaz türbini enerji santrali için atık ısı geri kazanımı, güneş enerjisi ve absorbsiyonlu soğutma döngüsünün entegrasyonuna odaklanıyor. Konfigürasyon, Al-Qayyarah gaz türbini enerji santralinden ve parabolik oluklu kollektör (PTC) alanından gelen egzoz gazlarını, düşük sıcaklıktaki havayı besleyen bir absorpsiyonlu soğutma döngüsüne ek olarak, yüksek geri kazanımlı buhar üretim prosesi kullanarak buhar üretmek için kullanır. Brayton döngüsü. Al Qayyarah enerji santralinin konfigürasyonları için 4E değerlendirmesi, enerji, ekserji, eksergoekonomik ve çevresel çalışmalara yönelik termoekonomik bir analiz. NGCC, ISCC ve ISCC-ARC sistemleri tarafından üretilen güç sırasıyla 493,5 MW, 547,4 MW

ve 581,6 MW olup, toplam enerji ve ekserji verimliliği NGCC için %44,84 ve %43,35, ISCC için %50,89 ve %49,14'tür ve ISCC-ARC için %51,15 ve %49,4. ISCC-ARC sisteminin genel spesifik maliyetleri Haziran'da 62,33$/MWh ile Aralık'ta 72,18 $/MWh arasında değişmektedir; ISCC sistemi için de Haziran'da 70,08 $/MWh ile Aralık'ta 76,79 $/MWh arasında değişen benzer dalgalanmalar gözlemlenmiştir. Ayrıca NGCC için Haziran'da 79,4 $/MWh ile Aralık'ta 80,05 $/MWh arasında değişiyor. Yıl boyunca sistemin karbondioksit salınımına bağlı olarak yapılan çevresel analizde, ISCC-ARC yılı boyunca Aralık ayında 405,3 $kgCO_2$/MWh ve 373,5 $kgCO_2$/MWh arasında değişen CO_2 emisyonlarına kıyasla emisyonlar seyrek dalgalanmalarla azalmaktadır. Haziran ayında MWh ve NGCC için Aralık ayında 439,7 $kgCO_2$/MWh ve Haziran ayında 447,4 $kgCO_2$/MWh olarak değişti.

Anahtar Kelimeler : Al-Qayara gaz türbini, güneş enerjisi, atık ısı geri kazanımı, absorpsiyonlu soğutma çevrimi, çoklu üretim, ekserji, eksergoekonomik ve çevresel.

Bilim Kodu: 91408

ACKNOWLEDGMENT

In the name of Allah, the Most Gracious, the Most Merciful, all praise is due to Allah, the Lord of all worlds, and peace and blessings be upon His Messenger, Muhammad, and his family and companions.

I want to start by sincerely thanking Allah Almighty for giving me the courage, direction, and persistence to start this academic path and finish my Ph.D. I have always been accompanied by His blessings and kindness, and I will always be grateful for His boundless grace and direction.

I would like to sincerely thank my supervisor, Assist. Prof. Dr. Abdulrazzak Ahmed Saleh AKROOT, Throughout my Ph.D. program for all his important advice, encouragement, and support. Also, thanks to Prof. Dr. Emrah DENİZ and Prof. Dr. Ahmet KABUL for their knowledge, tolerance, and unshakable commitment have greatly influenced the course of my research and promoted my scholarly development.

I am appreciative of the Karabük University staff and administration, whose assistance and administrative support have made my doctoral work go more smoothly. We are very grateful for their professionalism and help.

I would like to express deep appreciation to my colleagues and my research partners for their cooperation, friendship, and intellectual interchange. Their varied viewpoints and combined efforts have made this study project a success.

Lastly, I want to express deep thanks to my family for their constant support, love, and tolerance during this trip. Their constant encouragement and selflessness have been my inspiration and source of strength.

Thank you to everyone who helped and encouraged me. I also dedicate my achievement to my beautiful country, Iraq, and my favorite city, Mosul, which is unwavering in its people, as well as to Turkey, which welcomed me during my study period.

CONTENTS

Page

Page

Page

LIST OF FIGURES

Page

Page

LIST OF TABLES

Page

SYMBOLS AND ABBREVIATIONS INDEX

NOMENCLATURE

A_{ap}	Area of the solar field (m^2)
$\dot{C}$	Cost rate ($/h)
DNI	Direct normal irradiance of the sun
$\dot{E}$	Exergy rate (kJ)
$\dot{E}_D$	Exergy destruct
$\dot{E}_q$	Heat loss exergy
$\dot{E}_w$	Exergy of power
$\dot{m}$	Mass flow rate (kg/s)
h	Specific enthalpy (kJ/kg)
N	Number of operating hours
LHV	Fuel's lower heating value
$\dot{Q}$	Heat transfer rate (kW)
T	Temperature
Tcond	Temperature of the condenser
T_{sun}	DNI sun temperature
$\dot{W}$	Power (kW)
$\dot{Z}_k$	Represents the entire cost rate

SYMBOLS

η	Energy efficiency
η_I	Energy performance
η_{II}	Exergy efficiency
φ	Maintenance factor
i	Interest rate

Ψ	Exergy efficiency

SUBSCRIPTS

D	Destruction
e	Exit
i	Inlet
f	Fuel
p	Product
q	Related to heat
w	Related to work
tot	Total
Th_VP	Therminol VP-1

ABBREVIATIONS

AC	Air compressor
ARC	Absorption refrigeration cycle
BC	Brayton cycle
CC	Combustion chamber
CCPP	Combined cycle power plant
Con	Condenser
CRF	Capital recovery factor
CSP	Concentrating solar power
DSG	Direct steam generator
EES	Engineering equation solver
GE	General electric
GT	Gas turbine
GTIT	Gas turbine inlet temperature
HRSG	Heat recovery steam generation
HPST	High-pressure steam turbine
ISCC	Integrated solar of combined cycle

ISCC-ARC	Integrated solar combined cycle with absorption refrigeration cycle
LFR	Linear fresnel reflector
LiBr	Lithium bromide
MED	Multi-effect distillation
MSF	Multistage flash
MW	Megawatt
NGCC	Natural gas of combined cycle
NPV	Net produce value
LPST	Low-pressure steam turbine
ORC	Organic rankine cycle
PFC	Predictive function control
PI	Proportional-integral
Pr	Pressure ratio
PTC	Parabolic trough collector
SAM	System analyzer modeler
SFF	Static feed-forward
SPT	Solar power tower
ST	Solar tower
STP	Thermal power plants

PART 1

INTRODUCTION

1.1 OVERVIEW OF THE THESIS

Integrating renewable energy sources into traditional power plant generation systems has been accepted recently as a method to improve power sustainability and reduce environmental effects. Although Iraq is set apart with high solar direct average radiation DNI, there is much potential to discover the integration of solar power into the present electrical network. Because of their significant efficiency and flexibility, the combined cycle for power plants has become a technology usually used to construct power plants and electricity. However, fossil fuels are the primary power source for conventional combined cycles for plants, increasing questions about energy safety and greenhouse gas emissions. Investigators and scientists are focusing more on solar integration with combined system stations that use solar and fossil fuel power to produce electricity to overcome these problems. This multiple-expertise method improves the flexibility and reliability of the energy supply and makes it simple to decrease carbon dioxide emissions. For this, it is essential to conduct a complete analysis of the thermoeconomics for solar integration with combined cycle (ISCC) in the power station in Iraq. This study is responsible for valuable visions into the environmental profits and economic possibility of solar integration within the local power environment.

The places of power stations and transmission stations in Iraq are shown in Figure 1.1, "Power Generation and Power Transmission," which is taken from the General Electric (GE) webpage illustrating the operations of these stations in Iraq. The country has more places than one might suppose, given that Iraq's oil resources are in the southern region, although Iraq's significant population conurbations distribution is in the north. Energy output facilities, power stations, and transmission facilities are illustrated on

the map. Power stations generate electricity from fossil fuel combustion or by consuming alternative energy sources like solar and wind energy. The produced energy was brought to stations through high-voltage transmission lines, which changed to lower-voltage distribution lines for transfer to domestic and commercial segments.

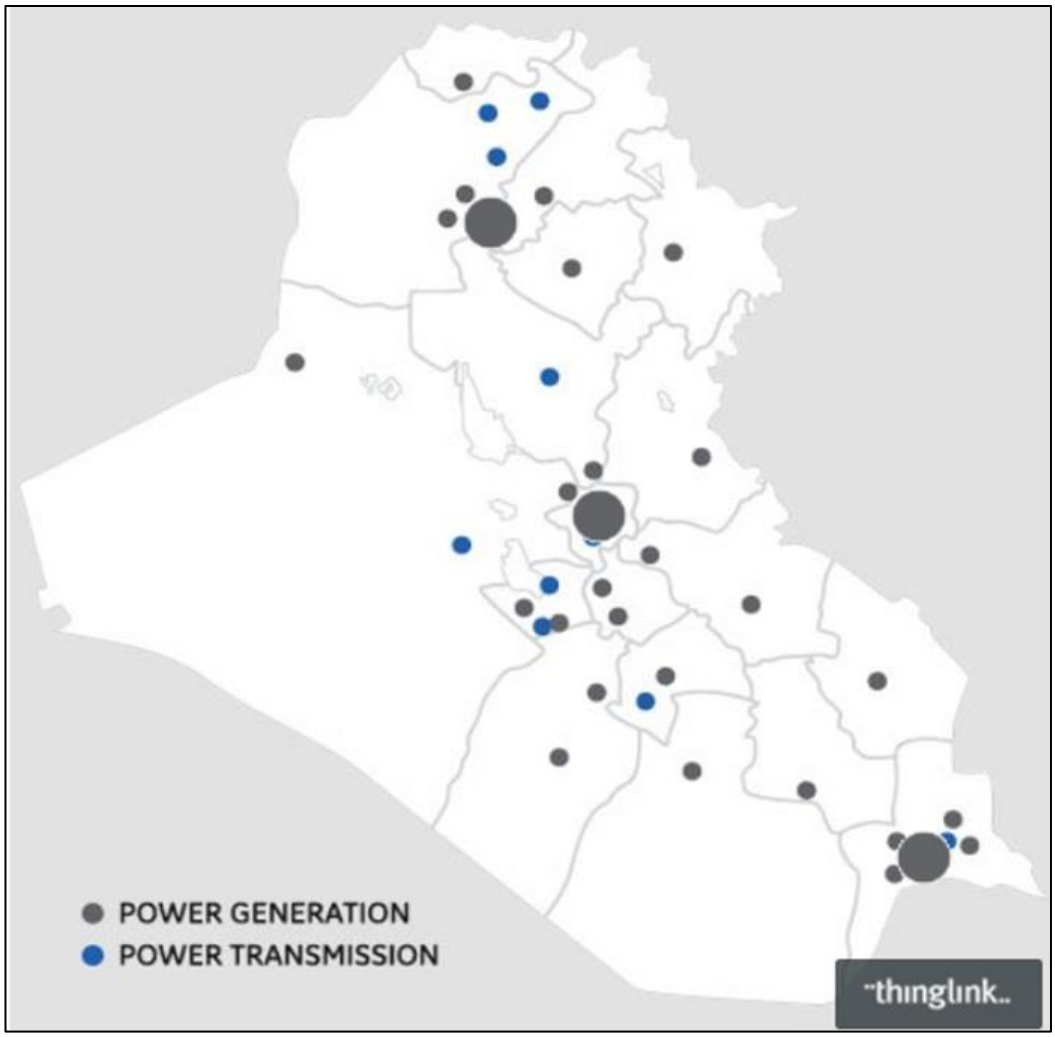

Figure 1.1. Iraq power generation and power transmission [2]

Globally friendly and sustainable energy generation technologies have seen a prominent change in the global power vision in recent years. The shift in low-carbon emissions and renewable power sources is immediately needed to increase worries about climate variation, power security, and resource reduction [3,4]. Merging solar energy with conventional energy production technologies and counting combined cycle systems is a method to address these subjects. Power plants with integrated solar and combined cycle (ISCC) technology present an infrequent chance to benefit from

the sun's abundant power while maximizing the reliability and efficiency of the present fossil fuel depending on the infrastructure. [5]. By merging solar thermal power with gas turbine technologies and serial heat integration strategies, ISCC plants can reach higher power change efficiencies, decrease emissions, and improve complete performance [6].

1.2 OVERVIEW POLYGENERATION FOR THE SYSTEMS

The change to new combined systems and effective and sustainable power generation equipment is more significant than today as the world's traditional power systems are about to undertake a genuine conversion. This transformation is driven by several factors:

- Raising demand for power on a global level.
- Require decreasing carbon releases.
- The continuous search for power effectiveness and efficiency.

For these contexts, the polygeneration approaches show up as an appropriate example of innovation, presenting a complete piece of equipment to solve this trouble direct. This research investigates the advance of power plants through polygeneration, frameworks its primary philosophies, and explains how influential polygeneration is in generating sustainable power in the future [7].

Moving between conventional, single-output power stations to the advanced, multi-output designs nowadays represents a critical turning point in the history of energy production. Whether for cooling, heating, or electrical power, power systems in the past were created with a single purpose. However, this method frequently resulted in significant ineffectiveness, wasting much power as temperature. An initial move toward eliminating this ineffectiveness came with the introduction of regeneration systems, which use exhaust heat to produce electrical power for heat. The following big step ahead is called polygeneration, which builds on the concepts of regeneration to generate various power results from a single fossil fuel resource, such as heating

and cooling. The integration of conventional power plants with renewable solar electricity in a polygeneration system offers several benefits, including:

- Polygeneration systems optimize energy efficiency by harnessing waste heat from one process, such as a conventional power plant, to power another process, such as solar thermal generation, by integrating several kinds of energy production.
- By diversifying energy sources, these systems strengthen energy security and diminish reliance on fossil fuels.
- Polygeneration enables the generation of various energy outputs, including electricity, heating, and cooling, via a unified system, maximizing resource use.

These systems may effectively reduce greenhouse gas emissions compared to conventional standalone power plants.

1.2.1 Description of Polygeneration

The potential of polygeneration to participate in the production of numerous power resources to reach a variety of power demands is what identifies it. This technique requires unequaled changeability to handle fluctuating power needs while enhancing the complete efficiency of power generation. During the use of many types of machinery and procedures, such as Brayton cycle power station, absorption cooling system, and solar-driven steam turbine, polygeneration systems can generate a helpful power production combination by using a comprehensive variety of fuels, containing both traditional fossil fuels and alternative power resources.

Polygeneration significantly benefits by effectively reducing waste heat and maximizing power use. Polygeneration, in contrast to traditional systems, efficiently decreases fuel consumption and gas emissions by harnessing and using waste heat created during the generation of more energy. Furthermore, including renewable energy sources such as solar power in polygeneration methods enhances the overall sustainability of the power generation process [8].

1.2.2 Importance of Polygeneration in Systems

The shift towards polygeneration methods is of greater significance than technology advancements since it represents a holistic approach to power management that aligns with the concepts of sustainable development [9]. The requirement for polygeneration systems increases as the world faces problems of resource decline, environmental change, and rising power needs. They present a practical choice that affects an evaluation of ecological responsibility, efficiency, and flexibility, presenting them as a necessary segment of power stations [10,11].

In summary, the start of polygeneration systems, characterized by their environmentally friendly operation and capability for various results, indicates the beginning of an innovative period in power generation. This demonstrates the possibility of a significant beneficial effect on universal energy performance and examines the difficulties and utilizes of these systems, mainly through the viewpoint of a creative polygeneration system integrating solar power, gas turbines, and absorption cooling. This examination develops the academic discussion on power approaches and suggests practical recommendations for creating an extra sustainable and actual power in the future. [12].

1.3 INVESTIGATING SOLAR-POWER RANKINE STEAM SYSTEM

Today, combining traditional energy production technology with alternative sources is fundamental in searching for renewable power options. The Rankine steam system, which utilizes solar power to produce electrical energy with high efficiency and minimal environmental effect, represents one of these important strategies. [13,14].

The thermodynamic process of the Rankine steam cycle consists of four major steps:

- The working fluid is heated through the boiler until it boils and converts into steam.
- The steam expands through a steam turbine, generating power.
- This steam is then cooled and condensed back into liquid form in a condenser.

- The cycle completes with the compression of the condensed liquid.
- This system's efficiency is essential in calculating the operation liquid choices and organization elements design in power plants.

1.3.1 Improving Systems with Solar Power

The globe faces an energy crisis and significant environmental concerns, such as the greenhouse effect, global warming, and pollution. The dependence on conventional energy sources, such as fossil fuels, mainly causes the problems mentioned. Therefore, it is essential to integrate renewable energy sources in conjunction with traditional power plants. Presently, the primary emphasis on energy development is on green energy sources and ecologically sustainable energy-producing techniques. Solar power is a prominent and highly efficient renewable energy source for generating electricity and is known for its cleanliness.[15].

Solar energy is propagated as electromagnetic radiation, which may propagate in a vacuum without a medium. Solar photovoltaic panels and solar thermal collectors capture solar radiation and transform it into practical thermal and electrical energy. Solar power systems may be classified into active and passive ways based on the technology used for energy collection and distribution. Active solar power systems harness radiant energy by utilizing equipment such as photovoltaic cells and solar water heaters. Passive solar approaches enhance active systems by adjusting the alignment of solar energy equipment to optimize sunshine exposure.[16].

A substantial proportion of global energy generation relies on the combustion of non-renewable fossil fuels such as coal, oil, and natural gas. This practice contributes to environmental and economic problems and exacerbates challenges related to their escalating costs, limited availability, and increasing demand. Furthermore, the combustion of these fuels emits detrimental pollutants that contribute to climate change and provide health hazards. Transitioning to ecologically sustainable and renewable energy sources would have a substantial impact on reducing greenhouse gas emissions and enhancing the climate.[17]. As a result, governments, businesses, and consumers are increasingly focused on developing methods to harness energy from

renewable sources like solar power. Unlike conventional sources, which are becoming prohibitively expensive, renewable energy is affordable and plentiful. Presently, the field of solar power production is seeing a significant expansion because of technological breakthroughs. The advantages of selecting solar electricity are detailed below:

- Solar energy has a distinct advantage over fossil fuels due to its infinite nature since it is produced from the Sun's rays rather than by limited conventional sources.
- Recent advancements in solar technology enable the efficient gathering and distribution of electricity during periods of high customer demand.
- Solar technology has the advantage of flexibility and scalability, eliminating the need for the elaborate infrastructure that is necessary for conventional power plants.
- Solar energy production has little environmental consequences in comparison to other energy production technologies.

1.3.2 Using Solar-Powered Rankine Steam System in Polygeneration

The Solar-Powered Rankine Steam System combines solar energy technology with standard thermal power generating technologies in a novel way. This system uses the Rankine cycle, a key concept in thermodynamic engines, to collect solar sunlight and create steam. The steam then powers turbines, which in turn provide electricity. The solar-powered Rankine system differs from traditional ones because it uses concentrated solar panels or mirrors to convert sunlight into heat instead of burning fossil fuels to generate steam [18].

The solar thermal collector is a crucial solar-powered Rankine steam system component. The objective of this device is to concentrate sunlight to elevate the temperature of a fluid to a range of 250 to 600 degrees Celsius. The hot fluid transfers thermal energy to water, converting it into high-pressure steam. Steam is used to drive turbines, producing mechanical energy, which a generator converts into electricity.

Solar-powered Rankine steam systems provide several advantages over conventional energy sources. The main benefits are:

- Solar power generates electricity, a sustainable and ecologically friendly alternative.
- They exhibit notable flexibility and may be tailored to meet the requirements of both small residential settings and large industrial projects.
- These methods reduce reliance on imported fuels, hence enhancing energy security.
- The efficiency and cost-effectiveness of solar thermal and steam turbine systems are constantly improving due to technological advancements.
- These devices cut greenhouse gas emissions and pollutants.

1.3.3 Opportunities and Challenges for the Project

While merging solar energy with the Rankine steam system in polygeneration organizations has various benefits, there remain many challenges to recovering. Since direct solar irradiation changes, power storage, and hybrid techniques are needed to ensure a consistent energy requirement. Further challenges to using solar power techniques are their big beginning investment cost and complicated technological strategy. Continuing technical improvement, declining solar energy element costs, and the present opportunity to recover from these problems predict an additional environmental effect and economic future for the power of organizations [19,20].

Combining solar and conventional power plants brings distinct potentials and problems. Using solar energy may reduce carbon emissions and the utilization of coal or natural gas plants during peak daylight hours, improving efficiency and lowering costs [21].

These points outline solar energy opportunities for integration with the Rankine steam system in polygeneration:

- Improves energy conversion efficiency by using solar and conventional waste heat.
- Energy efficiency lowers operating expenses.
- Reduces fossil fuel use and promotes renewable energy.
- Renewable solar energy reduces greenhouse gas emissions.
- Energy diversification improves dependability and security.

Also, these points describe solar energy integration issues with the Rankine steam system in polygeneration:

- Solar technology integration requires significant amounts of money.
- Integrated system management requires advanced control methods and technologies.
- Solar energy is location-dependent.
- Infrastructure retrofitting is complicated and expensive.

1.4 INCORPORATING ABSORPTION REFRIGERATION

Integrating an absorption cooling system into a polygeneration design, which combines traditional power plants with renewable solar energy, offers several benefits. This hybrid approach harnesses waste heat generated from both conventional and solar power generation to power the absorption cooling process, enhancing the system's overall efficiency [22].

Unlike traditional refrigeration technology that relies on mechanical compression, absorption cooling solutions use a heating energy cycle. Absorption systems provide cooling without requiring additional electrical energy by harnessing waste heat or solar energy from gas turbines or solar power conversion sources.

The absorption cooling system utilizes waste heat to drive a refrigeration cycle, generating chilled water for air conditioning or industrial cooling. This integration is particularly advantageous in hot countries, such as Iraq, where there is a high need for cooling and a plentiful supply of solar energy.

The primary benefits of incorporating an absorption cooling system into a polygeneration system that encompasses conventional power plants and renewable solar power plants are as follows:

- Reduces reliance on fossil fuels, resulting in decreased levels of greenhouse gas emissions.
- Harnesses waste heat from traditional and solar power sources, enhancing energy efficiency.
- Offers consistent and dependable cooling solutions, particularly in areas with significant cooling requirements.
- Decreases operating expenses by using waste heat for cooling, hence eliminating the need for further fuel usage.
- Facilitates the adoption of sustainable energy practices by combining renewable solar energy with conventional systems.
- Expand the range of energy sources, hence strengthening energy security and decreasing dependence on foreign fuels.

1.5 PROBLEM STATEMENT

Already, there is a significant shortage of electrical systems in Iraq. All this happened because of frequent wars such as the war between Iraq and Iran, which began in 1980 and ended in 1988, as well as the Gulf War in 1991 between Iraq and Kuwait, and finally, the American invasion of Iraq in 2003, which is destroyed and damaged the country's economy, Infrastructure of the country and power plant organization.

To improve Iraq's power infrastructure, it is essential to upgrade the Qayyarah power station by adding a steam turbine to the existing gas turbine, converting it into a combined-cycle power plant. Additionally, integrating an absorption refrigeration cycle for the air entering the power station and utilizing solar energy by exploiting available space is crucial. Iraq has vast, underutilized areas unsuitable for agriculture that can be transformed into solar energy fields. With over 3,300 hours of sunshine annually and solar radiation exceeding 2000 kWh/m², Iraq has an excellent opportunity to enhance its electrical energy production, as illustrated in Figure 1.2.

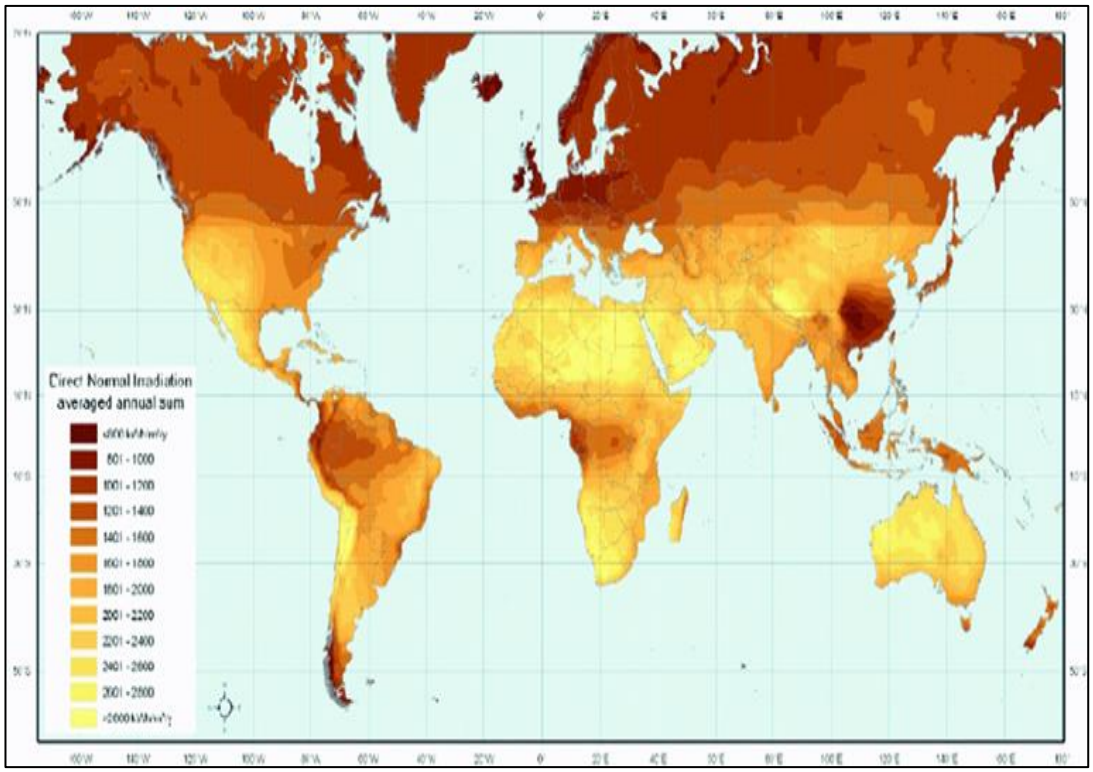

Figure 1.2. Annual irradiation in the world [23].

Power generation in Iraq by using solar energy can meet the electrical needs of these areas and neighboring countries. This thesis examines the enhancement of the Al Qayyarah power plants in northern Iraq by utilizing the region's direct normal radiation (DNI) to recover combustion products from the gas turbine exhaust. The plant features a 750 MW gas turbine, 375 MW steam turbines, and an absorption refrigeration cycle (ARC) powered by solar energy and gas turbine exhaust.

Integrating ARC and solar thermal energy into combined power stations can significantly improve efficiency, reduce emissions, and enhance heat recovery. However, further research is needed to understand the operation of solar-integrated combined cycle plants under different solar and climate conditions, particularly for the Al-Qayyarah Power Plant.

1.6 OBJECTIVES

The main objectives of this research can be summarized as:

- Integrate solar thermal power, steam turbines, and an absorption refrigeration cycle with the existing 750 MW gas turbines to improve power generation capacity.
- Solar power and waste heat are used in steam turbines to optimize energy efficiency and performance under various climatic conditions.
- Incorporate clean energy sources to decrease the environmental footprint of power generation and evaluate the system's performance and financial viability based on operational data.

1.7 OUTLINES OF THE PROJECT

The first section summarizes the present research, including historical background on Natural Gas Combined Cycle (NGCC), solar energy, and thermal energy from earlier studies. It also outlines the main goals of the present study. The pertinent literature for the present inquiry is thoroughly reviewed in Chapter Two. The suggested system's principal components and operation methods are discussed in detail in the third chapter of this thesis. Furthermore, the third section covers the inputs provided by the system variables and the thermodynamic and exergoeconomic equations used for the technique's energy, energy, economic, and environmental analyses. The study's findings and analysis are presented in the fourth chapter. Chapter Five offers some closing thoughts and possible directions for future research.

PART 2

LITERATURE REVIEW

2.1 INTRODUCTION

At present, there is a notable focus on the implementation of polygeneration systems and the enhancement of energy efficiency, particularly with power plant technologies. Integrating renewable energy sources, including solar energy, with traditional power generation techniques has been the subject of numerous studies to increase overall efficiency and lessen environmental effects. Furthermore, it has been shown that using waste heat recovery systems and absorption refrigeration cycles are viable approaches to improve system performance and maximize energy use. This literature review investigates previous research and practical implementations of solar integrated with combined system power stations, waste heat recovery, and absorption refrigeration cycles.

AlKassem [24] showed a techno-economic evaluation of adopting an ISCC power station with solar tower (ST) equipment in Saudi Arabia. The outputs for the ISCC model were compared quantitatively with other traditional and alternative power resources. The results demonstrated that, at a capacity factor of 49.9%, the hybridized ST area in the ISCC generator may achieve an efficiency ranging from 53 to 59% annually. ich is better than other intermittent renewable energy equipment. Solar capacity is demonstrated to be about 9.11% of the entire power station's ability, and the production is up 10.7% of the total output.

Siddiqui and Dincer [25] raised the global requirements for primary energy by almost 50% between 2016 and 2030. Using thermodynamic investigation into the exergy and energy techniques for solar-based hybrid systems that utilized ammonia as a fuel cell substitute, the study raised system efficiency by approximately 19.3%. The rise had

the potential to connect hydrogen to single-production systems and increase the exergy efficiency related to single-production mechanisms by approximately 17.8%.

Martins et al. [26] investigated fossil petroleum power consumption and fossil fuel depletion, considering factors such as environmental impact, energy demand, and the role of alternative energy in total final energy consumption. They carried out statistical and mathematical studies to give decision-making information and raise consciousness regarding fossil fuel use in European countries. While several European nations rely significantly on fossil fuels, the report highlighted the importance of low-carbon power infrastructure and a shift to alternative energy. The article focused on the negative repercussions of utilizing fossil fuels, such as global warming, pollution of the environment, and health hazards. Furthermore, the study employed mathematical modeling and comparisons to highlight the demand for European countries to decrease their reliance on natural gas, coal, and oil by the year 2050.

Akbar and Nemati [27] investigated gas turbine generators with an emphasis on maintenance methods for enhancing the operation of power stations. They observed critical variables in over 80% of power plants worldwide, identifying machinery that needs specific attention and those that can be used as standards for comparison. The study highlighted important elements and monitoring approaches for power stations. The investigators examined the isentropic efficiency of gas turbines and their correlation with the compressor temperature ratio, providing valuable insights into the performance of gas turbines. They highlighted the significance of evaporative coolers in enhancing efficiency and increasing energy production. The research also emphasized the need for more accurate combustion modeling equations. Recommendations included comparing all turbines with turbine one during overhauls and evaluating other compressors against specific reference compressors.

Hamouda et al. [28] developed mathematical models for a proposed multi-effect distillation (MED) system combined with reverse osmosis (RO) and conducted a techno-economic analysis of a solar cogeneration system. This system integrates a solar accumulator with the turbine sequence in power stations for water production. The study compared two heat utilization approaches: one using exhaust heat from a

turbine to enhance energy production via the organic Rankine cycle, and the other using exhaust heat to operate a multistage flash (MSF) system for water production. The cogeneration model, implemented using the MATLAB Simulink toolbox, demonstrated reduced costs, lower total water costs, and decreased CO_2 emissions. The paper introduced a novel system combining a concentrated solar tower (CST) with a gas turbine cycle (GTC) and hybrid desalination (MSF or RO), exploring its feasibility compared to traditional systems. It provided technical design results for the desalination component of the first scenario, including steam thermal power transfer, desalinated water productivity, and energy consumption.

Ni et al. [29] enhanced the turbine sequence for high efficiency and solar-assisted Brayton cycle integration using a solar-chemicals recovered turbine system combined with two-stage fuel-steam improvements. Their thermodynamic analyses aimed to achieve 47.7% thermal efficiency and 75.0% solar participation in the power plant, significantly surpassing other solar-turbine combinations. The study promoted converting low-level thermal energy to high-level chemical energy and discussed practical strategies for further system enhancements based on exergetic investigations. The proposed system reduced overall exergy destruction by upgrading waste heat and solar thermal power to high-level biochemical energy. This approach improved power generation by approximately 38.2% from gas turbine waste heat and about 17.4% from solar power.

Al-Kouz et al. [30] proposed a 140-MW solar power station with storage in Ma'an, Jordan, modeled after the Solana solar power plant in Gila Bend, AZ, US. They evaluated the plant's performance and effectiveness using the System Advisor Model (SAM) software, comparing environmental conditions and electricity production between Ma'an and Gila Bend. The study highlighted Ma'an's advantages in solar irradiance, humidity, and minimum temperature. Before the implementation, the technology readiness level for concentrated solar power parabolic trough (CSP PT) with thermal energy storage (TES) was improved.

Temraz et al. [31] conducted an exergy analysis of a solar-integrated combined cycle (ISCC) power station in Kuraymat, Egypt, using data from planning and design

documents. They assessed the power station's performance and efficiency based on exergy calculations, focusing on exergy destruction, particularly in the combustion chamber (CC). The study examined the overall thermal and dual-law efficiency of the ISCC and identified the lowest exergy efficiency within the system. The findings discussed sources of exergy destruction in high-temperature components, such as the CC and solar power systems, which had the highest exergy destruction percentages. The research identified opportunities for improving the operation of each element in the Kuraymat power station.

Manente et al. [32] enhanced the performance of fossil fuel power stations by integrating them with solar power and analyzing various solar strategies in a combined cycle to achieve high solar energy-to-electricity conversion efficiencies of around 30% using sensible heat. They discussed methods for incorporating solar resources into fossil fuel-powered stations. They examined different concentrating solar power technologies suitable for high integration, such as linear Fresnel, solar towers, and parabolic the research suggested a hybrid integration cycle using solar radiation to evaluate the effectiveness of different configurations of solar-combined systems.

Wang et al. [33] performed a comprehensive analysis to assess the efficiency and economic viability of ISCCS. The investigators examined the reasons and locations of inefficiency in the ISCCS and identified areas for enhancement by examining losses of energy in different parts of the system. Becoming the initial investigation to do an exoergic analysis on an ISCC technology with a two-drag-one mode GTCC for energy production and refrigeration, the study closes a research gap by offering insights into the exergy efficiency and losses of the overall system. The suggested ISCC system's environmental friendliness and economic viability are demonstrated by the ecological and economic evaluations, which also emphasize the system's potential for sustainable energy production and refrigeration.

Kannaiyan et al. [34] showed the initial fundamental design of the PTC utilizing thermominol oil and the layout of the Linear Fresnel Reflector (LFR) utilizing water as the fluid of operation. Performance measurements acquired from different scenarios were used to assess the controller's operation. Further, it is suggested that an ongoing

proportional-integral (PI) regulator with predictive function control (PFC) or static feed-forward control (SFF) be designed for the best results and conclusion. The research and publications on solar collector closed-loop applications controller development, which improves the lifespan of Solar Thermal Power plants (STP), including conventional controllers (PID, FF, Cascade) and advanced control techniques.

Adnan et al. [35] presented a financial evaluation of a gasification combined cycle (IGCC) hybridized beside a solar power tower (SPT) to regenerate (electricity, methane, and ammonia). Discussed the two designs of the solar power tower (SPT) were imitation and enhanced for Pakistani climate environments and analysis varies hybrid strategies and thermo-economic performance, containing efficiency, effectiveness, solar efficiency, power charge, entire station costs, and repair prices. The efficiency for 100% power hybrid is 38.77%, and the effectiveness and energy efficiency enhance to 39.10% with the integration of SPT and Specific CO_2 emissions after hybridization, with the minimum achieved being 42.1 kg/MWh evaluated two aspects one of them thermodynamic and the other is economic assessments included electric effectiveness, energy efficiency, besides solar-change to-electrical efficiency for the financial evaluation included price of power, entire station budgets, and operational and maintain costs for mixture stations.

Alqahtani and Echeverri [36] quantified the thermos-economic and environmental profits of an ISCC power station in Palmdale, California, and displayed that it decreased the price of solar energy electricity by around 35-40% compared to Concentrating Solar Power (CSP) also, the study compared the commercial capability of solar combine cycle (ISCC) plus the NGCC. Examined the economic viability of ISCC for NGCC stations, finding that ISCC was great economic for natural gas cost around 13.5 MMBtu and ISCC reaches minor charge of CO_2 reduction for petroleum cost around 8.5 MMBtu and compared that the benefits of ISCC relation for NGCC which based on the ability parameter. The assumed conditions for the NGCC station of the GE FlexEfficiency-60 are for Combined Cycle and solar element ISCC to match the CSP with solar accumulators.

2.2 DISCUSSION OF PREVIOUS STUDIES

Saeed et al. [37] examined and analyzed the present and upcoming power in Iraq, including the power revolution, energy part extension strategy, and climatic effect, and showed the abilities of non-fossil fuel sources in power introduction like solar or wind, which is called renewable power, and substituted it with alternative power focusing using renewable and nuclear energy in Iraq and calculated their environmental effect for sustainable and difference in power production to identify the current shortage and imagine power demand rise and lack solutions for forecasts the quick rise in power needs in Iraq for the following 15 years—used Long-range Energy Alternative and Planning (LEAP) System to analyze electricity generation and future expansion plans and simulate the environmental impact of different technologies.

Hassan et al. [38] analyzed constructing solar irradiance possible in Iraq for a 20 MW power station. Studied parameters like wind speed, solar energy irradiance strength, and ambient temperature, which are foundations for calculation. Also, the study shows that complete power production relies on solar energy irradiance intensity for support and examines power production in various areas of Iraq. The outcomes demonstrated that power production varies in different areas in Iraq, with maximum power production in the midwestern area and minimum in the northeast areas.

Kazem and Chaichan [39] Inspected alternative power resources that could be significant to Iraq's utilization of alternative power in the future, like biomass, solar, and wind energy. A study was carried out to investigate the viability of developing a 20 MW PV project in Iraq for producing power. The assessment looked at how DNI, $T_{ambient}$ and wind affected the overall power production. The study also examined the effectiveness of solar panels in hot weather and dusty conditions. Also, they investigated Iraq's untapped biomass power potential and the government's assistance and cost needs for the industry's expansion.

Amani et al. [40] developed a method to calculate the quantity of steam mass flow produced through daytime hours in the heat exchanger in the ISCC station in Hassi R'Mel, Algeria. The ISCC Hassi R'Mel generating station

superheated, economizer, and evaporator thermal stability were evaluated. Also, an economic assessment was conducted on the ISCC power plant, with the LCOE estimated and compared to the standard combined cycle generators.

Wang et al. [41] studied an ISCC system comprising a lithium bromide refrigeration unit, a combined cycle gas turbine, and a PTC direct steam generator. They used gray-box modeling and Epsilon software to conduct an exergy analysis, focusing on exergy losses in components like the CC, solar DSG system, HRSG, ST, and condenser.

Faisal et al. [42] conducted an energy and exergy analysis of a GE turbine at the Shatt Al-Basra station in Iraq, noting reduced performance and efficiency due to high temperatures in summer. They suggested improving inlet air cooling and utilizing waste heat energy, demonstrating higher exergy and thermal efficiencies in February. The study analyzed actual operating data from 2017, both at full-load and part-load conditions, and recommended enhancing the use of waste heat. The analysis neglected kinetic and potential energy. The paper contributed to understanding the impact of different atmospheric temperatures on gas turbine operation, thermal efficiency, and power output.

Pirzadi1 and Ghadimi [43] evaluated the performance and effectiveness of a 1 MW solar power station in Arak, Iran, using data collected over 12 months. They discussed the impact of performance and grid failures on the plant's operation and suggested solutions to reduce energy loss due to system inefficiencies. The study presented performance metrics, including component performance, system energy, element loss, and efficiency indicators, according to the IEC 61724-1 standard. The performance and effectiveness of the Arak solar power station were compared with other power stations globally, highlighting the potential for photovoltaic power in Arak. Additionally, the study examined the relationship between power plant performance and electricity network operations and failures, recommending strategies to minimize power loss. The article emphasized the need for an automation system to improve the supervision and operation of the 1 MW power station in Iran.

Salah et al. [44] conducted an exergy and energy analysis of a gas turbine unit under actual climate conditions using ChemCad simulation software. They identified weaknesses and losses in the system by evaluating the gas turbine's performance under various external influences. The study assessed the thermal performance of the gas turbine unit (K3) using the first and second laws of thermodynamics, revealing that fuel consumption increases with higher atmospheric temperatures, while exergy efficiency peaks in November at 19.39°C. The combustion chamber was identified as the primary source of power loss and the main contributor to the destruction of available energy. The study highlighted the significant impact of the combustion chamber on overall power efficiency and system performance.

Ahmed et al. [45] investigated the exergy and energy of the 150-megawatt Bryton cycle power station using the Dataflow sheet in Iraq in the city of Kirkuk. Both laws for thermodynamics are utilized to calculate losses. Second law efficiency increased from 82.34% to 95.57%. First law efficiency also increases from 42.32% to 94.11%. The study represented the results by using Sankey and Grasmann diagrams for thermodynamics examination. The entire thermal efficiency for the component was determined to be around 33.069%, although the exergy efficiency was around 32.397%. Consequences presented efficiency in the combustion chamber, compressor, exhaust, and gas turbine.

Alaa et al. [46] explored the influence of various design parameters on the performance of a Gas Steam Organic Combined Cycle (GSOCC), focusing on factors like intake temperature and isentropic efficiency and their impact on thermodynamic performance and overall cost. The study demonstrated that integrating the Taji station with a steam and organic steam turbine can recover waste heat, generate additional electricity, and reduce emissions. Under optimal conditions, the GSOCC system produced 258.2 MW of electrical energy, while the gas turbine alone generated 167.3 MW. Compared to the gas turbine alone, which had a power of 28.74% and an efficiency of 27.75%, the GSOCC arrangement demonstrated an overall power of 44.37% and an efficiency of 42.84%. Economic production cost was 9.03 $//MWh for the GSOCC system and 8.24 $/MWh for the BC.

Li et al. [47] improved efficiency, and a dual-stage direct steam generation (ISCC-DSG) system which introduced. While they examined ISCC-DSG techniques, they found that the dual-stage ISCC approach worked more than 30% better than single-stage systems when speaking of net solar-to-electricity operation. The increased solar which parts in energy production and solar-to-electricity efficiency practical, enhances the operational parameters for the Heat Recovery Steam Generator (HRSG) and steam turbine to reach solar integration in the new ISCC structure. This work also discussed the effect of solar power entrance on the complete efficiency of the ISCC structure and recommended efficient methods to enhance procedure and system operation. The outcomes of the initial simulations utilizing the ASPEN PLUS code are offered, saving an understanding of the operation of the new ISCC-DSG structure.

Zhang et al. [48] introduced a unique calculation technology for investigating different ISCC structures, through enchanting solar power integration into the explanation and innovated various essential ISCC system representations depending on the power cascade utilizing both laws of thermodynamics. Similarly, the effect of integrating solar power with ISCC systems is offered, containing the efficiency upgrade factor's efficiency improvement and the saving of fuel factor's covered impact, and the calculation method is utilized on actual-world conditions, present understanding assistance for extra ISCC system estimation study.

Contreras et al. [49] discussed utilizing SOLEEC software, the thermal investigation of a solar energy capability in Mexico presented that a DSG structure with different PTC designs capacity to decrease solar power by around 35%. The applying parabolic trough solar collectors beside a (DSG) structure in a combined cycle power station in Mexico is estimated through the designing and performing of a mathematical system to calculate the exact geometric elements for the (PTC) gatherer, visual efficiency, and software program authentication utilizing simulated information. The determined outcomes of the proposed solar utilization DSG in one style can satisfy the vapor needs and decrease the entire installed reign of the solar.

Ameri and Mohammadzadeh [50] compared solar stations in ISCC have a minor environmental effect than traditional combined cycle power plants (CCPP) and

investigated thermodynamic analysis to identify the elements through great exergy destruction, gas turbines, combustion chambers, air compressors, and solar accumulators. The life cycle assessment (LCA) of solar power plants shows that they have a negligible influence on human health and environmental protection. The research also assessed energy dissipation, ecological consequences, and investment economics, quantifying the environmental implications of both solar and conventional energy generation. It discussed the methodologies used, including the Eco-indicator 99 technique, LCA, the NEEDS database, and the Open LCA software employed for the project.

Adibhatla and Kaushik [51] conducted exergy, energy, and economic (3E) analyses on a theoretical power station integrating solar power into the Rankine cycle of a natural gas combined cycle power plant (CCPP). The study achieved about 7.84% power generation with a modest solar energy capacity of 50 MWh at the design point. Using a direct steam generation (DSG) system with parabolic trough collectors (PTC), the solar power efficiency was found to be 53.79%, energy efficiency about 27.39%, and the cost of energy generation reduced to 6.7 cents per kWh from 7.4 cents per kWh. The study discussed various solar integration technologies, such as Brayton cycle intake air refrigeration and heating the gas turbine compressor discharge air, providing insights into performance parameters, geometrical and optical parameters, and inlet factors of the gas turbine station.

Migla et al. [52] improved solar refrigeration systems by integrating various phase change materials (PCM) and thermal energy storage to reduce the environmental impact of refrigeration systems powered by non-renewable energy. They used TRNSYS simulation software and experimental data for system validation. The system, validated using experimental data from a research laboratory, showed a 6.2% reduction in auxiliary energy consumption with PCM usage and a 27.8% increase in the duration the temperature exceeded 90°C in the storage tank of the liquid heat carrier. Additionally, solar power supplied approximately 98% of the refrigeration load under different climate conditions. The study optimized the potential of solar cooling systems and reduced the environmental impact of refrigeration systems relying on non-renewable energy.

Kwon et al. [53] introduced the concept of a simultaneous dual cooling scheme for coolant pre-cooling, comparing intake air and heating elements refrigeration using an absorption cooler to enhance gas turbine power station performance during hot seasons. They conducted an economic analysis and compared a combined power station utilizing an H-class machine with a dual cooling system to conventional cooling systems, such as simple intake air refrigeration using a mechanical or absorption cooler. The study predicted that the combined cycle power station's energy output could be about 8.2% higher than other systems, highlighting the significant benefits of using an absorption cooler for coolant and intake air refrigeration.

Nezammahalleh et al. [54] compared a techno-economic evaluation of the ISCCS-DSG to two conventional arrangements: a solar electric generating system (SEGS) with a solar combined cycle based on the heat transfer fluid (HTF) method. It gave an extensive description of the solar combined cycle and the (DSG) method, which replaces oil in DSG and results in lower operational costs and capital investment. The study found that the levelized energy consumption (LEC) for solar combo equipment employing the DSG method is lower due to lower operation and maintenance (O&M) costs and higher net heat-generating efficiency. Furthermore, it was revealed that SEGS had the lowest CO_2 release.

Aqachmar et al. [55] highlighted the most prominent solar power installations in Africa and the Middle East, with a particular emphasis on Morocco's Noor 1 production place. In 2016, this power plant generated 160 MW of electricity with parabolic trough solar technology. The study looked at the operation of Noor 1, a parabolic trough solar thermal power station, against other comparable facilities throughout the world that produce 2000 MW of sustainable power. The comparison revealed that Noor 1's specific energy generation was 61.5% of that of other similar solar thermal power plants.

Rovira et al. [56] proposed a novel methodology to assess station operation and perform economic calculations, demonstrating its suitability for understanding the results. They introduced a solar combined cycle incorporating a Brayton cycle with partial recovery, a novel approach in this field. The study utilized an advanced

technique to propose, analyze, and improve the solar combined cycle, which includes a gas turbine with partial recovery. They detailed methods for identifying energy in the hybrid station, referencing selected and isentropic efficiency to address uncertainties and emphasizing energy allocation methods and economic assessments in their conclusions.

Sachdeva et al. [57] conducted a thermodynamic investigation based on the first and second laws of thermodynamics for a solar-driven triple combined system comprising a gas turbine, steam turbine, and organic steam turbine, achieving 33.15% thermal efficiency in the Indian context. This triple combined cycle generates zero emissions and carbon-free energy while addressing the cycle's inefficient components while maintaining high efficiency. The study evaluated performance parameters, identified optimal operating conditions, and estimated the second law efficiency at 97.07% for the main elements of the triple combined cycle system. The findings from this investigation can serve as a model for future experiments and developments in this field.

Temraz et al. [58] designed a solar-assisted combined cycle power station. They conducted energy and exergy analyses to calculate all components' overall exergetic and thermal efficiencies at different solar energy capacities. They examined the energy losses within the solar system. They found that solar energy yields the lowest exergetic efficiency, followed by the condenser, at an ambient temperature of 20°C and a solar input temperature of around 50 MW. The study noted that exergetic and thermal efficiencies decrease with rising ambient temperatures. However, integrating solar support in combined cycle power stations increases efficiency and reduces CO_2 emissions. Their research enhances the understanding of exergy and energy performance in solar-supported combined cycle stations and provides insights for efficiency improvements.

Roshanzadeh et al. [59] proposed enhancing the thermodynamic performance of combined cycle power stations by using solar refrigerating equipment to cool intake air and generate additional electricity during high-temperature summer seasons in various cities. They identified a decline in energy production under hot ambient

conditions. They determined that the optimal economic performance is achieved with a combination of flat plate solar collectors and dual-effect absorption coolers. The study simulated the performance and financial viability of four different types of solar collectors and two kinds of absorption cooler components. The study offered valuable information on the optimal techniques for using intake air refrigeration in areas with high humidity.

Baghernejad and Yaghoubi [60] developed an approach for assessing and improving the price and efficiency of a 400-MW ISCC. Their methodology depends on a genetic algorithm. The study focused on the novel application of exergoeconomic evaluation in an ISCCS, which has not been comprehensively examined in the previous research. The improvement resulted in an 11% decrease in the objective operation, which reduced manufacturing costs for steam and gas turbine generation. The study underlined the efficacy of using algorithms for exergoeconomic enhancement in power generation, notably solar energy, which has shown substantial promise for different nations in recent years.

Rahman et al. [61] provided a complete examination of Saudi Arabia's present power generation and the resulting greenhouse gas release. The nation's discussion focused on a variety of GHG reduction actions, such as the use of conventional gas, cogeneration systems, combined cycle plants, CO_2 collection, alternative energies, and energy-saving measures. The alternative energy targets outlined in Saudi Vision 2030 aim to significantly reduce GHG release and help the country meet its Nationally Determined Contributions (NDCs). The recommended choices include the use of efficient internal combustion, polygeneration, integration of renewable energy into distributed and microgrid mechanisms, biomass generators, and ocean power conversion plants.

Nourpour et al. [62] integrated a system that uses natural gas turbines, solid oxide fuel cells (SOFC), with steam generator turbines to generate additional energy in compressor operations. The proposed process was evaluated utilizing the 6E system, involving exergoeconomic, emergoeconomic, emergoenvironmental, energy, exergy, and advanced exergy assessments. The researchers used the 6E assessment to

compare five various organic liquids for the ORC. The investigation revealed that R11 is among the best-recommended liquids. The station's thermal performance improved significantly, with a rise of approximately 21 MW which is equal to 53.76%, approximately 13.07% relative to the baseline plant. The LCOE, or the mean cost for generating power through the lifetime of a thermal plant, has been calculated to be roughly $41.2 (MWh).

Abdelhay et al. [63] utilized parametric evaluation and optimization with several goals for comparing the nanofiltration Multi Effect Desalination (MED) method for trigeneration. The assessment was carried out from an energy, exergoeconomic, and environmental perspective. They demonstrated the integration of a solar energy system to significantly cut annual CO_2 release through the utilization of waste heat rather than electricity for cooling. The study found that involving NF-MED in the trigeneration plant results in higher performance ratio amounts, longer evaporator life, and more energy savings than MED plants.

Abubaker et al. [64] addressed the limitations of the Brayton cycle, a unique cascaded method was devised and integrated into a combined process. The technology utilized PTC to heat the air when it reached the combustion chamber. The equipment featured an absorption air entry refrigeration technique to regulate the temperature of the air entering the compressor. The analysis identified model improvements for the combustion chamber and the location of the PTC, which might lower power losses by roughly 303.6 MW and 58.9 MW, respectively. They utilized information gathered by the EES program that is related to MATLAB, as well as an Artificial Neural Network (ANN), to optimize multiple objectives. Relative to the previous model, the ANN lowered total exergy destruction to 489.4 MW while increasing power exergy efficiency reach 46.19%.

Wang et al. [65] Compared an integrated refrigeration, heating, and energy process with thermoelectric production to improve power efficiency, although increased expenses and CO_2 release. They investigated the suggested system's environmental and techno-economic features, which obtained an exergy effectiveness of 42.62%, generated 923.55 kt CO_2, with a thermal efficiency of 67.88%, and a price of $10.60

per hour. While comparing two different techniques for combined systems, the study found that merging ORC and CO_2 systems resulted in better economic operation and efficiency than the proposed system.

Evangelos and Tzivanidis [66] explored solar trigeneration technology with PTC for heating, cooling, and power. Statistical research was conducted to assess the evaluated variables' impact on system energy efficiency, exergy efficiency, producing electricity, heating production, and cooling generation. The study investigated the effects of numerous parameters on the system's exergy efficiency, energy efficiency, and manufacturing output. They also analyzed the investment's economic viability. They calculated that a realistic system design incorporating PTC, ORC, and an absorption pump could have an easy repayment period of 8.1 years in building applications.

Duan and Wang. [67] looked at numerous ISCC systems that utilize lithium bromide absorption cooling to chill the entry air. The investigators simulated the entire system using Aspen Plus and EBSILON programs, comparing the innovative system's thermodynamic and economic performance to that of a normal ISCC plant without air inlet cooling. The results showed that the upgraded system had higher thermal efficiency and a lower levelized price for solar energy. The study focused on improving the efficiencies of photoelectric and exergy, as well as raising the system's daily and annual thermal efficiency. The investigators assessed the feasibility of coupling absorption refrigeration with the ISCC mechanism, accounting for variations in DNI and the surrounding temperature throughout the year to determine the best approach to integrate solar power.

Eduardo et al. [68] showed a rise in overall power generation and investigated the average cost for each kWh of electricity utilized for exergy. To reduce exergoenvironmental and environmental consequences, it was emphasized that condenser performance should be improved to promote exergetic efficiency and reduce expenditures on investment. The study thoroughly examined every element, providing detailed insights into exergy destruction, economic rate, exergetic efficiency, and environmental consequences of the exergy process.

Settino et al. [69] investigated solar integration into a standard gas combined plant, with a focus on energy efficiency as well as CO_2 release. The investigators found that the most effective concept featured a 17.9 compression ratio, one intercooling stage, and a solar converting efficiency of approximately 33%. As a result, energy efficiency was determined to be roughly 69.5%. The study examined two types of systems, one with a single-stage intercooler and the other with a two-stage intercooler, to determine the best hybrid design. For one-year experiment done in Messina and Torino revealed that the annual efficiency of changing solar power to electricity was approximately 32%. The study found that employing this solar power technology resulted in yearly decreases of 7.7% and 5.8% in natural gas usage in Messina and Torino, respectively.

Hasan et al. [70] Researched the merging of combined cycle power stations using conventional desalination equipment and multi-effect distillation. Utilizing Thermoflex programs, the investigators verified the combined cycle power plant (CCPP) using multi-effect distillation (MED) and reverse osmosis (RO). They assessed exergy, exergoeconomics, and exergoenvironment. Gas turbines have the largest capital investment price from an economic standpoint, but the MED element had the greatest environmental effect at a level of 0.025. The combination increased the use of fuel by approximately 3.79% while improving the system's exergy efficiency. The study also investigated the economic and environmental implications, including evaluating gas turbine investment costs and the ecological impact associated with the MED element.

Ahamad et al. [71] Improved and analyzed the efficiency of using solar power in conjunction with a turbine that uses steam. The refrigerants were selected using a 4-E assessment that considered energy efficiency, exergy losses, and thermodynamic operation characteristics. The aim was to increase the efficiency of solar power cogeneration equipment. The inclusion of the regenerative part increased the system's power efficiency by approximately 75.07%. To develop a dependable electricity source, the researchers investigated the effects of flow rate, solar normal irradiation, and turbine parameters on energy efficiency, cost savings, environmental footprint, and loss of power. The combination resulted in a considerable

reduction of about 68% in energy costs while increasing ecological effectiveness by roughly 16% when compared to standard configurations.

Bonforte et al. [72] examined component cost and environmental values for integrated cycle power stations, we employed a comprehensive Life Cycle Assessment (LCA) model tool together with exergoeconomic and exergoenvironmental assessments. They increased ecological development by utilizing an approach that forecasts plant operation and environmental benefits. The study looked at the relationship involving exergy loss in solar gathering parts in ISCCGTs, exergy destruction, environmental effects, and economic factors. The findings showed that adding solar power into a Combined Cycle plant may enhance the environment while not compromising cost considerations. This combination reduces CO_2 emissions by roughly 9% while only slightly increasing initial expenses and having little influence on the payback of investment. stressed the environmental advantages of integrated solar installations.

Elmorsy et al. [73] examined the three solar thermal methods in terms of energy, exergy, and economics for parabolic trough collectors (PTC), solar power towers, and linear Fresnel reflectors. Based on their findings, Fresnel collectors have the highest exergetic efficiency around 44.1%, while solar towers have the smallest efficiency around 33.2%, as measured by exergetic assessment. Based on the findings, direct steam-producing equipment with solar produced the most cost-effective energy, spending $36.75 (MWh). The economic analysis revealed that establishing concentrated solar power might be done at acceptable costs and would profit from learning technology when included as an integrated energy unit of a combined power plant. This combination would lead to a significant decrease in economic investment expenses.

Moussa and Ghenaiet. [74] proposed a revolutionary thermal storage device to improve power plant efficiency, improve solar power conversion, and enhance the electrical system, all while significantly lowering costs. The study analyzed the LCOE and economic benefits of the refurbished station, focusing on potential reductions in fuel use and the environment. They increased the efficiency of the solar integrated

cycles plant by installing creative thermal storage technology. The redesigned ISCC-PTC system contributed to a $30 million decrease in gas utilization. Solar energy proportions may rise to around 14%, for energy and exergy efficiency rates of 56.06% and 53.29%, respectively. The updated ISCC-PTC power station has an electricity price of around 9.75 cents (kWh), which significantly reduces natural gas costs.

Tiwari et al. [75] conducted an exergy analysis on the NTPC Dadri power station in India, that comprises a BC element, an RC element, and an HRSG. The investigators observed that the combustion chamber for GT accounts for 35% of total exergy destruction, thus being the largest source of exergy loss. Various station elements' exergy destruction ranged from 7% to 21% depending on the operational conditions. The study looked at how variables including pressure ratio, pressure dips in the combustion chamber, turbine inlet temperature, and HRSG affected the power plant's energy losses. They expressed their gratitude to the National Thermal Power Corporation (NTPC) in Dadri, India, for supplying critical data for the study. They also acknowledged the Executive Engineers who assisted them on the site.

Khandelwal et al. [76] combined systems, such as gas turbines operating at full and partial capacities were evaluated for efficiency. The study compared the performance of various heat transfer liquids, involving melted salt and water, for the ISCC mechanism. According to research, ISCCs made using molten salt are 1.51% greater inefficient than those made with water. The efficiency of water-based ISCCs is measured at 50.87%. The study underlined the benefits of integration, including increased efficiency, fuel economy, and cost savings. The study also analyzed the emissions linked to the integrated system, showing insignificant outputs. Moreover, the researchers deliberated on the arrangements of solar generating in conjunction with conventional generation.

Besevli et al. [77] introduced a waste heat recovery system for steel and iron companies that use various systems, including the SRC, KC, ORC, and trans-critical CO_2 system (t-CO_2) to produce electricity. The system attained a thermal efficiency of 0.19 and generated 596.6 kW of power. The research examined four distinct cycles for

using the waste heat from the reheat heater. These cycles were assessed based on their thermal efficiency, ability to reduce emissions, net energy output, and cost of energy generation. According to the research, combining cycles may decrease CO_2 emissions by 23.16 tons per day and generate energy at a minimum price of 0.1972 $/kWh while still attaining low energy production costs.

The literature contains significant studies into the precise evaluation of combined solar elements, notably PTC, and their impact on system efficiency and economic viability. Past studies on solar with triple combined cycle power stations in Iraq provide useful insights into their thermoeconomic operation under climatic conditions, but it is not comprehensive. Previous research has mostly focused on the characteristics of gas turbines and HRSG, failing to effectively address solar integration and its interaction using standard power-generation technologies. Iraq's power constraint highlights the importance of using waste heat in power plant techniques, suggesting creative solutions. This investigation seeks to fill this gap by conducting a thorough examination of the use of solar power in conjunction with combined cycle power plants in Iraq. The emphasis is on how PTCs enhance energy production, economic viability, and waste heat use. The effort aims to close this gap by providing vital data that will enhance the efficiency and viability of solar power plants in similar environments. Table 2.1 lists some of the world's ISCCs.

Table 2.1. Some ISCCs in the world.

Project name	**Location**	**DNI kWh/m²**	**Solar technology**	**Total output (MWe)**	**Solar contribution (MWe)**	**Solar share %**	**Status**
Kuraymat	Egypt	2400	PTC	140	40	28.57	Operation 2011 [78]
Palmdale	California	2200	PTC	555	62	11.17	Operation 2010 [79]
Hassi R'Mel	Algeria	2300	PTC	130	25	19.23	Operation 2011 [80]
Yazd	Iran	2100	PTC	430	67	15.58	Operation 2011 [81]
Agua Prieta	Mexico	2821	PTC	480	31	6.45	Operation 2017 [82]
AinBeni Mathar	Morocco	2300	PTC	472	20	4.23	Operation 2011 [83]
Waad Al shamal	Saudia Arabia	2700	PTC	1390	50	3.59	Planned 2026 [84]
Dadri	India	22000	PTC	210	14	6.7	Operation 2020 [85]

PART 3

MATERIALS AND METHODS

3.1. INTRODUCTION

ISCC power station's analysis and optimization process has been described in detail in the third chapter of the thesis. After establishing the goals of the study, practical information and technology details regarding the presently operating Al-Qayyarah generator are collected. Next, based on thermodynamic principles, numerical designs are created for every part of the ISCC system utilizing data collected from other studies. The EES program runs simulations and analyzes energy, exergy, exergoeconomic, and environmental to assess the system's effectiveness. This systematic methodology guides the thesis's following chapters and makes thorough study and improvement of the ISCC power station possible.

3.2. THE MAIN COMPONENT

3.2.1 Simple Gas Turbine

A simple gas turbine's primary work is to change the power from fuel burning into mechanical power through several steps. It begins with atmospheric air taking in the compressor, which increases pressure and temperature. Then, in a combustion chamber, this air is burned with fuel to generate gas at high pressure and temperature. This gas rolls the blades of the turbine that are connected to a shaft, generating mechanical power. Gas turbines release gases from the exhaust, which is called waste heat [86]. Turbines are used in manufacturing practices, air navigation, and power plants. They usually work in combined system power generation because the Rankine cycle, which is run by the waste heat from these components, raises total power efficiency [87].

3.2.2 Steam Turbine.

While utilizing the gas turbine exhaust heat, the working of the steam turbine in a combined system power generation raises total power efficiency. Hot waste gases from the turbine exhaust heat the liquid in the HRSG, generating vapor with high pressure. This vapor or steam rotates thermal power into mechanical power and, lastly, into electrical power. In small words, the vapor rotates the steam turbine. A HRSG rolls the steam and condenses it to generate the steam. Merging the gas and steam turbines raises complete efficiency and effectiveness and increases financial viability by generating more power from exhaust heat [88].

3.2.3 Combined Cycle

The recent energy-producing technology developed in combined systems power generation, where gas turbines merged with steam turbines. For that, the more considerable energy-generating ability of the Rankine cycle is combined with the efficiency of gas turbines. The core portion of the combined system was identified for rapid startup working and worthy efficiency at various loads, gas turbines, or Brayton cycles. HRSG regains exhaust heat to generate vapor instead of releasing it into the atmosphere. Also, a PTC enhances the HRSG's vapor production with solar power, which raises workability and efficiency for the power plant [89]. A steam turbine is driven by steam produced by exhaust heat recovery and solar power. Because of this merging, combined system power generation is between the most efficient incomes of producing power, both solar energy and fossil fuel, with total efficiency above 60% [90].

3.2.4 Solar Energy Parabolic Trough Collector (PTC)

In the integrated combined system power generations, the PTC is the important element that utilizes solar power to enhance the heat produced by the HRSG. The bent glasses in its system track sunshine routine to concentrate the solar onto a response tube. The fluid that transfers energy, like heated salt and thermal oil, is included in this tube and heated by absorbing solar energy. Later, the heated liquid is guided to a heat

exchanger, which converts thermal solar power to steam or vapor [91]. The PTC improves steam generation by engaging solar power to exhaust heat recovery. This rising and growing of steam assists in producing electricity by driving a Rankine turbine, which is joined to an electric producer. Also, to increase efficiency, innovative control systems adjust the liquid flow rates and reflect the location of the PTC. The PTC utilizes solar power to support steam production, enhancing the total efficiency of combined system power generation [92].

3.2.5 Heat Recovery Steam Generating (HRSG)

In the present work, solar energy (SE) with the combined cycle power station that recovers heat for the steam generator (HRSG) also plays a vital role in increasing performance and power efficiency by catching the exhaust heat from the gas turbine and using the SE in the power plant. The HRSG is a heat exchanger approach that separates thermal power from the exhaust high-temperature heat gases of the superficial gas turbine. These heated gases go forward during the HRSG, heating the working fluid that moves everywhere in the heat recovery steam generation. Then water absorbs heat. It is transformed into high-pressure superheated vapor. This superheated vapor then goes to a Rankine steam turbine, expanding and leading the turbine's rotary motion, producing extra power [93]. For now, chilled exhaust air exits from the Brayton cycles and is released into the environment. By effectively regaining the waste heat air coming from the Brayton cycle, the HRSG allows combined-system power stations to reach better complete efficiency compared to conventional power stations. Furthermore, the HRSG permits adaptable working, as it can adjust variations in energy needs and offer additional steam generation while required. In general, the HRSG is an essential element in the combined system, supporting its effectiveness and efficiency, dependability, and financial sustainability [94].

3.2.6 Absorption refrigerant cycle (ARC)

Refrigeration systems working by absorption are fundamental in merging Solar with Combined Cycle (ISCC) power stations, using exhaust heat and solar energy from power plants in gas turbines to present refrigeration. The performance for these cycles

by sucking and emitting refrigerant airs using sucker fluid like lithium bromide (Li Br) and ammonia with water [95].

Exhaust heat at the exit of HRSG directs the absorption refrigeration system. Refrigerant steam is sucked into the absorbent fluid at minimal pressure and temperature, emitting temperature to the environment cooling. After that, the refrigerant-wealthy absorbent mixture is injected to upper pressure and temperature, normally by a heat exchanger, emitting refrigerant steam. The steam condensed again into fluid, emitting extra temperature. The exhaust absorbent fluid comes again to the sucker to finish the system. By applying exhaust heat, the absorption refrigeration cycle improves ISCC power plant performance and efficiency, presenting power electricity and cooling output together. The absorption refrigeration cycle generally increases ISCC plant sustainability and possibility cost by enhancing resource operation and use [96].

3.3. DATA COLLECTION AND ANALYSIS

Figure 3.1 from the London Geographical Institute illustrates the location of the AL Qayyarah electrical facility on the Turkish border. It is located near the city of Nineveh in the northern part of Iraq called Al-Qayyarah power station. Approximately 124 miles separate it away from the Turkish border. The power station's advantageous position puts it close to critical infrastructure and major cities, making it easier to distribute power to the neighboring regions. Furthermore, given its closeness to Turkey's border, there might be potential for international partnerships in energy or commerce in items like gasoline or repair parts.

Compiling the technology parameters and operating information on the current Al-Qayyarah power station is necessary for complete investigation and improvement. This procedure entails gathering comprehensive data on the plant's operational and architectural features. The 750 MW power of the plant, the kinds of energy production (gas turbine frame 9E coming from GE), energy source kinds (crude oil, gasoline, and gas from natural sources), efficiency indicators, operational factors (temperatures, pressures), and devices specifications for the main parts (gas turbines and steam

turbines) are some of the essential information points. It's also critical to comprehend the plant's service connections, maintenance histories, procedures for operation, and respect for the environment. Researchers can evaluate the plant's execution, discover areas for development, and make well-informed decisions to raise its reliability and efficacy by gathering this data.

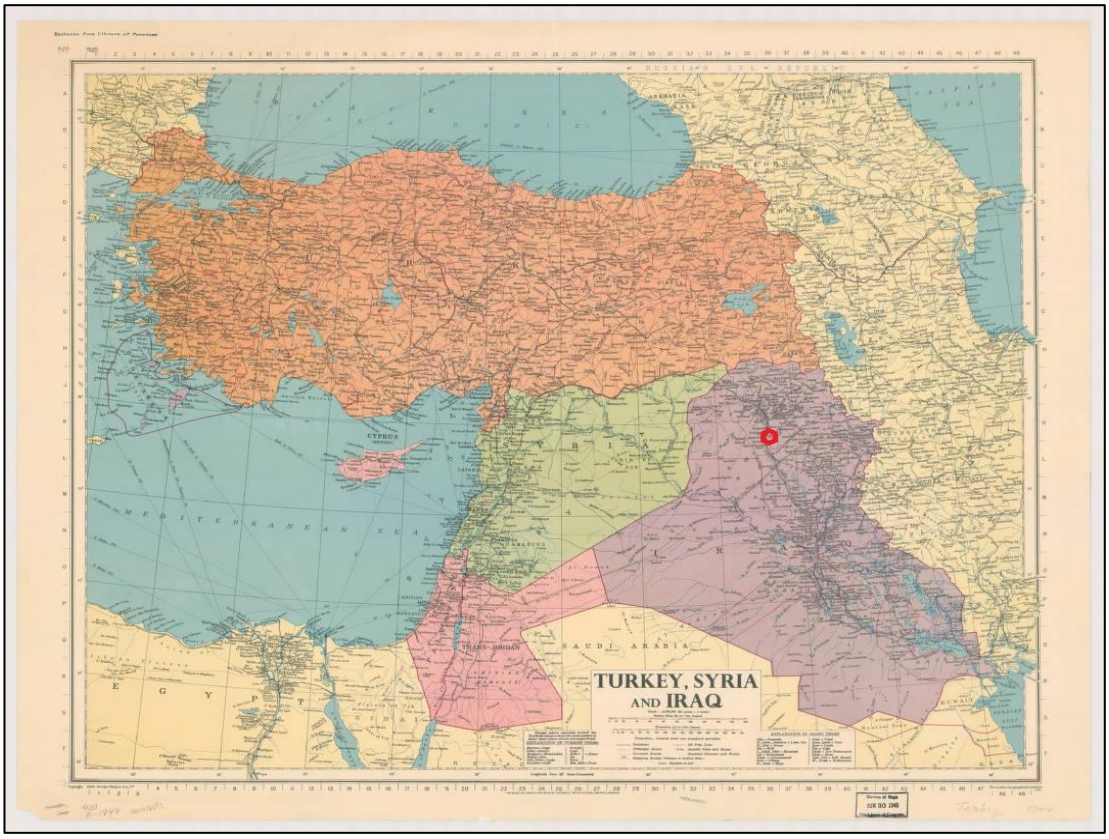

Figure 3.1. The location of the power plant to the border of Turkey from the London Geographical Institute [97].

The location is 35°46'52.11' E and 43°15'01.46" N. The details of the Al Qayyarah generating plant are displayed in Figure 3.2. It is a large power plant generation that is essential to power generation in the area. Gasoline and natural gas are the primary fuels the power station uses to produce energy. The Al-Qayyarah generator, which has a capacity of about 750 MW, substantially contributes to supplying Mosul and the neighboring territories with power.

Figure 3.2. Location of Al Qayyara power plant [1].

Table 3.1 describes the supplied variables and displays the environmental factors at the air compressor's intake for thermodynamic evaluation.

Table 3.1. Characteristics of the monthly environmental conditions at the compressor intake air

Mounts	**DNI (W/m^2)**	**Temperature (°C)**	**Humidity (%)**
Jan	3.94	7.43	56.39
Feb	4.33	9.76	56.45
March	5.18	12.54	55.76
Apr	5.63	21.86	34.1
May	6.87	28.88	20.51
June	7.96	32.24	15.26
July	7.77	36.38	17.18
Aug	7.28	35.65	17.45

Sep	6.49	29.28	20.39
Oct	5.28	22.84	27.39
Nov	4.56	15.09	54.07
Dec	3.87	8.81	54.07

3.4. SYSTEMS DESCRIPTION

Al-Qayyarah power plant does have the same problems that affect other thermal power stations in Iraq, including outdated infrastructure, maintenance problems, and the need to increase efficiency. Despite these challenges, the Al-Qayyarah generator remains essential for the area's consistent power supply. Figure 3.3 depicts the suggested NGCC system layout simply as it will incorporated into a gas turbine system. Just three of the six 125 MW gas turbines at the Al-Qayyarah gas power station are employed in the simulation in this investigation. It's critical to comprehend how gas turbines operate. The air compressor, which brings in outside air and compresses it to more excellent heat and pressure, starts with the procedure. After that, air that has been compressed is fed into a combustion chamber, after which it combines with fuel and burns to produce a high-pressure, high-temperature gas. By expanding via a turbine, this heating gas produces energy from motion and power. The turbine revolves and powers the shaft linked to the compressor and a generator that produces electricity. The cycle is completed when the waste gases leave the turbines through an exhaust after the power is extracted. Finally, the HRSG model will receive these waste heat gases from the gas turbines and use them to operate RC.

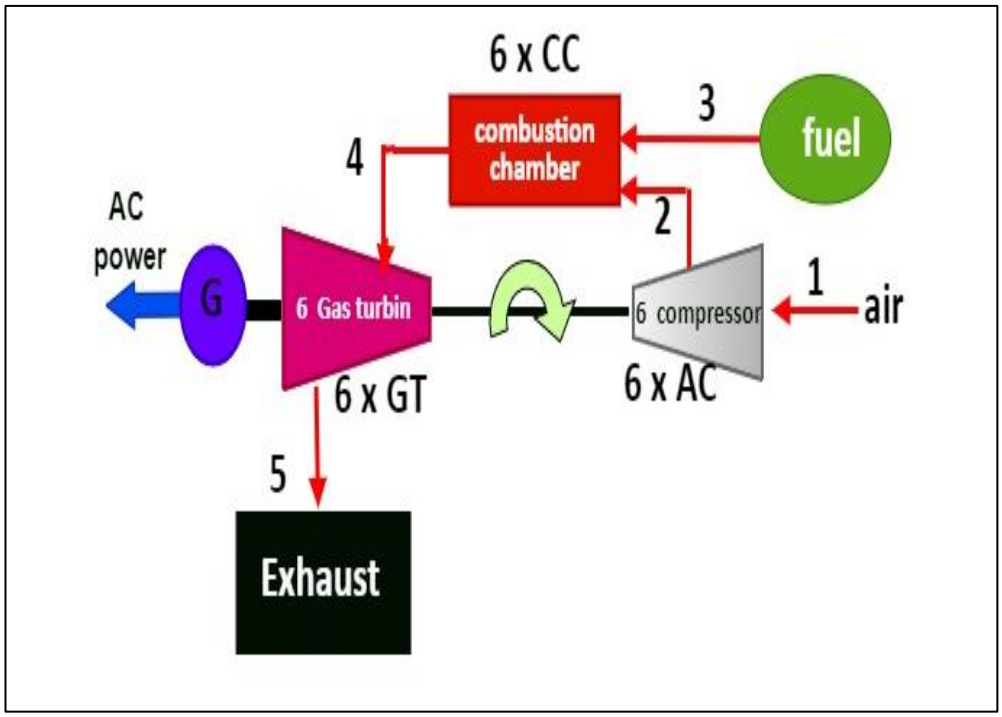

Figure 3.3. Bryton cycle power generation of Al-Qayyarah.

The heat recovery steam generation method is used to guide the gas turbine's emission of heat gases to increase the system's general efficiency and generate additional electricity through the process known as the Rankine cycle. The mixed process of the Al-Qayyarah natural gas turbine, which increases the quantity of steam produced in the HRSG, is shown in Figure 3.4. Here, exhaust heat is used to power steam turbines by heated water or another thermal-transfer fluid. Further electrical power plants are powered by the rotating mechanical power generated by these turbines, increasing electricity generation even more.

The heat that remains latent in the steam is released when it condenses back into the fluid in a condenser following its passage across the steam turbines. This continuous water circulation technique guarantees the effective use of available resources. The manufacturing organization demonstrates its dedication to power efficiency and sustainability by using a variety of control mechanisms and monitoring tools to manage fuel consumption, enhance combustion methods, and guarantee safe and effective running during the entire process.

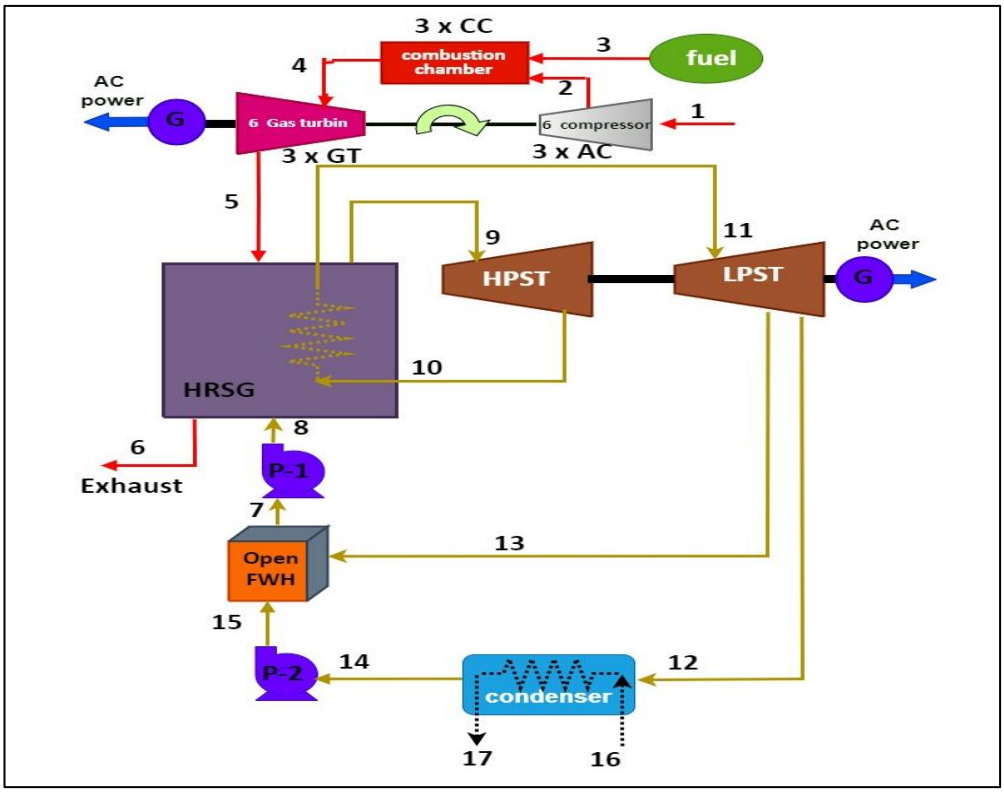

Figure 3.4. Simple combined cycle (NGCC) [98].

The planned combination of PTCs with the combined cycle technology of the Al Qayyarah power station is depicted in Figure 3.5. Enhancing the combined cycle generation station operation and efficiency, especially when mixing solar energy, requires a thorough understanding of how gas turbines operate. as a calculated attempt to maximize energy production. The main goal of this project is to use solar power to increase the amount of steam produced by HRSG. PTCs are widely recognized in this configuration for their capacity to focus on solar energy. PTCs allow boiling salt or heated oil, a heat transfer liquid, to be heated by absorbing and transforming solar power into heat. This heated liquid enhances the HRSG's internal steam generation analysis, increasing the power station's total steam output capability.

The combined technique allows for a concentrated examination of the suggested changes because it emphasizes three natural gas turbine components. This integration project aims to realize the opportunity for higher production and efficiency using mathematical modeling and analysis, opening the door for a more reliable and sustainable power-producing infrastructure at the Al Qayyarah power station.

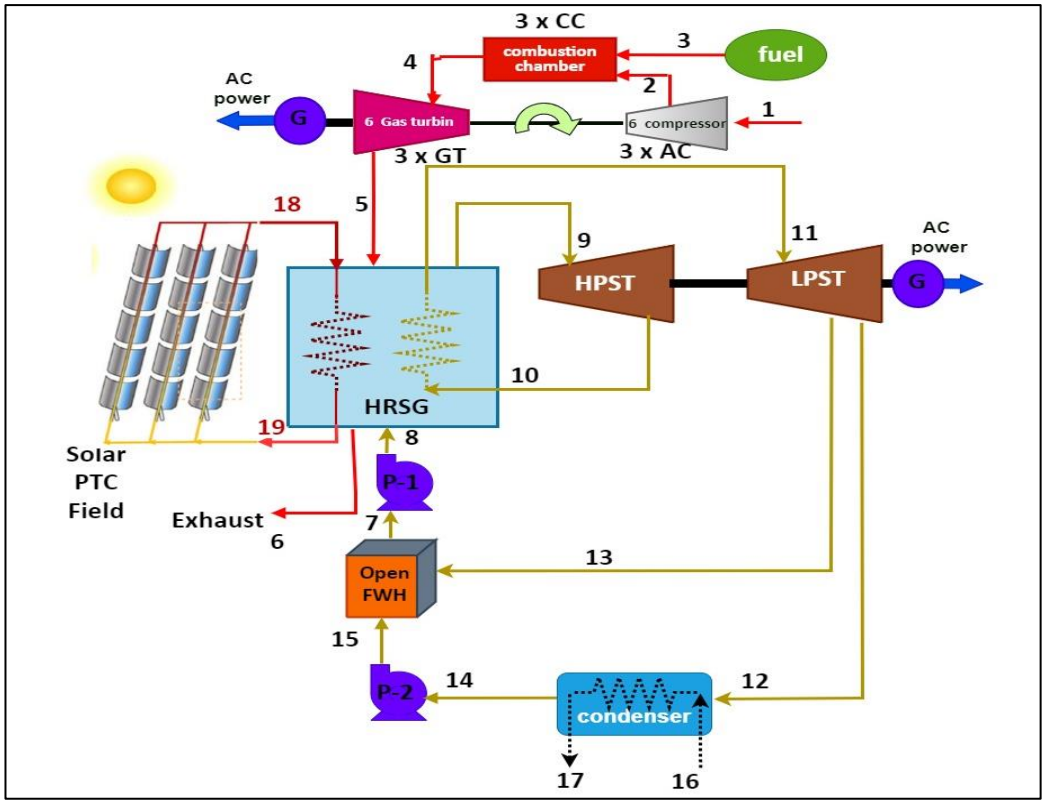

Figure 3.5. Integrated solar energy with Al-Qayyarah combined cycle [98].

A significant development in the production of electricity technique is shown in Figure 3.6, which integrates the absorption refrigeration cycle (ISCC-ARC) with the solar combined cycle. In this configuration, the ARC uses the thermal energy from the HRSG's exhaust gases. This process enables the ARC to lower the temperature of the surrounding air to 283 K before it reaches the air compressors in the gas turbine components. By reducing the power consumption of the compressors, this configuration enhances the performance of the ISCC-ARC, particularly during the hot months.

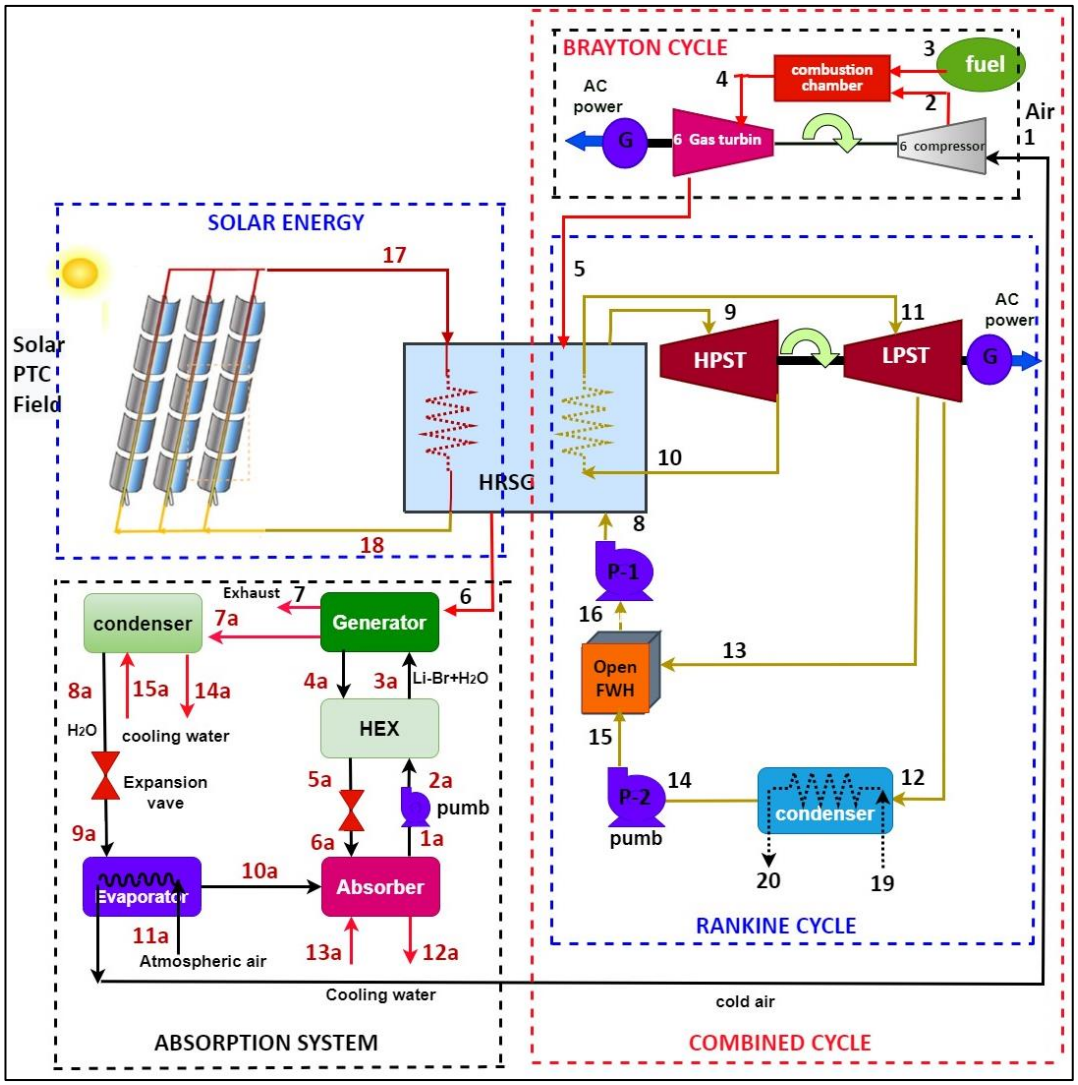

Figure 3.6. Solar energy, combined cycle, absorption cooling process, and integrated solar combined cycle (ISCC-ARC) [99].

3.5. MODELING

The current subsection covers the computational modeling and operation examination of the transmitted solar heat exchangers, Absorption Refrigeration cycle, PTCs, and combined cycle. The integrated system is developed, verified, assessed, and analyzed using EES. The independent components' assumptions and performance evaluations are the same as those of the absorption cooling device, the combined cycle, and the PTCs. Figure 3.7 illustrates a flow chart for the relationship between every component and how each system may provide input to one another, which will help to learn the relationship between components best. Nevertheless, integration is innovative since

the impacts of a particular system may be noticed by each other. First, the HRSG is operated by the exhaust of the gas turbine, and in exchange, the HRSG improves its operation using solar energy by collecting thermal waste heat and producing additional power through the steam turbine. Second, the PTC is run by solar energy. By lowering the energy input in the compressors, the Absorption Chilling Component improves the Gas Turbine and is thermal powered by the PTC via SHE2. ARC, nevertheless, would use more NG and exhaust it more, enabling the PTC to reduce this increased fuel use by the SHE1.

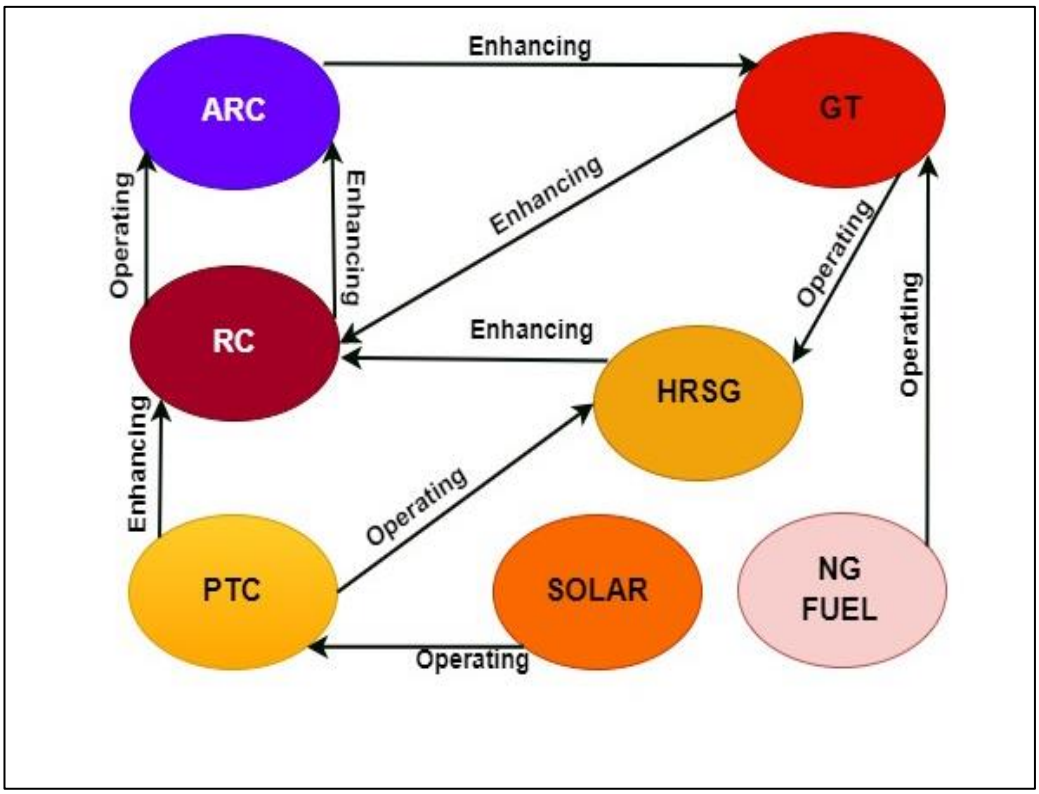

Figure 3.7. Flow chart of all systems.

3.6. THERMODYNAMIC ANALYSIS

The EES program is used to evaluate, investigate, and model the suggested systems in this work. Thermodynamic characteristics like pressure, temperature, entropy, and exergy have been computed using this software. The following assumptions are taken into account during the design and analysis:

- Steady-state process.
- The impact of friction effect, loss of heat, and pressure drops caused by the layout of tubes and heat exchangers are all negligible.
- Air is considered an ideal gas.
- For simplicity in calculations, natural gas is assumed to be composed entirely of methane.
- The differences in potential and kinetic energy across components are disregarded.
- Pumps, turbines, and compressors are numerically represented through adiabatic simulations
- Heat loss to the surroundings is not considered.

Explanation of the power transformation procedures in power stations, mainly ISCC systems, requires a fundamental knowledge of the first law of thermodynamics. The first law offers an essential system for the thesis that emphasizes improving the effectiveness of ISCC generators by integrating solar power and absorption cycles for cooling. It directs the study of heat transfer, energy production, and power consumption by regulating how power is changed and transmitted through the system. Under the use of first law concepts, the studies can evaluate the ISCC technique's balance of energy, enhance power conversion procedures, and eventually improve the power station's total performance and efficiency. Mass and energy balances for each system component (control volume) are established in this study as follows:

$$\sum_{in} \dot{m} = \sum_{out} \dot{m} \tag{3.1}$$

$$\dot{Q}_{in} + \dot{W}_{in} + \sum_{in} \dot{m}(h_{in}) = \dot{Q}_{out} + \dot{W}_{out} + \sum_{out} \dot{m}(h_{out}) \tag{3.2}$$

For the air compressors, the energy equation is:[100]:

$$\dot{W}_{AC} = \dot{m}_{air}(h_2 - h_1) \tag{3.3}$$

Where:

$\dot{W}_{AC}$: The work rate is done through an air compressor (kW).

$\dot{m}_{air}$: The mass flow rate of entering air to the compressor (kg/s).

h_1: Specific enthalpy of the air inlet to the compressor expressed (kJ/kg).

For the combustion chamber, the energy equation is [101]:

$$\dot{m}_{air} h_2 + \dot{m}_{fuel} \, LHV_{CH_4} = (\dot{m}_{fuel} + \dot{m}_{air}) h_4 \quad (3.4)$$

Where:

h_2: The specific enthalpy of the air at the compressor's output and intake of the combustion chamber (kJ/kg).

$\dot{m}_{fuel}$: Rate of flow mass for fossil fuel (kg/s).

LHV_{CH_4}: Lower Heating Value of the fuel (kJ/kg).

h_4: The specific enthalpy of the gas's combustion products that enter the turbine (kJ/kg).

While for the gas turbines, the energy equation is: [102]:

$$\dot{W}_{GT} = \dot{m}_4 (h_4 - h_5) \quad (3.5)$$

Where:

$\dot{W}_{GT}$: Work done rate through the turbine (kW).

$\dot{m}_4$: Rate of flow mass for gases into the gas turbine (kg/s).

h_5: Specific enthalpy of the gases that leave from a gas turbine (kJ/kg).

The heat transfer balance between cold fluids and hot fluids for the HRSG is defined as follows:

$$\dot{Q}_{HRSG} = \dot{m}_4 (h_5 - h_6) + \dot{m}_{17} (h_{17} - h_{18}) = \dot{m}_8 (h_9 - h_8) + \dot{m}_{10} (h_{11} - h_{10}) \quad (3.6)$$

Where:

$\dot{Q}_{\mathrm{HRSG}}$: Heat rate is engaged by the HRSG (kJ/s).

h_{16}: The specific enthalpy of the steam entering the HRSG (kJ/kg).

$\dot{m}_8$: Rate of flow mass for steam exiting the HRSG (kg/s).

$\dot{m}_{10}$: Rate of flow mass for water inlet the HRSG (kg/s).

$h_5, h_6, h_{16}, h_{17}, h_9, h_8, h_{11}$, and h_{10}: The specific enthalpies of the subsequent conditions in the HRSG (J/kg). [103]:

$$\dot{W}_{\mathrm{HPST}} = \dot{m}_9(h_9 - h_{10}) \tag{3.7}$$

$$\dot{W}_{\mathrm{LPST}} = \dot{m}_{11}(h_{11} - \mathrm{h}_{13}) + \dot{m}_{12}(h_{13} - \mathrm{h}_{12}) \tag{3.8}$$

Where:

$\dot{W}_{\mathrm{HPST}}$: The work rate generated by the HPST (kW).

$\dot{m}_9$: Rate of flow mass for steam arriving at the HPST (kg/s).

$\dot{W}_{\mathrm{LPST}}$: The work rate generated by the LPST (kW).

$\dot{m}_{11}$ and $\dot{m}_{12}$: Rates of flow mass for steam inlet and leaving the LPST correspondingly (kg/s).

h_{11}, h_{12} and h_{13}: Specific enthalpies of the subsequent states for HRSG (kJ/kg).

The heat extracted from the hot steam condenses into liquid water and transfers thermal energy to the cooling water through the condenser. The energy balance equation for the condenser is written as [104]:

$$\dot{Q}_{\mathrm{Con}} = \dot{m}_{14}(h_{12} - h_{14}) \tag{3.9}$$

Where:

$\dot{Q}_{\mathrm{Con}}$: Heat rate, which is a transfer from the condenser (kJ/s).

$\dot{m}_{14}$: Flow mass rate for the chilling water moving during the condenser (kg/s).

h_{12} and h_{14}: Specific enthalpies of the subsequent states at the condenser entering and exiting correspondingly (kJ/kg).

The energy balance equations for pump 1 and pump 2 are represented by the following equation:

$$\dot{W}_{\mathrm{P1}} = \dot{m}_7(h_8 - h_{16}) \tag{3.10}$$

$$\dot{W}_{\mathrm{P2}} = \dot{m}_{14}(h_{15} - \mathrm{h}_{14}) \tag{3.11}$$

Where:

$\dot{W}_{\mathrm{P1}}$: The work rate is consumed by pump 1 (kW).

$\dot{m}_7$: Rate of flow mass for water being sent by Pump 1 (kg/s).

h_7 and h_8: Specific enthalpies of the subsequent states of Pump 1's exit and enter correspondingly (kJ/kg).

$\dot{W}_{\mathrm{P2}}$: The work rate is consumed by pump 2 (kW).

$\dot{m}_{14}$: Rate of flow mass for water sent through Pump 2 (kg/s).

h_{15} and h_{14}: Specific enthalpies of the subsequent states at Pump 2's exit and enter correspondingly (kJ/kg).

The energy balance for the OFWH is written as:

$$\dot{Q}_{\mathrm{OFWH}} = \dot{m}_{15}(h_{16} - \mathrm{h}_{15}) = \dot{m}_{13}(h_{13} - \mathrm{h}_{16}) \tag{3.12}$$

Where:

$\dot{Q}_{\mathrm{OFWH}}$: Heat rate, which transfers in the OFWH (W).

$\dot{m}_{14}$: Rate of flow mass for the water arriving at the OFWH (kg/s).

$\dot{m}_{13}$: Rate of flow mass for the water exiting OFWH (kg/s).

The following formula for exergy balance will be used to determine each part's exergy destruction: [105].

$$\dot{\mathrm{E}}_{\mathrm{Q}} - \dot{\mathrm{E}}_{\mathrm{W}} = \sum \dot{\mathrm{E}}_{\mathrm{out}} - \sum \dot{\mathrm{E}}_{\mathrm{in}} - \dot{\mathrm{E}}_{\mathrm{D}} \tag{3.13}$$

Where:

$\dot{E}_Q$: Exergy rate for heat transfer (kW).

$\dot{E}_W$: Exergy rate for work transfer (kW).

$\dot{E}_{out}$: Exergy rate for system transfers out (kW).

$\dot{E}_{in}$: Exergy rate for system transfer in (kW).

$\dot{E}_D$: Exergy destruction rate (kW).

$\dot{E}_Q$: The variation between the balance state temperature and the environment temperature for systems, multiplied by the quantity of energy transfer, is how the formula depicts the exergy transfer with heat. The stream exergy rate by heat is determined using the following equation [106]:

$$\dot{E}_Q = \left(1 - \frac{T_0}{T_i}\right) \dot{Q}_i \tag{3.14}$$

Where:

T_0: Environment temperature for a dead state (K).

T_i: System boundary temperature for heat transfer happens (K).

$\dot{Q}_i$: Heat transfer rate (kW).

The fuel exergy of the solar field, associated with solar radiation (Ės), is defined as follows:

$$\dot{E}_{Q,solar} = \left(1 - \frac{T_0}{T_{sun}}\right) \dot{Q}_{solar} \tag{3.15}$$

The exergy transfer connected with work is expressed correspondingly by this equation [107]:

$$\dot{E}_W = \dot{W} \tag{3.16}$$

Where:

$\dot{E}_{Q,solar}$: Exergy rate for solar radiation (kW).

T_{sun}: Solar radiation temperature (K).

$\dot{Q}_{solar}$: Solar radiation rate (kW).

$\dot{E}_W$: Work exergy rate (kW).

$\dot{W}$: Work rate (kW).

3.7. ENERGY AND EXERGY EQUATION OF THE SYSTEM

The term "exergy destruction" describes irreversible processes and inefficiencies that cause every element of the system to lose its useful power [108]. Temperature variations, reductions in pressure, friction, and various other elements that cause the system's system to vary from optimal conditions lead to energy annihilation. Enhancing general effectiveness and efficiency can be achieved by understanding regions where enhancements can be made by studying the exergy destruction for every part of the entire system. For instance, inadequate combustion in the combustion chamber or inefficient heat transmission in the heat exchangers might destroy exergy. In the same way, friction between liquids and energy losses can cause exergy destruction in pumps, turbines, and compressors. Exergy destruction for every system element can be computed to enable focused optimization procedures to reduce wastage and enhance the general efficiency of ISCC, the generating plant.

The exergy destruction by the air compressor can be calculated by the following equation:

$$\dot{E}_{D,\mathrm{AC}} = \dot{W}_{\mathrm{AC}} + \dot{E}_1 - \dot{E}_2 \tag{3.17}$$

Where:

$\dot{E}_{D,\mathrm{AC}}$: Exergy destruction rate for air compressor,

$\dot{W}_{\mathrm{AC}}$: Work input rate for air compressor.

$\dot{E}_1$: Exergy flow in rate for air compressor.

$\dot{E}_2$: Exergy flow out rate for air compressor.

The exergy destruction by the air combustion chamber can be determined as follows:

$$\dot{E}_{D,\mathrm{CC}} = \dot{E}_2 + \dot{E}_3 - \dot{E}_4 \tag{3.18}$$

Where:

$\dot{E}_{D,\mathrm{CC}}$: Exergy destruction rate for the combustion chamber,

$\dot{E}_2$&$\dot{E}_3$: Exergy flow in rate for the combustion chamber,

$\dot{E}_4$: Exergy flow out rate for the combustion chamber.

The exergy destruction in the gas turbine is determined as:

$$\dot{E}_{D,\mathrm{GT}} = \dot{E}_4 - \dot{E}_5 - \dot{W}_{\mathrm{GT}} \tag{3.19}$$

Where:

$\dot{E}_{D,\mathrm{GT}}$: Exergy destruction rate for gas turbines.

$\dot{E}_4$: Exergy flow in rate for gas turbine.

$\dot{E}_5$: Exergy flow out rate for gas turbine.

$\dot{W}_{\mathrm{GT}}$: Work produced rate for gas turbine.

The following formula can be used to determine HRSG exergy destruction:

$$\dot{E}_{D,\mathrm{HRSG}} = \dot{E}_5 - \dot{E}_6 + \dot{E}_8 - \dot{E}_9 + \dot{E}_{10} - \dot{E}_{11} + \dot{E}_{17} - \dot{E}_{18} \tag{3.20}$$

Where:

$\dot{E}_{D,\mathrm{HRSG}}$: Exergy destruction rate for HRSG.

$\dot{E}_8$: Exergy flow in rate for HRSG.

$\dot{E}_9$: Exergy flow out rate for HRSG from HPST.

$\dot{E}_{10}$: Exergy flow in rate for HRSG from LPST.

$\dot{E}_{11}$: Exergy flow out rate for HRSG from the feedwater intake.

$\dot{E}_{17}$: Exergy flow in rate for HRSG from flue gas exit.

$\dot{E}_{18}$: Exergy flow out rate for HRSG from the air intake.

The following formula can be used to determine HPST exergy destruction:

$$\dot{E}_{D,\mathrm{HPST}} = \dot{E}_9 - \dot{E}_{10} - \dot{W}_{\mathrm{HPST}} \tag{3.21}$$

Where:

$\dot{E}_{D,\mathrm{HPST}}$: Exergy destruction rate for HPST,

$\dot{E}_9$: Exergy flow in rate for HPST,

$\dot{E}_{10}$: Exergy flow out rate for HPST from LPST,

$\dot{W}_{\mathrm{HPST}}$: Work output rate for HPST.

The following formula can be used to calculate LPST exergy destruction:

$$\dot{E}_{D,LPST} = \dot{E}_{11} - \dot{E}_{12} - \dot{E}_{13} - \dot{W}_{\mathrm{LPST}} \quad (3.22)$$

Where:

$\dot{E}_{D,LPST}$: Exergy destruction rate for LPST.

$\dot{E}_{11}$: Exergy flow in rate for LPST.

$\dot{E}_{12}$: Exergy flow out rate for LPST of the condenser.

$\dot{E}_{13}$: Exergy flow out rate LPST from LPST.

$\dot{W}_{\mathrm{LPST}}$: Work output rate for LPST.

The following formula can be used to find the condenser exergy destruction.:

$$\dot{E}_{D,\mathrm{Con}} = \dot{E}_{12} - \dot{E}_{14} + \dot{E}_{20} - \dot{E}_{19} \quad (3.23)$$

Where:

$\dot{E}_{D,\mathrm{Con}}$: The rate of exergy destruction for the condenser,

$\dot{E}_{12}$: Exergy flow in rate for condenser from HPST,

$\dot{E}_{14}$: Exergy flow out rate for the condenser to the condensate,

$\dot{E}_{20}$: Exergy flow rate for condenser from OFWH,

$\dot{E}_{19}$: Exergy flow out rate for the condenser to cooling water.

The following formula can be used to determine exergy destruction for Pump1:

$$\dot{E}_{D,\mathrm{P1}} = \dot{W}_{\mathrm{P1}} + \dot{E}_{16} - \dot{E}_8 \quad (3.24)$$

Where:

$\dot{E}_{D,\mathrm{P1}}$: Exergy destruction rate for Pump1.

$\dot{W}_{\mathrm{P1}}$: Work rate for the inlet towards Pump 1.

$\dot{E}_{16}$: Exergy flow in rate for Pump1 from OFWH.

$\dot{E}_{8}$: Exergy flow out rate for Pump1 towards HPST.

The pump2 exergy destruction is calculated by this equation:

$$\dot{E}_{D,\mathrm{P2}} = \dot{W}_{\mathrm{P2}} + \dot{E}_{14} - \dot{E}_{15} \tag{3.25}$$

Where:

$\dot{E}_{D,\mathrm{P2}}$: Exergy destruction rate for Pump2.

$\dot{W}_{\mathrm{P2}}$: Work input rate for Pump 2.

$\dot{E}_{14}$: Exergy flow in rate for Pump2 from the condenser.

$\dot{E}_{15}$: Exergy flows out rate for Pump2 to OFWH.

The following formula may be used to calculate the exergy degradation for OFWH:

$$\dot{E}_{D,\mathrm{OFWH}} = \dot{E}_{13} + \dot{E}_{15} - \dot{E}_{16} \tag{3.26}$$

Where:

$\dot{E}_{D,\mathrm{OFWH}}$: Exergy destruction rate for OFWH.

$\dot{E}_{13}$: Exergy flow in rate for OFWH from LPST.

$\dot{E}_{15}$: Exergy flow in rate for OFWH from the condenser.

$\dot{E}_{16}$: Exergy flow out rate for OFWH to HPST.

The net electrical power output from the system is defined as follows:

$$\dot{W}_{BC} = \dot{W}_{\mathrm{GT}} - \dot{W}_{\mathrm{AC}} \tag{3.27}$$

$$\dot{W}_{ISCC} = \dot{W}_{GT} - \dot{W}_{AC} + \dot{W}_{HPST} + \dot{W}_{LPST} - \dot{W}_{\mathrm{pumps}} \tag{3.28}$$

The following formulas are used to determine total the performance of the system [109]:

$$\eta_{BC} = \frac{\dot{W}_{\mathrm{GT}} - \dot{W}_{\mathrm{AC}}}{\dot{Q}_{\mathrm{in,\ BC}}} \tag{3.29}$$

$$\eta_{BC} = \frac{\dot{W}_{GT} - \dot{W}_{\mathrm{AC}}}{\dot{Q}_{\mathrm{in,\ BC}}} \tag{3.30}$$

$$\eta_{ISCC} = \frac{\dot{W}_{GT} - \dot{W}_{AC} + \dot{W}_{HPST} + \dot{W}_{LPST} - \dot{W}_{\mathrm{pumps}}}{\dot{Q}_{in}} \tag{3.31}$$

$$\Psi_{ISCC} \quad \frac{\dot{W}_{GT} - \dot{W}_{AC} + \dot{W}_{HPST} + \dot{W}_{LPST} - \dot{W}_{\mathrm{pumps}}}{\dot{E}_{in}} \tag{3.32}$$

Where:

η_{BC}: Brayton efficiency.

$\dot{W}_{GT}$: Work production for gas turbines.

$\dot{W}_{\mathrm{AC}}$: Work enters for air compressor.

$\dot{Q}_{\mathrm{in,\ BC}}$: Heat inlet for Brayton cycle.

η_{ISCC}: ISCC efficiency.

$\dot{W}_{HPST}$: Work production by HPST.

$\dot{W}_{LPST}$: Work production by LPST.

$\dot{W}_{\mathrm{pumps}}$: Total work consumed by pumps.

$\dot{Q}_{in}$: Total heat inlet to ISCC.

$\dot{E}_{in}$: Total exergy inlet to ISCC.

To evaluate the technique's general effectiveness, it is critical to measure the exergy losses in every element from the perspective of the second thermodynamics law. Calculations for the mass, energy, and exergy balance are used for every part of the system. The formulae listed in Table 3.2 provide the numerical design for ISCC-ARC. It provides an overview of balance formulas for the power and exergy stability for each ISCC-ARC system element. Table 3.2 contains the formulae used to calculate the

entire system and its constituent parts' second law efficiency, exergy quantities, and exergy destruction number. The exergy quantity, exergy loss quantity, and Second Law's efficiency for every element were computed using the formulas provided in Table 3.2, specifically created for the system's components.

Table 3.2. Energy and Exergy equations for every component of the ISCC-ARC system.

Element	Energy	Exergy
Air Compressor	$\dot{W}_{AC} = \dot{m}_{air}\,(h_2 - h_1)$	$\dot{E}_{D,AC} = \dot{W}_{AC} + \dot{E}_1 - \dot{E}_2$
Combustion chamber	$\dot{m}_{air}h_2 + \dot{m}_{fuel}LHV = (\dot{m}_{fuel} + \dot{m}_{air})h_4$	$\dot{E}_{D,CC} = (\dot{E}_2 + \dot{E}_3) - \dot{E}_4$
Gas turbine	$\dot{W}_{GT} = \dot{m}_4(h_4 - h_5)$	$\dot{E}_{D,GT} = (\dot{E}_4 - \dot{E}_5) - \dot{W}_{GT}$
HRSG	$Q_{HRSG} = \dot{m}_4(h_5 - h_6) + \dot{m}_{17}(\dot{h}_{17} - h_{18})$	$\dot{E}_{D,HRSG} = \dot{E}_5 - \dot{E}_6 + \dot{E}_8 - \dot{E}_9 + \dot{E}_{10} - \dot{E}_{11} + \dot{E}_{17} - \dot{E}_{18}$
HPST	$\dot{W}_{HPST} = \dot{m}_9(h_9 - h_{10})$	$\dot{E}_{D,HPST} = \dot{E}_9 - \dot{E}_{10} - \dot{W}_{HPST}$
LPST	$\dot{W}_{LPST} = \dot{m}_{11}(h_{11} - h_{13}) + \dot{m}_{12}(h_{13} - h_{12})$	$\dot{E}_{D,LPST} = \dot{E}_{11} - \dot{E}_{12} - \dot{E}_{13} - \dot{W}_{LPST}$
Condenser	$\dot{Q}_{Con} = \dot{m}_{14}(h_{12} - h_{14})$	$\dot{E}_{D,Con} = \dot{E}_{12} - \dot{E}_{14} + \dot{E}_{20} - \dot{E}_{19}$
Pump1	$\dot{W}_{Pump1} = \dot{m}_7(h_8 - h_{16})$	$\dot{E}_{D,P1} = \dot{W}_{P1} + \dot{E}_{16} - \dot{E}_8$
Pump2	$\dot{W}_{Pump2} = \dot{m}_{14}(h_{15} - h_{14})$	$\dot{E}_{D,P2} = \dot{W}_{P2} + \dot{E}_{14} - \dot{E}_{15}$
OFWH	$\dot{Q}_{OFWH} = \dot{m}_{15}(h_{16} - h_{15}) = \dot{m}_{13}(h_{13} - h_{16})$	$\dot{E}_{D,OFWH} = \dot{E}_{13} + \dot{E}_{15} - \dot{E}_{16}$
PTC	$\dot{Q}_{solar} = \eta_{PTC} * A_{ap} * DNI$	$\dot{E}_{Q,solar} = \left(1 - \frac{T_0}{T_{sun}}\right)\dot{Q}_{solar}$
Generator	$\dot{Q}_{Gen} = \dot{m}_{7a}h_{7a} + \dot{m}_{4a}h_{4a} - \dot{m}_{3a}h_{3a} = \dot{m}_6(h_6 - h_7)$	$\dot{E}_{D,Gen} = \dot{E}_6 - \dot{E}_7 + \dot{E}_{3a} - \dot{E}_{7a} - \dot{E}_{4a}$
Absorber	$\dot{Q}_{Abs} = \dot{m}_{10a}h_{10a} + \dot{m}_{6a}h_{6a} - \dot{m}_{1a}h_{1a}$	$\dot{E}_{D,Abs} = E_{10a} - \dot{E}_{1a} + \dot{E}_{6a} + \dot{E}_{13a} - \dot{E}_{12a}$
HEX	$\dot{Q}_{HEX} = \dot{m}_{2a}(h_{3a} - h_{2a})$	$\dot{E}_{D,HEX} = \dot{E}_{4a} - \dot{E}_{5a} + \dot{E}_{2a} - \dot{E}_{3a}$
Pump3	$\dot{W}_{P3} = \dot{m}_{1a}(h_{2a} - h_{1a})$	$\dot{E}_{D,P3} = \dot{W}_{P3} + \dot{E}_{2a} - \dot{E}_{1a}$
Evaporator	$\dot{Q}_{Evap} = \dot{m}_{10a}(h_{10a} - h_{9a})$	$\dot{E}_{D,Evap} = \dot{E}_{10a} - \dot{E}_{9a} - \dot{E}_{11a} + \dot{E}_1$
Expansion valve 1	$\dot{m}_{5a}h_{5a} = \dot{m}_{6a}h_{6a}$	$\dot{E}_{D,valv1} = \dot{E}_{5a} - \dot{E}_{6a}$
Expansion valve 2	$\dot{m}_{8a}h_{8a} = \dot{m}_{9a}h_{9a}$	$\dot{E}_{D,valv2} = \dot{E}_{8a} - \dot{E}_{9a}$

Solar field

The thermal energy received by the collector is calculated as follows [110]:

$$\dot{Q}_{solar} = \eta_{PTC} * A_{ap} * DNI \tag{3.33}$$

Where:

$\dot{Q}_{solar}$: Thermal energy for PTC.

A_{ap}: The solar areas.

DNI: The direct normal irradiance.

η_{PTC}: The PTC's efficiency.

This depicts the amount of solar radiation that falls on a specific area perpendicular to the solar in Mosul (35.35° N 43.16° E) during the attention period.

The useful energy ($\dot{Q}_{solar}$) delivered to the working fluid in the receiver is determined as follows [111]:

$$\dot{Q}_{solar} = m_{Th\_VP} Cp_{Th\_VP} \left(T_{Th\_VP,out} - T_{Th\_VP,in}\right) \quad (3.34)$$

Where:

$\dot{Q}_{solar}$: Isolation solar transmitted for a collector.

m_{Th_VP}: Mass flow rate for working liquid (usually a thermal oil or molten salt).

Cp_{Th_VP}: Specific heat for working liquid.

$T_{Th\_VP,out}$: Outlet temperature for the working liquid of the collector.

$T_{Th\_VP,in}$: Inlet temperature for the working liquid of the collector.

3.8. Exergoeconomic analysis

Exergoeconomic analysis of energy systems, which integrates principles of exergy analysis and cost analysis, serves as a potent tool. Its primary aim is to offer valuable insights into the costs associated with useful and destroyed exergy in each component of the system. This information is crucial for identifying components that have significant potential for optimization.

Initially, the exergy of each stream and the exergy destroyed in each component should be quantified through exergy analysis. Subsequently, exergoeconomic analysis involves several crucial steps: (1) defining the desired exergy output (product exergy) and the net exergy input (fuel exergy) for each component; (2) establishing cost rate balance equations for each component, typically presented as follows [112]:

$$\sum_e \dot{C}_{e,k} + \dot{C}_{w,k} = \dot{C}_{q,k} + \sum_i \dot{C}_{i,k} + \dot{Z}_k \quad (3.35)$$

Where:

$\sum_e \dot{C}_{e,k}$: Summation of external flows contributing to the cost of the element.

$\dot{C}_{w,k}$: Consumption rate cost of resources (e.g., water, electricity) for the component *k*.

$\dot{C}_{q,k}$: Rate cost of heat for the component *k*.

$\sum_i \dot{C}_{i,k}$: Summation of internal flows contributing to the cost of the element.

$\dot{Z}_k$: Rate of economic benefit generated by element *k*.

Table 3.3 displays the main constant factors that were utilized to calculate the cost of the supplied items. Additionally, the reference [113] provides suitable factors for the exergoeconomic assessment of the entire system. According to [114], the investment cost and cost recovery parameters are ascertained.

An economic indicator called the Cost Recovery Factor (CRF) determines an investment's comparable regular yearly cost throughout its economic life. It enables an analysis of investments with various cash flows and considers the value of time for money. The CRF and $\dot{Z}_k$ is calculated by the following equations [115]:

$$\mathrm{CRF} = \frac{i(1+i)^n}{(1+i)^n - 1} \tag{3.36}$$

$$\dot{Z}_k = Z_k \cdot CRF \cdot \varphi/(N \times 3600) \tag{3.37}$$

Where:

CRF: Cost recovery factor.

i: Discount rate (interest rate).

n: Economic life of investment in years.

$\dot{Z}_k$: Total monetary benefit generated by element k.

φ: Number of hours the element works per year.

N: Number of seconds in an hour (3600 seconds).

This formula generally determines the annualized income for component k, utilizing the CRF and the operational hours per year.

Table 3.4 is an overview of the basic equations for the cost balance of every integrated system element and the auxiliary equations that go with it. Moreover, the overall investment cost for every part of this system is listed in Table 3.4. The exergoeconomic analysis uses performance metrics to evaluate the system. The following are the definitions of the cost per unit exergy of fuel and product:

$$c_{F,k} = \dot{C}_{F,k}/\dot{E}_{F,k} \tag{3.38}$$

$$c_{P,k} = \dot{C}_{P,k}/\dot{E}_{P,k} \tag{3.39}$$

The exergoeconomic performance of each component was evaluated based on the cost rate of destroyed exergy ($\dot{C}_{D,k}$) and the exergoeconomic factor (f), as detailed below:

$$\dot{C}_{D,k} = c_{F,k}\dot{E}_{D,k} \tag{3.40}$$

$$f_k = \dot{Z}_k/\left(\dot{Z}_k + c_{F,k}\dot{E}_{D,k} + \dot{E}_{L,k}\right)\Big) \tag{3.41}$$

Table 3.3. Economic investigation

Element	**Exergetic cost formula**	**Auxiliary formula**
AC	$\dot{C}_1 + \dot{C}_{W,AC} + \dot{Z}_{AC} = \dot{C}_2$	$c_{w,AC} = c_{w,GT}$
CC	$\dot{C}_2 + \dot{C}_3 + \dot{Z}_{CC} = \dot{C}_4$	$\frac{\dot{C}_2}{\dot{E}_2} = \frac{\dot{C}_4}{\dot{E}_4}$, $c_3 = 12$
GT	$\dot{C}_4 + \dot{Z}_{W,GT} = \dot{C}_5 + \dot{C}_{GT}$	$\frac{\dot{C}_4}{\dot{E}_4} = \frac{\dot{C}_5}{\dot{E}_5}$
HRSG	$\dot{C}_5 + \dot{C}_{17} + \dot{C}_8 + \dot{C}_{10} + \dot{Z}_{HRSG} = \dot{C}_6 + \dot{C}_{18} + \dot{C}_9 + \dot{C}_{11}$	$\frac{\dot{C}_5}{\dot{E}_5} = \frac{\dot{C}_6}{\dot{E}_6}$
HPST	$\dot{C}_9 + \dot{Z}_{W,HPST} = \dot{C}_{10} + \dot{C}_{HPST}$	$\frac{\dot{C}_9}{\dot{E}_9} = \frac{\dot{C}_{10}}{\dot{E}_{10}}$
LPST	$\dot{C}_{11} + \dot{Z}_{W,LPST} = \dot{C}_{10} + \dot{C}_{11} + \dot{C}_{LPST}$	$\frac{\dot{C}_{11}}{\dot{E}_{11}} = \frac{\dot{C}_{12}}{\dot{E}_{12}} = \frac{\dot{C}_{13}}{\dot{E}_{13}}$
Condenser 1	$\dot{C}_{12} + \dot{C}_{19} + \dot{Z}_{cond1} = \dot{C}_{13} + \dot{C}_{20}$	$\frac{\dot{C}_{12}}{\dot{E}_{12}} = \frac{\dot{C}_{13}}{\dot{E}_{13}}$
Pump1	$\dot{C}_{16} + \dot{C}_{W,P1} + \dot{Z}_{P1} = \dot{C}_8$	$c_{w,P1} = c_{w,HPST}$
Pump2	$\dot{C}_{14} + \dot{C}_{W,P1} + \dot{Z}_{P1} = \dot{C}_{15}$	$c_{w,P2} = c_{w,HPST}$
OFWH	$\dot{C}_{13} + \dot{C}_{15} + \dot{Z}_{OFWH} = \dot{C}_{16}$	
PTC	$\dot{C}_{18} + \dot{C}_{q,solar} + \dot{Z}_{PTC} = \dot{C}_{17}$	$\dot{C}_{q,solar} = 0$
Generator	$\dot{C}_6 + \dot{C}_{3,a} + +\dot{Z}_{Gen} = \dot{C}_7 + \dot{C}_{7,a} + \dot{C}_{4,a}$	$\frac{\dot{C}_{4,a} - \dot{C}_{3,a}}{\dot{E}_{4,a} - \dot{E}_{3,a}} = \frac{\dot{C}_{7,a} - \dot{C}_{3,a}}{\dot{E}_{7,a} - \dot{E}_{3,a}}$
Pump3	$\dot{C}_{1,a} + \dot{C}_{W,P3} + \dot{Z}_{P3} = \dot{C}_{2,a}$	$c_{w,P3} = c_{w,HPST}$

SHEX	$\dot{C}_{2,a} + \dot{C}_{4,a} + \dot{Z}_{SHEX} = \dot{C}_{3,a} + \dot{C}_{5,a}$	$\frac{\dot{C}_{4,a}}{\dot{E}_{4,a}} = \frac{\dot{C}_{5,a}}{\dot{E}_{5,a}}$
EV1	$\dot{C}_{5,a} + \dot{Z}_{EV1} = \dot{C}_{6,a}$	
Absorber	$\dot{C}_{6,a} + \dot{C}_{12,a} + \dot{Z}_{Abs} = \dot{C}_{1,a} + \dot{C}_{13,a}$	$\frac{\dot{C}_{6,a}+\dot{C}_{10,a}}{\dot{E}_{6,a}+\dot{E}_{10,a}} = \frac{\dot{C}_{1,a}}{\dot{E}_{1,a}}$, $c_{12,a} = 0$
Evaporator	$\dot{C}_{9,a} + \dot{C}_{11,a} + \dot{Z}_{Evap} = \dot{C}_1 + \dot{C}_{10,a}$	$\frac{\dot{C}_{7,a}}{\dot{E}_{7,a}} = \frac{\dot{C}_{8,a}}{\dot{E}_{8,a}}$, $c_{11,a} = 0$
EV2	$\dot{C}_{8,a} + \dot{Z}_{EV2} = \dot{C}_{9,a}$	
Condenser 2	$\dot{C}_{7,a} + \dot{C}_{14,a} + \dot{Z}_{cond2} = \dot{C}_{8,a} + \dot{C}_{15,a}$	$\frac{\dot{C}_{7,a}}{\dot{E}_{7,a}} = \frac{\dot{C}_{8,a}}{\dot{E}_{8,a}}$, $c_{11,a} = 0$

Table 3.4. Equipment price [116–118]

Part	**Purchased equation**
AC	$\left(71.11 \times \dot{m}_{air} \times (Pr)\right) / \left(0.90 - \eta_{comp}\right) \times \ln\ (Pr)$
CC	$(25.6 \times \dot{m}_{air}) / (0.995 - P_4/P_2) \times [(1 + \exp(0.0181 \times T_4 - 26.41))]$
GT	$(266.3 \times \dot{m}_{gas}) / (0.921 - \eta_{turb}) \times \ln(Pr) \times [1 + \exp(0.0360 \times T_4 - 54.4)]$
HRSG	$6570\left[\left(\dot{Q}_{HRSG}/\Delta T_{LMTD}\right)^{0.8}\right] + 21276\dot{m}_{water} + 1184.4\dot{m}_g^{1.2}$
HPST	$6000\left(\dot{W}_{HPST}^{0.7}\right)$
LPST	$6000\left(\dot{W}_{LPST}^{0.7}\right)$
Pump1	$3540\dot{W}_{P1}^{0.71}$
Pump2	$3540\dot{W}_{P2}^{0.71}$
OFWH	$5200\dot{m}_{water}$
PTC	$126A_{hel}$
Generator	$17500(A_G/100)^{0.6}$
Absorber	$16000(A_{abs}/100)^{0.6}$
SHEX	$309.14(A_{SHEX})^{0.85}$
Pump3	$17585(W_{P3}/100)^{0.71}\left(1 + \frac{0.2}{1-\eta_{P3}}\right)$
Evaporator	$16000(A_E/100)^{0.6}$
Ev1	$114.5\dot{m}_{water}$
Ev2	$114.5\dot{m}_{water}$

Given that exergoeconomic analysis provides a detailed view of the costs associated with exergy destruction, the objective function can be defined to minimize the total cost rate, ($\dot{C}_{total}$). This total cost rate includes the sum of all owning and operating costs as well as the total rate of exergy destruction costs [119]:

$$\dot{C}_{total} = \sum_k \dot{Z}_k + \sum_k \dot{C}_{D,k} \tag{3.42}$$

The entire cost of the investment may be calculated using the following calculation. [119]:

In the end, The entire cost of electricity per unit of power, or $/MJ, is determined by the following equation [119]:

$$\dot{C}_{\text{electricity,tot}} = \sum_{k=1}^{N} \dot{C}_{\text{total}} / \dot{W}_{\text{net}} \quad (3.43)$$

where $\dot{C}_{electricity,tot}$, is the overall cost power for each kWh of energy the system generates; it is commonly expressed in $/MJ.

3.9. ENVIRONMENTAL ANALYSIS

The amount of CO_2 released into the atmosphere because of human activity is measured by the CO_2 emission rate ($\boldsymbol{\epsilon_{CO2}}$) [120]. To calculate CO_2 emissions in the context of electricity generation, divide the total amount of CO_2 released produced over a certain period into the total amount of power generated during that same period. This formula is used to calculate this rate [121]:

$$\epsilon_{CO_2} = \frac{\dot{m}_{CO_2}}{\dot{W}_{net}} \quad (3.44)$$

$$\dot{m}_{CO_2} = y_{CO_2} \dot{m}_{g,5} \left(\frac{\bar{M}_{CO_2}}{\bar{M}_g} \right) \quad (3.45)$$

where y_{CO_2} *is* the mole percentage and $\bar{M}_{CO_2}$ is the mole weight of CO_2 are represented, respectively. Moreover, the mole fraction and mole weight of the exhaust gases at the end of the combustion chamber are represented by the values of $\dot{m}_g$ and $\bar{M}_g$.

PART 4

ESTIMATION AND DISCUSSION OF THE RESULTS

4.1 INTRODUCTION

The enhancement of the performance, cost, and environmental impact of the ISCC system by merging the exhaust heat recovery, RE, and ARC cycle has been investigated in this chapter. The primary target of the examined project is to utilize innovative energy generation techniques and alternative power resources to enhance the sustainability, effectiveness, and variation of Iraq's electric energy. It also requires the proposal of significant visions for these combined organizations' potential to increase energy production limits, improve power efficiency, and decrease environmental effects by assessing their financial viability and operation.

4.2 OVERVIEW OF RESULTS

This section is divided into two main segments. The first segment provides a 4E analysis of the NGCC and ISCC systems under optimal operating conditions. It also explores how the main operating conditions affect the performance and cost of these systems. After this segment, a comparative and detailed investigation is conducted on the monthly work net, exergy destruction, specific energy cost, and CO2 emissions for the existing BC power plant, NGCC, and ISCC systems. In the second section, the ISCC unit is combined with the Absorption Refrigeration Cycle (ARC) to improve system operation and electrical results, particularly in the heat of the summer. The findings of this combination are then compared to those from the isolated ISCC technology.

Table 4.1 presents validation results comparing two models for a natural gas combined cycle (NGCC) system: the Frame 9E model [122] and the present model. The current

model and the frame 9E model operate under identical atmospheric conditions, with a temperature of 288 K and a humidity of 60%. This consistency ensures that environmental variables do not affect the comparative analysis of other criteria. Both systems operate at the same atmospheric pressure of 1 bar and have identical mass flow rates of 418 kg/s. The Frame 9E and the present models have a pressure ratio of 12.6. The power output slightly differs, with the Frame 9E model producing 125 MW and the present model producing 124.2 MW. This small discrepancy might indicate slight variations in system efficiency or operational settings, but generally, it shows that the model aligns well with the actual system.

There's a notable difference in exhaust temperature, where the Frame 9E model has an exhaust temperature of 544°C, compared to 549°C for the BC model of the current study. This difference could affect the system's thermal efficiency. The Frame 9E models show a thermal efficiency of 34.6%, slightly higher than the 33.32% of the BC model of the current study. This suggests that the model might be more efficient in converting heat into power due to newer technology or better maintenance conditions in the theoretical model. The work output is marginally higher in the Frame 9E model (55.781 kW) than in the present model (55.238 kW), which aligns with the slightly higher power production. The thermal efficiency is also higher in the Frame 9E model at 30.15% compared to 29.17% in the present model.

The validation shows that the Frame 9E model aligns closely with the present model regarding power production, and thermal efficiency

Table 4.1. Validation results for the natural gas combined cycle.

Factors	**NGCC Frame 9E model** [123]	**Present Model**
Atmosphere temperature.	288K	288K
Humidity	60%	60%
Atmosphere pressure	1 bar	1 bar
Mass flow	418 kg/s	418 kg/s
Pressure ratio (Pr)	12.6	12.6
Power production	125 MW	124.2 MW
Exhaust temperature.	544°C	549°C

$\eta_{thermal}$	34.6 %	33.32 %
$\dot{W}_{ST}$ (kW)	55.781	55.238
η_{ST} (%)	30.15	29.17

The energy, exergy, exergoeconomic, and environmental impacts for the ISCC and ISCC-ARC systems were analyzed using the input parameter values listed in Table 4.2. Additionally, when performing calculations for system parameters, the component parameters default to the base case values specified in Table 4.2, unless specific component parameters are indicated.

Table 4.2. Systems input parameters under standard operating conditions[109][124].

	Parameter	**Importation**
	Quantity of (GT)	3
Bryton cycle	Compression Ratio (CR)	12.5
	Rate of flow mass	(420*3) kg/s
	Temp. Input	1,090 °C
	Environment temp.	25 °C
	Low Heat Value fuel (LHVF)	50,050 $kJ.kg^{-1}$
	AC efficiency	87 %
	GT efficiency	86 %
	CC efficiency	99.53 %
Steam turbine	HPST	100 bar
	LPST	20 bar
	Temperature of condensate	36 °C
	GT isentropic efficiency	87 %
	Pump isentropic efficiency	82 %
	Rate of HRSG	72 %
ARS	Generator Temp.	88 °C
	Condenser Temp.	39 °C
	Absorber Temp of outlet	48 °C
	SHE effectiveness	53 %
	Evaporator temp	5 °C
	Intake air temperature of the evaporator	50 °C
	Temperature of evaporator	10 °C
	Condenser temp. of enter	25 °C
	Condenser temp. of exit	35 °C

	Absorber temp. of enter	25 °C
	Absorber temp of exit	35 °C
Li Br Mix	Liquid strength	53 %
Solar Zone	Coordinate of Latitude	35.36°N(degrees)
	Coordinate of Longitude	43.17°E(degrees)
	Area	Mosul/Iraq
	Solar region	510,130 m^2
	Temperature of solar Outlet	395 °C
	Temperature of solar Inlet	295 °C
	Heat transfer of the liquid	Therminol VP-1

4.3 ISCC WITH WASTE HEAT RECOVERY

The performance of the ISCC cycle was assessed by applying the first and second laws of thermodynamics to each component and identifying the key properties for each state, as detailed in Table 4.3. These properties are crucial for analyzing the energy, exergy, and economic aspects of the ISCC cycle.

4.3.1 Energy, Exergy, and Exergoeconomic Analysis of the ISCC System

Table 4.3 outlines the operational differences between the ISCC and NGCC systems. According to the table, the NGCC system maintains a power output of 492.7 megawatts, a thermal efficiency of 44.76 percent, and an exergy efficiency of 43.22 percent. With the addition of solar energy, the ISCC system can generate 560.3 MW of power, elevating its first-law efficiency to 50.9 percent and its second-law efficiency to approximately 49.15 percent. Furthermore, Table 4.4 details the energy generation costs, with the ISCC at 6,876 $/ hr and the NGCC at 5,508 $/ hr. The cost per MW for the NGCC is 78.81 $, while it is 72.51$ for the ISCC. These figures indicate that integrating the NGCC and ISCC systems is highly advantageous from both commercial and thermodynamic viewpoints.

Table 4.3. Characteristics for every ISCC component at an ideal condition

Steps	Pressure (kPa)	Mass Flow (kg/s)	Temp. (K)	Enthalpy (kJ/ kg)	Entropy (kJ/ kg K)	Exergy (MW)
1	101	418.5	295	246.4	5.735	-
2	1276	418.5	659	623.4	5.832	145.5
3	101	7.33	288	-4672	11.53	380
4	1213	425.3	1360	240.6	8.041	405.8
5	104.5	425.3	822.8	-414.5	8.151	113.3
6	101	425.3	402.9	-880.4	7.372	13.93
7	121.6	144.9	372.6	417	1.301	12.12
8	10133	144.9	373.9	430.1	1.308	13.71
9	9829	144.9	794.8	3433	6.68	285.9
10	2007	144.9	581.8	3044	6.801	224.4
11	1946	144.9	774.8	3473	7.452	258.4
12	5.583	130.4	308	2437	7.942	78.42
13	121.6	14.49	463.3	2855	7.702	15.8
14	5.583	130.4	308	146	0.5031	6.603
15	121.6	130.4	308	146.2	0.5032	6.618
16	1000	427.7	665	780.6	1.675	120.3
17	1000	427.7	566	539.3	1.283	67.11
18	101	6617	295	91.66	0.3228	-
19	101	6617	307	141.8	0.4895	6.592

Table 4.4. Economic performance for ISCC and NGCC systems.

Factors	ISCC	NGCC
Brayton Cycle Network MW	363.1	363.1
Rankine Cycle Network MW	198.4	130.5
Production Energy MW	560.3	492.7
Complete Exergy Efficiency %	49.15	43.22
Complete Thermal Efficiency %	50.9	44.76
Economic of electrical energy $/h	6876	5508
Economic for each MW $	72.51 $	78.81 $

Table 4.5 presents the primary results of the exergy analysis for various components of the ISCC system. It provides detailed information on exergy generation and destruction for each component. The data table highlights the specific exergy destruction rates (Ψ) and destruction values ($\dot{E}_d$). The combustion chambers, with an exergy destruction rate of 55.1% and a destruction output of nearly 359.2 MW, are the most significant contributors to exergy loss within the ISCC system. In contrast, the solar collector and the condenser have lower exergy destruction rates of 9.29% and 9.91%, respectively. Table 4.5 shows that the turbines, specifically the GT, HPST, and LPST, are the most efficient components in terms of exergy within the ISCC process, with efficiencies of 95%, 91%, and 87%, respectively. Overall, the proposed ISCC process achieves an exergy efficiency of approximately 49.15%.

Table 4.5. ISCC system Exergy evaluation

Elements	**No**	**$\dot{E}_p$ (MW)**	**$\dot{E}_f$ (MW)**	**$\dot{E}_d$ (MW)**	**Ψ (%)**	**$\dot{E}_d$ (%)**
AC	3	436.6	472.3	36.22	92.34	5.55
GT	3	835.9	877.5	41.63	95.26	6.38
CC	3	1217	1577	359.2	77.21	55.1
HPST	1	56.33	61.56	5.23	91,51	0.79
HRSG	1	306.2	351.3	45.06	87.17	6.84
Condenser1	1	5.6	71.82	65.23	10.33	9.91
LPST	1	144	164.1	20.13	87.74	3.06
Pump2	1	0.015	0.02	0.004	80.64	0.0006
Pump1	1	1.59	1.90	0.301	84.1	0.046
PTC	1	53.23	114.4	61.17	46.53	9.29
OFWH	1	12.12	22.42	10.3	54.04	1.57

4.3.2 Effect of The Operation Conditions On The Performance, Cost, And Environmental Impact Of The NGCC And ISCC Systems

Figure 4.1 illustrates the impact of the pressure ratio (Pr) on the $\dot{W}_{net}$ of two systems. As shown in the figure, each system's net power output ($\dot{W}_{net}$) is negatively affected by the Pr. Higher pressure ratios require the compressors to use more energy, reducing energy production for each cycle. The data indicate that as the Pr increases from 6 to

18 bar, the $\dot{W}_{net}$ for the ISCC system drops from 602.1 MW to 505 MW. For the NGCC, the $\dot{W}_{net}$ decreases from 531.9 MW to 441.5 MW. The results also highlight that the heat supplied from solar panels to the HRSG is a key factor in why the ISCC outperforms the NGCC.

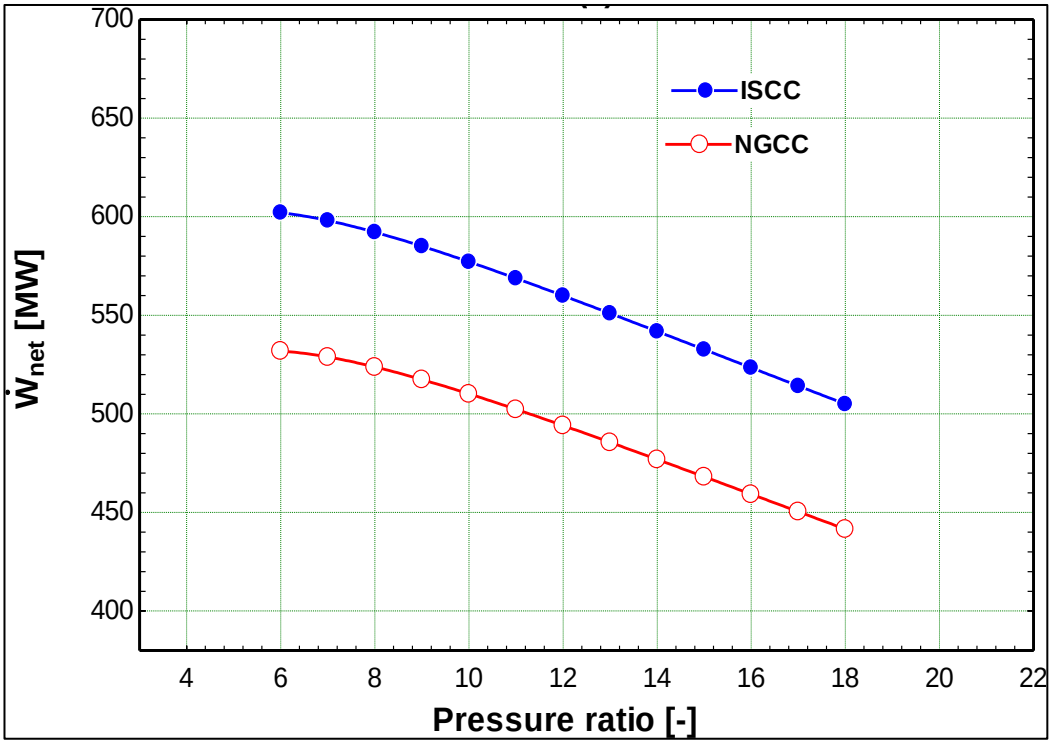

Figure 4.1. Impact of Pr on the $\dot{W}_{net}$ for the two systems.

Figures 4.2 and 4.3 effectively demonstrate the influence of the pressure ratio (Pr) on the overall efficiencies of various systems. The diagrams indicate that as Pr increases, the overall efficiencies of all systems initially rise, reach a peak, and then begin to decrease with further increases in Pr. Specifically, the energy efficiency (η_{energy}) for the ISCC system ranges from 46.42% to 51.10% as Pr increases from 6 to 18 bar. For the NGCC system, η_{energy} varies from 41.01% to 44.68%. Similarly, the exergy efficiency (η_{exergy}) for the ISCC system improves from 44.83% to 49.34%, while for the NGCC, it changes from 39.6% to 43.14% over the same Pr range.

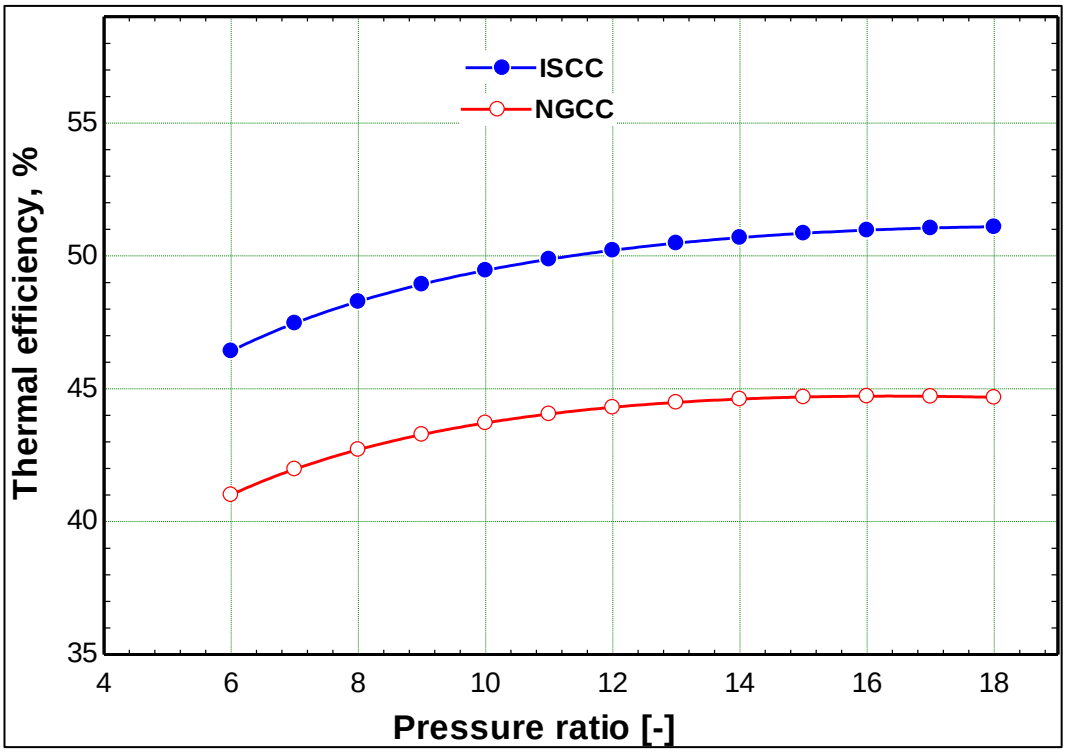

Figure 4.2. Impact of Pr on the thermal efficiency of the two systems.

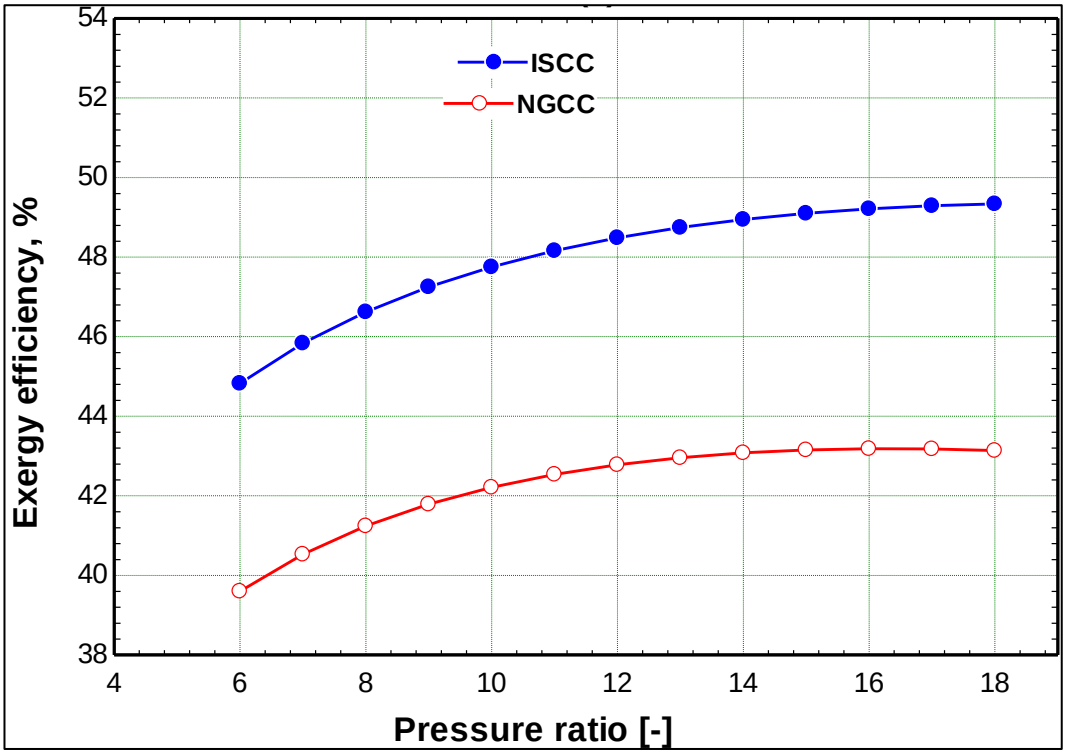

Figure 4.3. Impact of Pr on the exergy efficiency for the two systems.

As depicted in Figure 4.4, despite the increase in Pr from 6 to 18 bar, the total cost for electricity generation ($\dot{C}_{electricity}$) decreases slightly for both systems, moving from 79.16 $//MWh to 77.84 $//MWh for the ISCC and from 86.26 $//MWh to 84.85 $//MWh for the NGCC. The increase in $\dot{C}_{electricity}$ for the ISCC system can be attributed to the cost of solar panels.

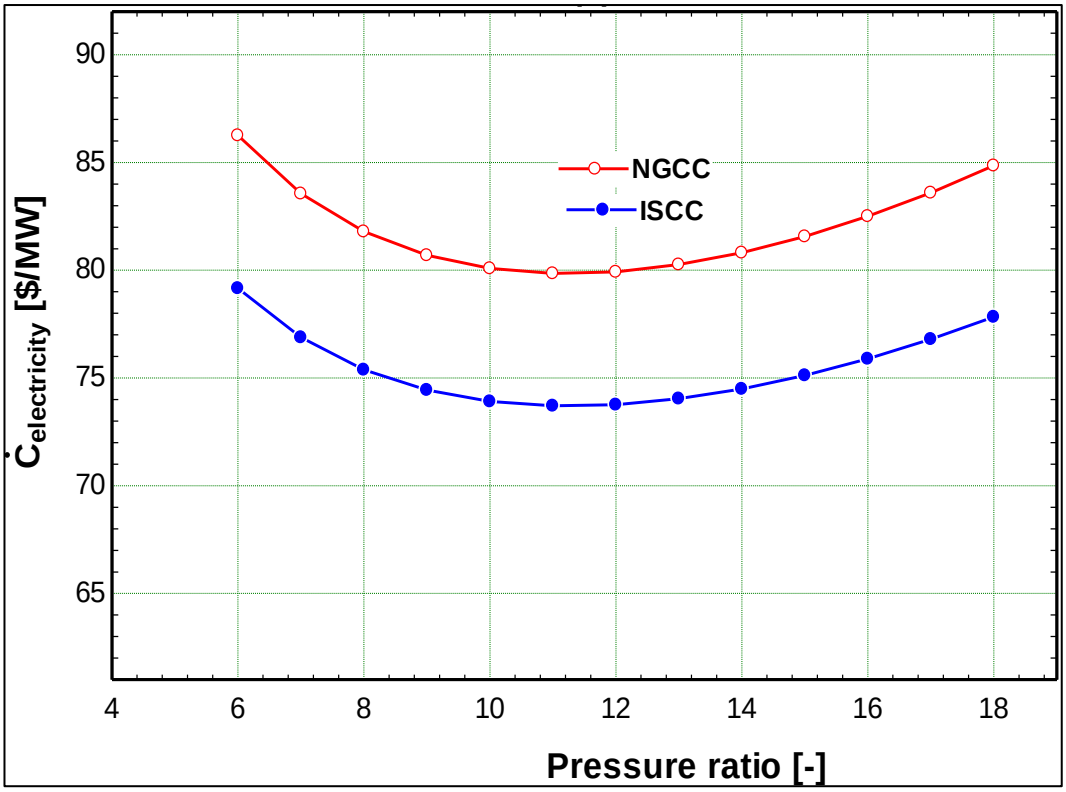

Figure 4.4. Impact of Pr on the costs for the two systems.

Figure 4.5 illustrates that as the pressure ratio (Pr) increases from 6 to 18 bar, the CO_2 emissions for the ISCC system decrease from 425 kg CO_2/MWh to 386.1 kg CO_2/MWh. The NGCC system's CO_2 emissions also declined because of the increase in Wnet in ISCC, ranging from 481.1 kg CO_2/MWh to 441.6 kg CO_2/MWh. These results further highlight why the ISCC system outperforms the NGCC regarding environmental impact.

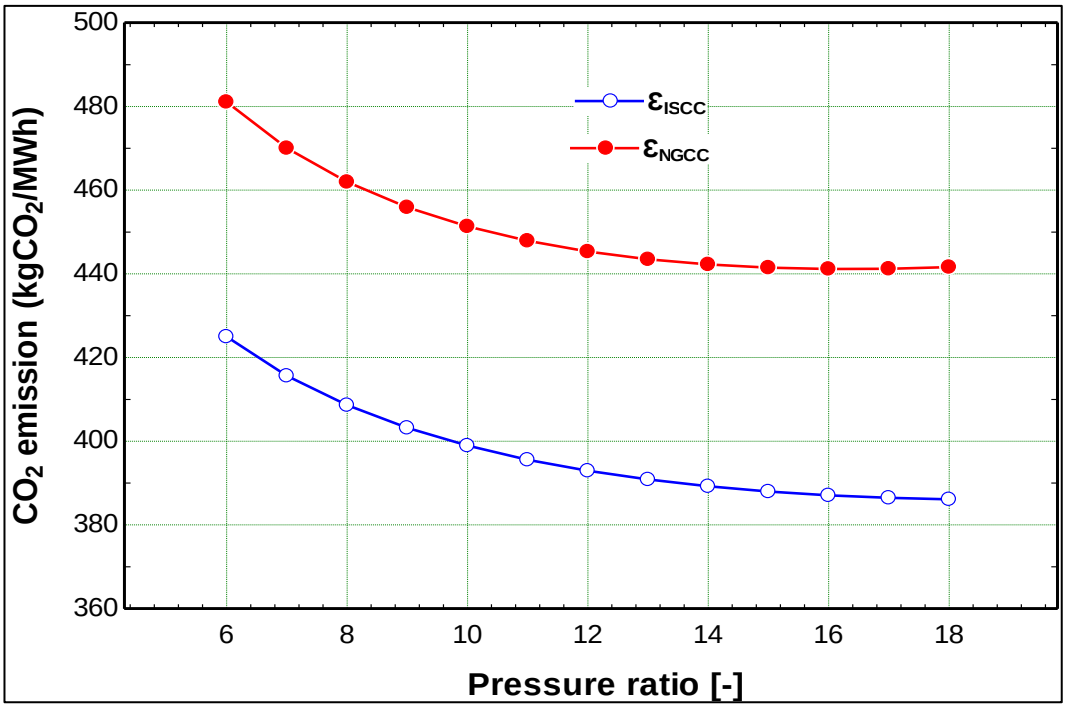

Figure 4.5. Impact of Pr on the CO_2 emission for the two systems.

Figure 4.6 shows the impact of gas turbine inlet temperature (GTIT) on the $\dot{W}_{net}$ of both ISCC and NGCC systems. The results illustrate how GTIT affects each system's power output. By increasing the temperature of waste emissions and the thermal energy at the gas turbines' entry point, GTIT improves the Wnet of the Brayton Cycle (BC) and Rankine Cycle (RC). The data indicate that as GTIT increases from 1250 K to 1550 K, the net power output ($\dot{W}_{net}$) of the ISCC system increases from 446.10 MW to 753.10 MW, while the NGCC system sees an improvement from 383.3 MW to 683.1 MW.

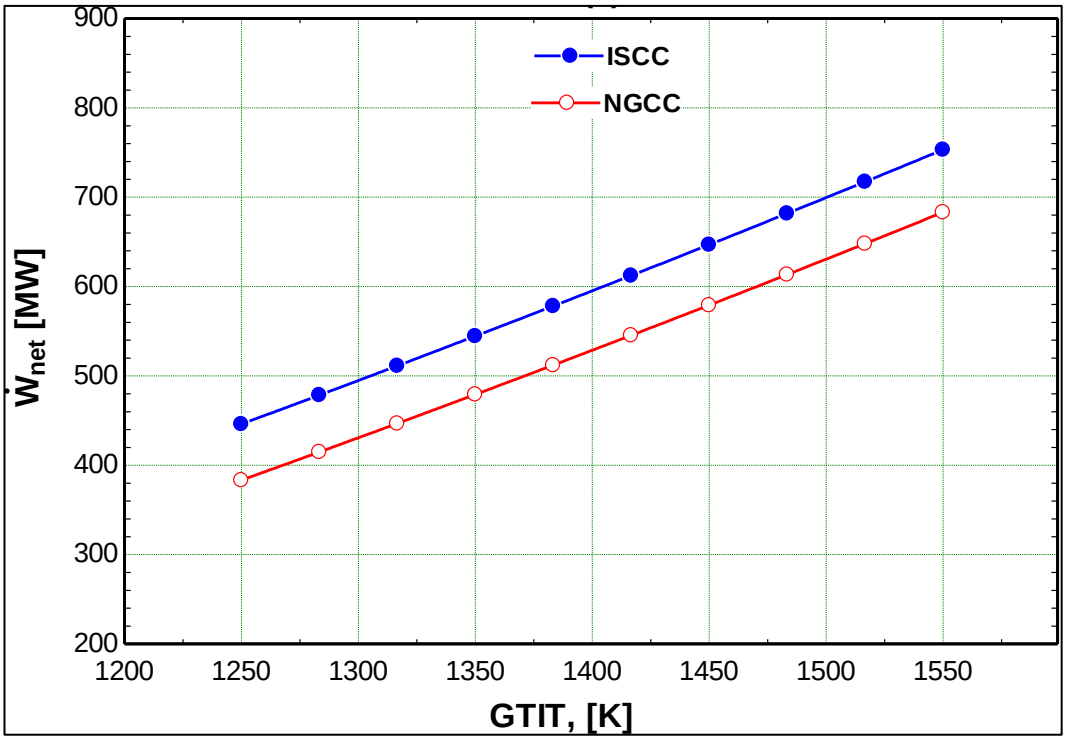

Figure 4.6. Gas turbine inlet temperature impacts the $\dot{W}_{net}$ for the two systems.

Figures 4.7 and 4.8 demonstrate that the overall efficiencies of both the ISCC and NGCC systems improve in conjunction with increases in GTIT. The addition of solar panels significantly enhances the system efficiencies of the ISCC compared to the NGCC. As GTIT ranges from 1250 to 1550 K, the ISCC system's thermal efficiency climbs from 49.02% to 52.04%, and its exergy efficiency increases from 47.33% to 50.25%. Meanwhile, for the NGCC system, the energy efficiency (η_{energy}) rises from 42.12% to 47.20%, and the exergy efficiency (Ψ_{exergy}) grows from 40.67% to 45.58%.

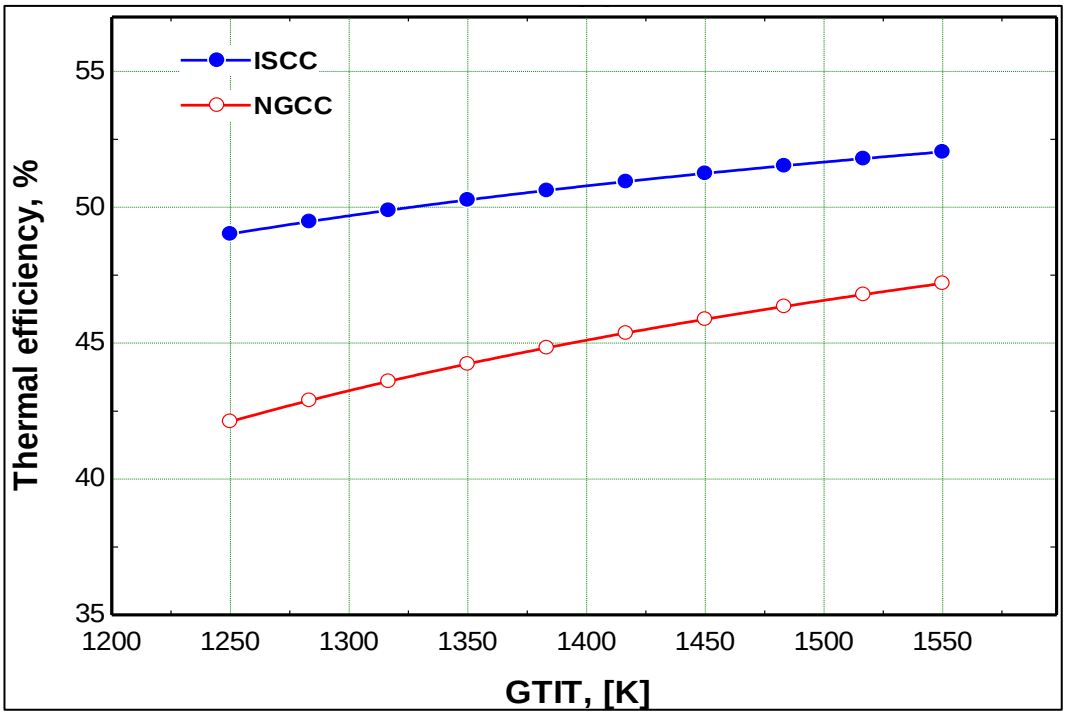

Figure 4.7. Gas turbine inlet temperature impacts the thermal efficiency of the two systems.

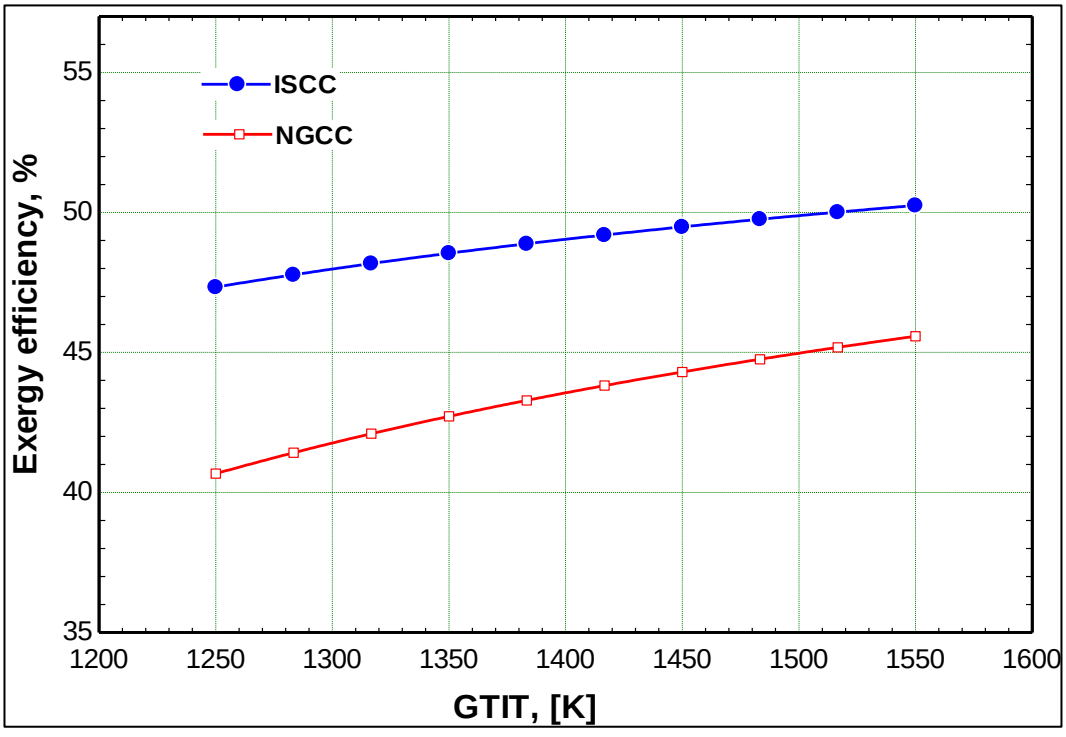

Figure 4.8. Gas turbine inlet temperature impacts the exergy efficiency of the two systems.

Figure 4.9 illustrates that the total cost of electricity generation ($\dot{C}_{electricity}$) decreases with an increase in GTIT, reaching a minimum before rising again as GTIT continues to increase. The costs associated with the combustion chamber (CC) and gas turbine (GT) escalate significantly with higher GTIT, which in turn raises the $\dot{C}_{electricity}$ for all systems. The figure also indicates that the optimal GTIT is 1517 K. At this temperature, the ISCC system achieves a $\dot{C}_{electricity}$ of 67.71 $//MWh, while the NGCC system's cost is slightly higher at 72.19 $//MWh. Also, Figure 4.10 shows that total CO_2 emissions decrease as the GTIT increases from 1250 K to 1550 K. For the ISCC, CO_2 emissions drop from 402.5 kg CO_2/MWh to 379.1 kg CO_2/MWh. In comparison, CO_2 emissions for the NGCC reduced from 468.4 kg CO_2/MWh to 418 kg CO_2/MWh.

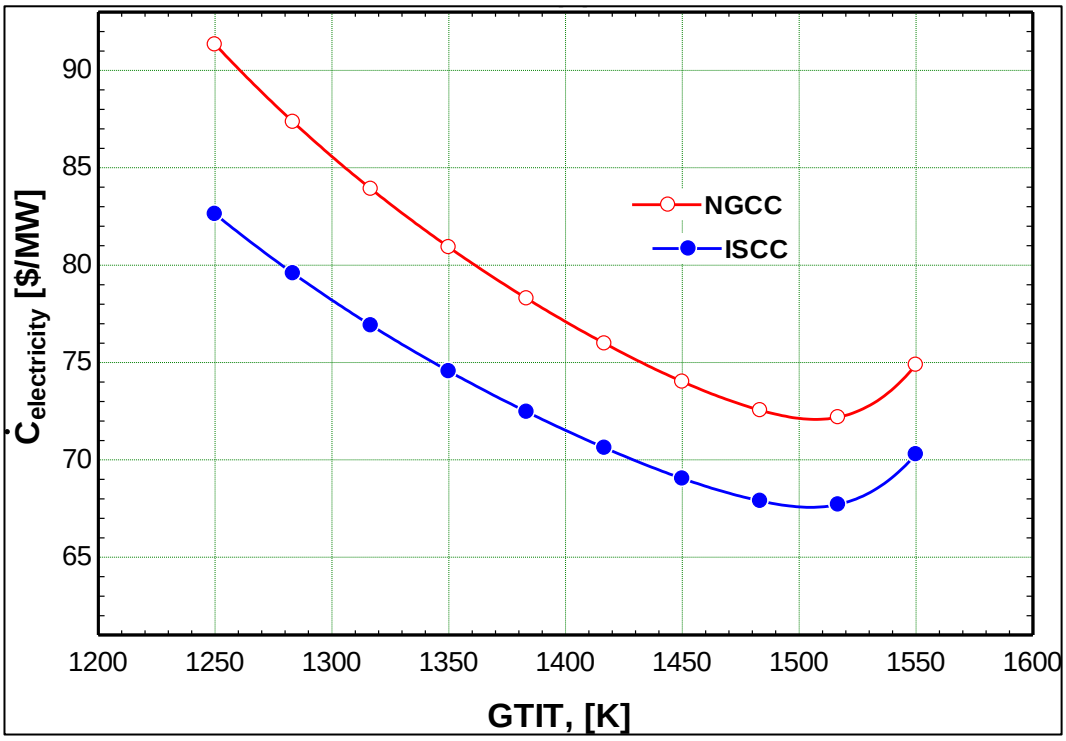

Figure 4.9. Gas turbine inlet temperature impacts the costs for the two systems.

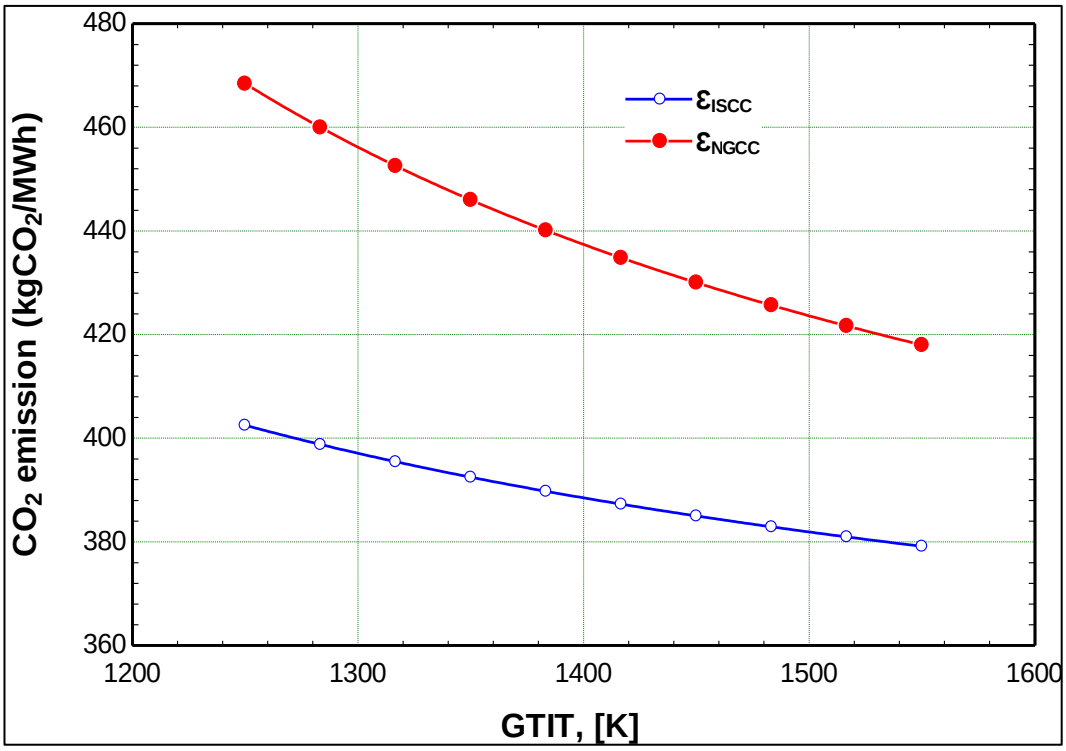

Figure 4.10. Gas turbine inlet temperature impacts the CO_2 emission for the two systems.

Figure 4.11 demonstrates the operational, economic, and efficiency impacts on the ISCC and NGCC systems concerning the high-pressure steam turbine intake pressure ($P_{HPST,\ in}$). The figure illustrates that as the enthalpy at the HPST intake increases, the net power output ($\dot{W}_{net}$) for both the ISCC and NGCC systems also increases. This rise in energy is due to the enhanced performance of the HPST and LPST as the intake enthalpy increases. Consequently, as $P_{HPST,\ in}$ improves from 80 to 125 bar, the $\dot{W}_{net}$ for the ISCC system increases from 551.2 MW to 557.3 MW, while for the NGCC, $\dot{W}_{net}$ rises from 486.8 MW to 490.8 MW.

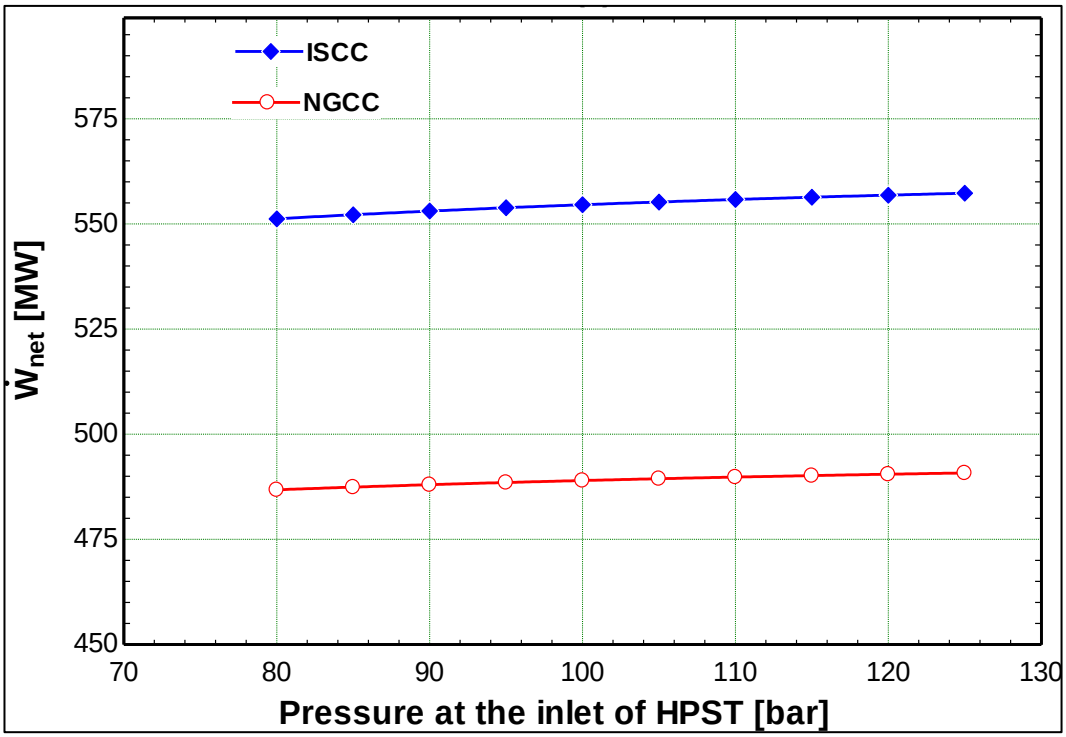

Figure 4.11. $P_{HPST,in}$ impact on the $\dot{W}_{net}$ for the two systems.

Figures 4.12 and 4.13 display the effects of $P_{HPST,\,in}$ on the efficiencies of the ISCC and NGCC systems. The results indicate that while the net power output ($\dot{W}_{net}$) shows a minimal increase at high $P_{HPST,\,in}$, the efficiencies of both systems exhibit modest improvements as $P_{HPST,\,in}$ rises. Specifically, in the ISCC process, as $P_{HPST,\,in}$ increases, the energy efficiency (η_{energy}) rises from 50.07% to 50.63%, and the exergy efficiency (Ψ_{exergy}) climbs from 48.35% to 48.89%. In the NGCC cycle, when $P_{HPST,\,in}$ in is elevated, η_{energy} advances from 44.22% to 44.58%, and Ψ_{exergy} improves from approximately 42.7% to 43.05%.

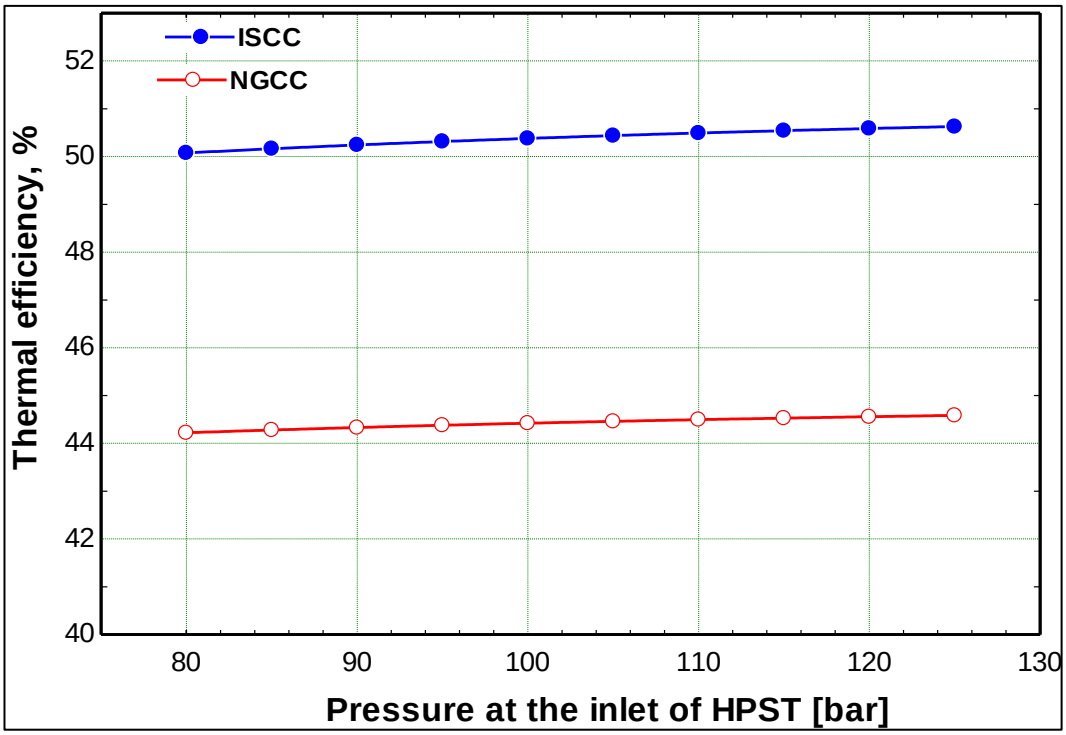

Figure 4.12. $P_{HPST,in}$ impact on the thermal efficiency for the two systems.

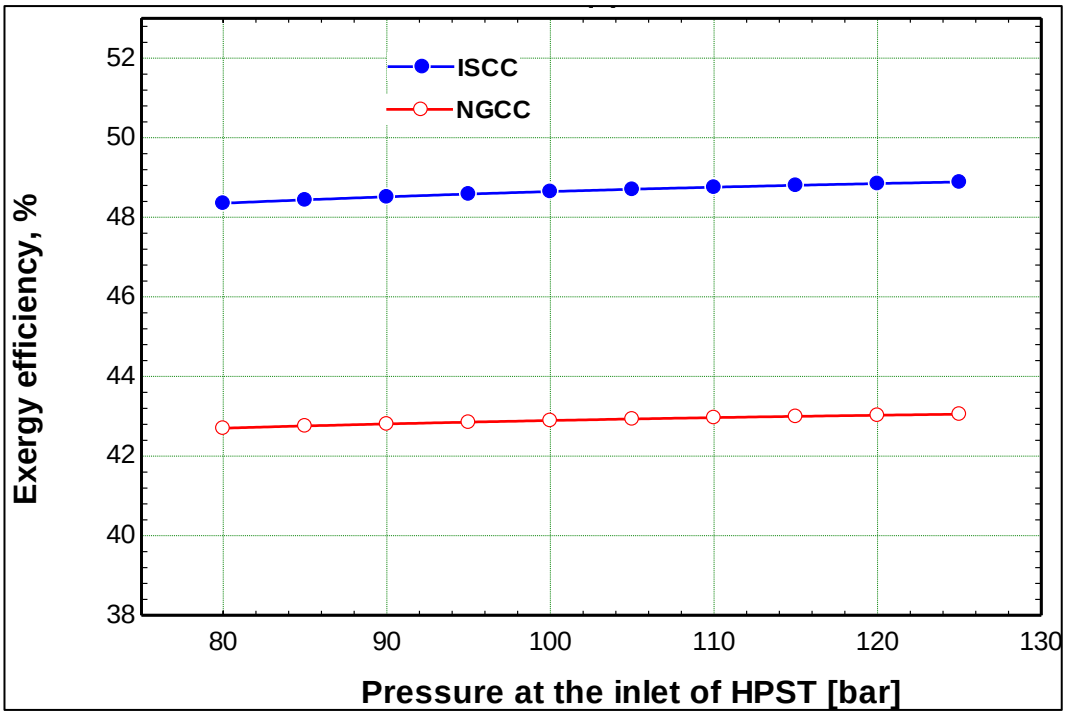

Figure 4.13. $P_{HPST,in}$ impact on the exergy efficiency for the two systems.

Figure 4.14 illustrates the minimal change in the total energy cost ($\dot{C}_{electricity}$) for each system as the $P_{HPST,\ in}$ increases. This cost stability is due to the corresponding increases in capital cost per unit of output ($\dot{C}_k$) and net power output ($\dot{W}_{net}$) for each component. The graph shows that the ISCC system's energy cost varies slightly from 74.91 to 73.09 $//MWh, while the NGCC system's cost ranges from 81.08 to 79.3 $//MWh.

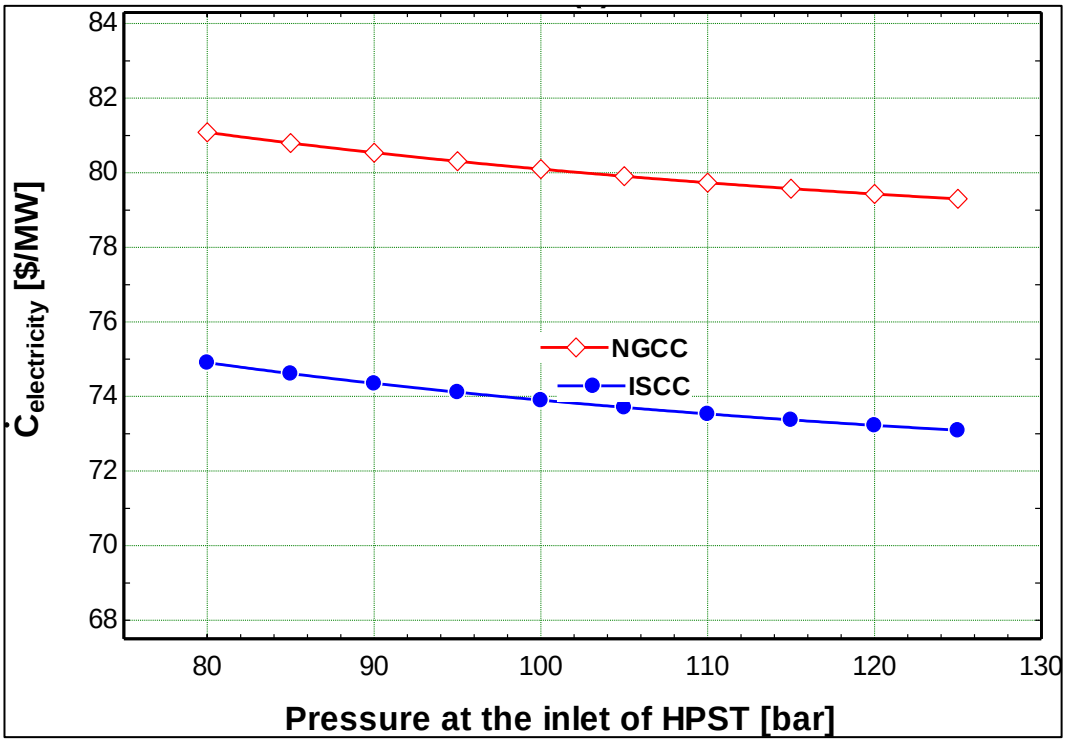

Figure 4.14. $P_{HPST,\ in}$ impact on the costs for the two systems.

Figure 4.15 shows that there is only a slight variation in the total CO_2 emissions for each system as the $P_{HPST,in}$ increases. This minimal change is attributed to the corresponding increase in the net power output ($\dot{W}_{net}$) for each component. The graph reveals a slight fluctuation in the CO_2 emissions for the ISCC system, ranging from 394 to 389.7 kg CO_2/MWh, while the NGCC system exhibits CO_2 emissions ranging from 446.2 to 442.5 kg CO_2/MWh.

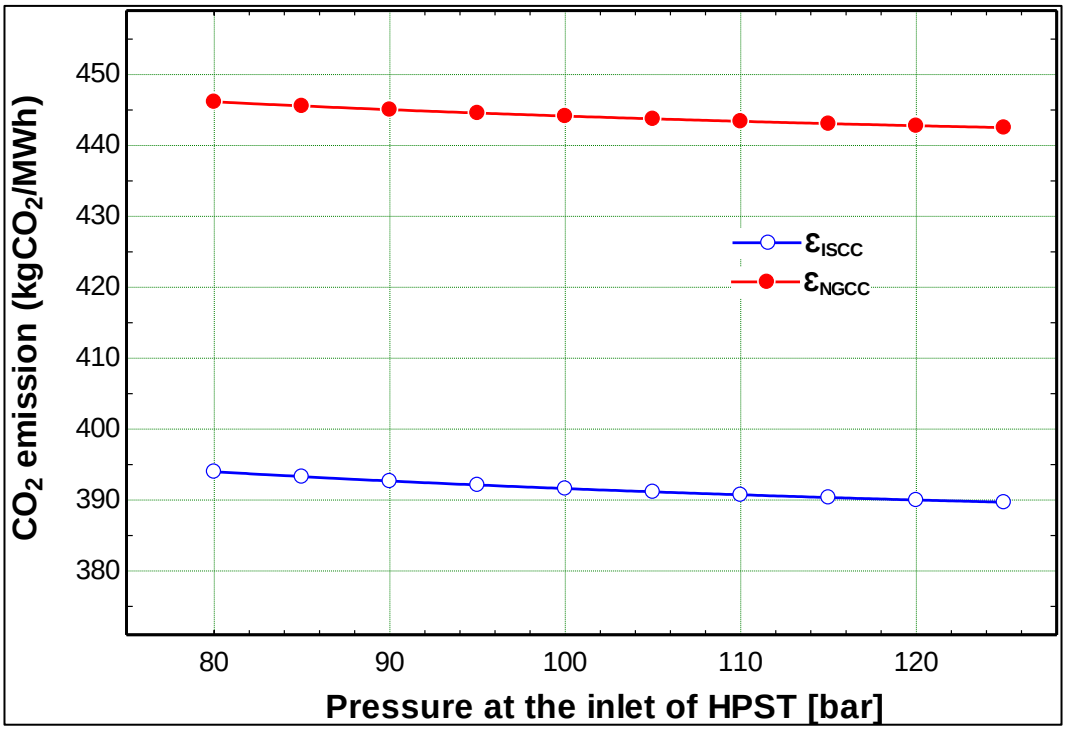

Figure 4.15. $P_{HPST,in}$ impact on the CO_2 emission for the systems.

Figure 4.16 illustrates the $\dot{W}_{net}$ of ISCC and NGCC systems as the condenser operating temperature (T_{cond}) varies from 25 to 70°C. The results indicate that an increase in T_{cond} negatively impacts both systems, reducing the power generated by the LPST. Specifically, the results show that the $\dot{W}_{net}$ for the ISCC system decreases from 560.3 MW to 533.7 MW, and for the NGCC system, it decreases from 492.7 MW to 475.3 MW as T_{cond} increases from 25°C to 70°C.

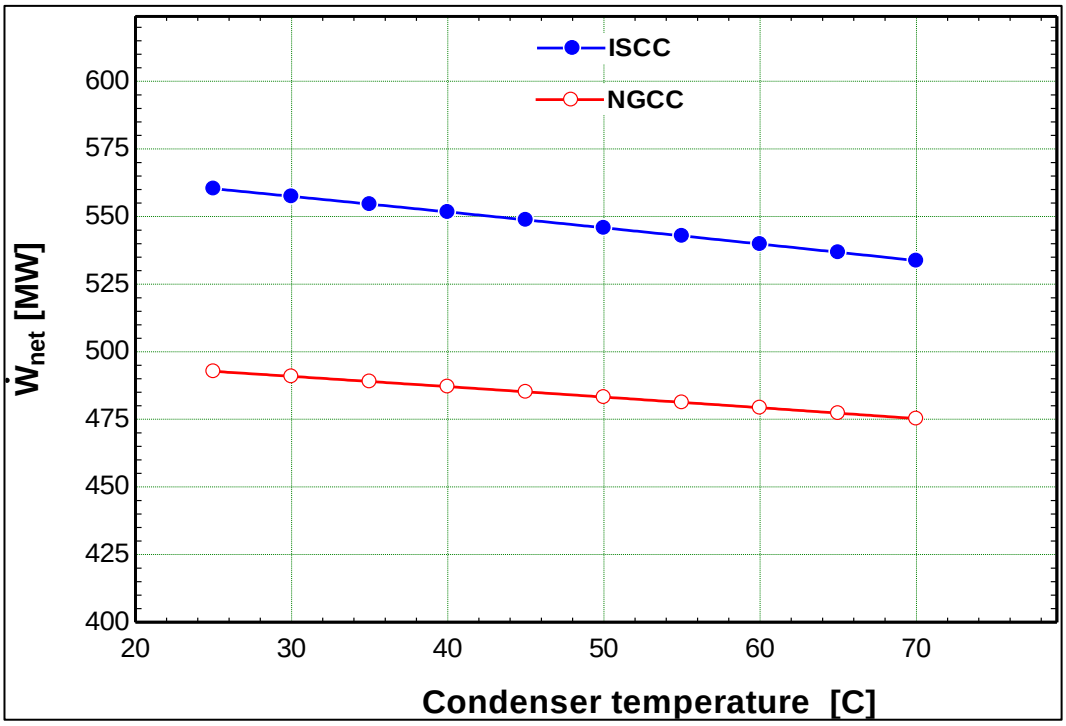

Figure 4.16. Effect of condenser temperature on the $\dot{W}_{net}$ for systems.

The impact of T_{cond} on the overall efficiencies of the NGCC and ISCC cycles is depicted in Figures 4.17 and 4.18. The diagrams show a decrease in η_{energy} and Ψ_{exergy} due to the reduction in $\dot{W}_{net}$ with increasing T_{cond}. The results indicate that for the ISCC system, η_{energy} decreases from 50.9% to 48.48%, and Ψ_{exergy} decreases from 49.15% to 46.81% as T_{cond} rises from 25°C to 70°C. For the NGCC cycle, η_{energy} decreases from 44.76% to 43.17%, while Ψ_{exergy} decreases from 43.22% to 41.69%.

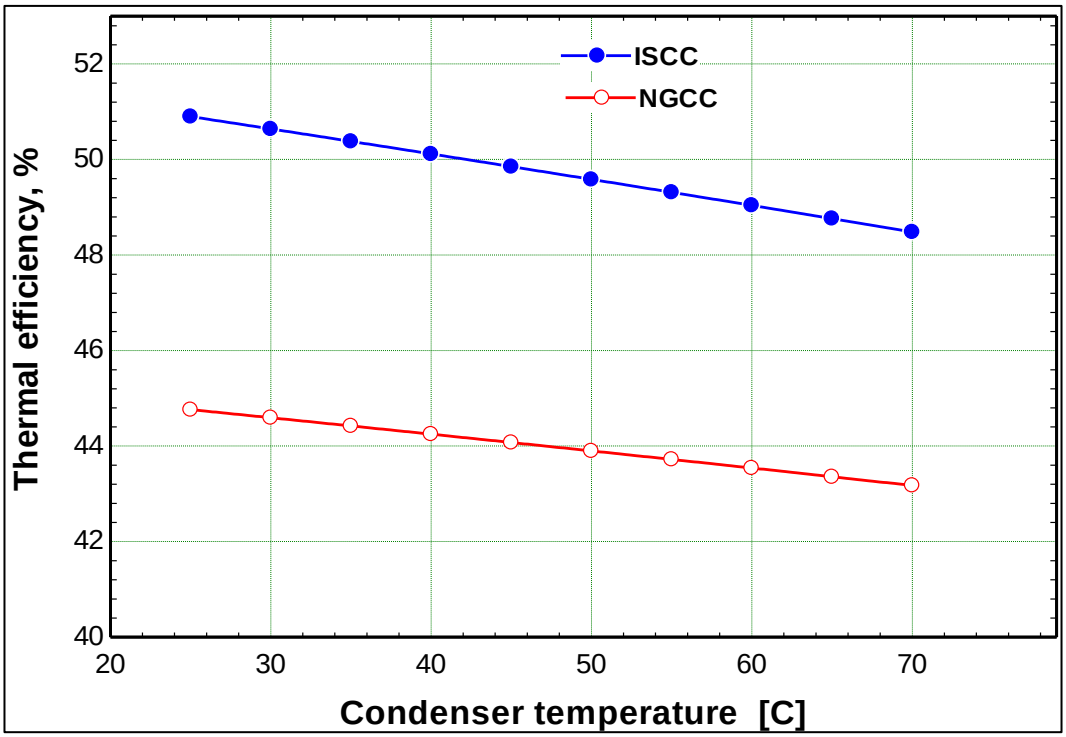

Figure 4.17. Effect of condenser temperature on the thermal efficiency for systems.

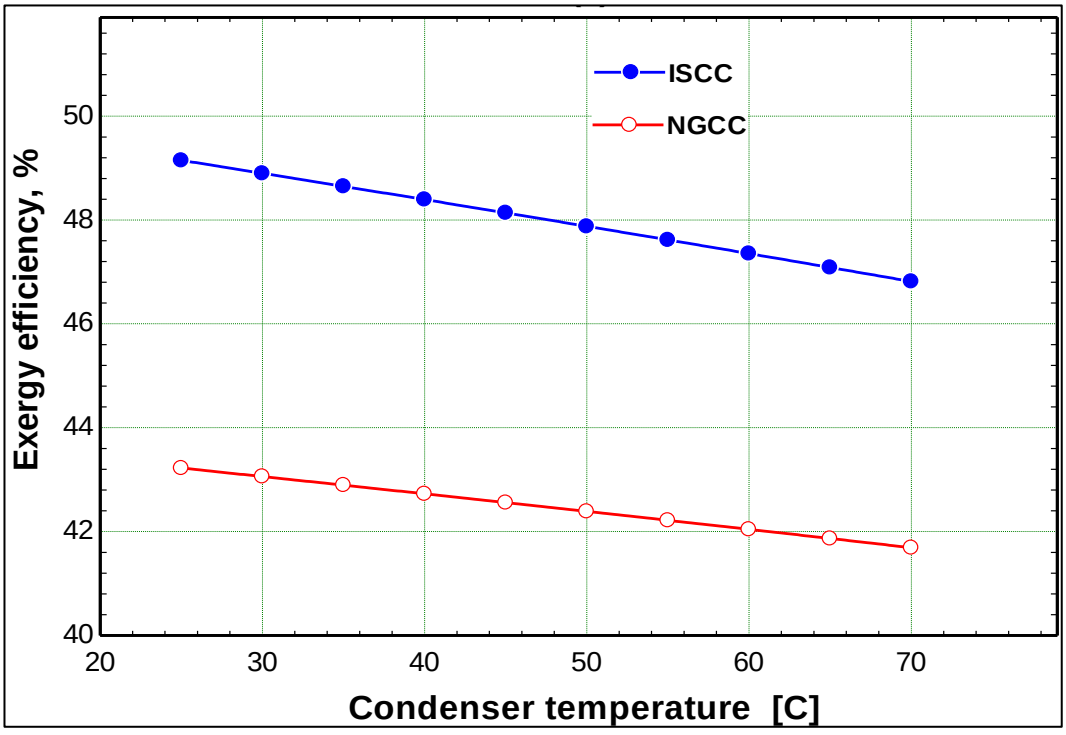

Figure 4.18. Effect of condenser temperature on the exergy efficiency for systems.

The entire cost of energy ($\dot{C}_{electricity}$) in the ISCC system increases between 72.51 $//MWh and 79.36 $//MWh while the ambient temperature varies between 25 and 70°C, although increases between 78.81 $//MWh and 85.04 $//MWh of the NGCC system, as shown in Figure 4.19.

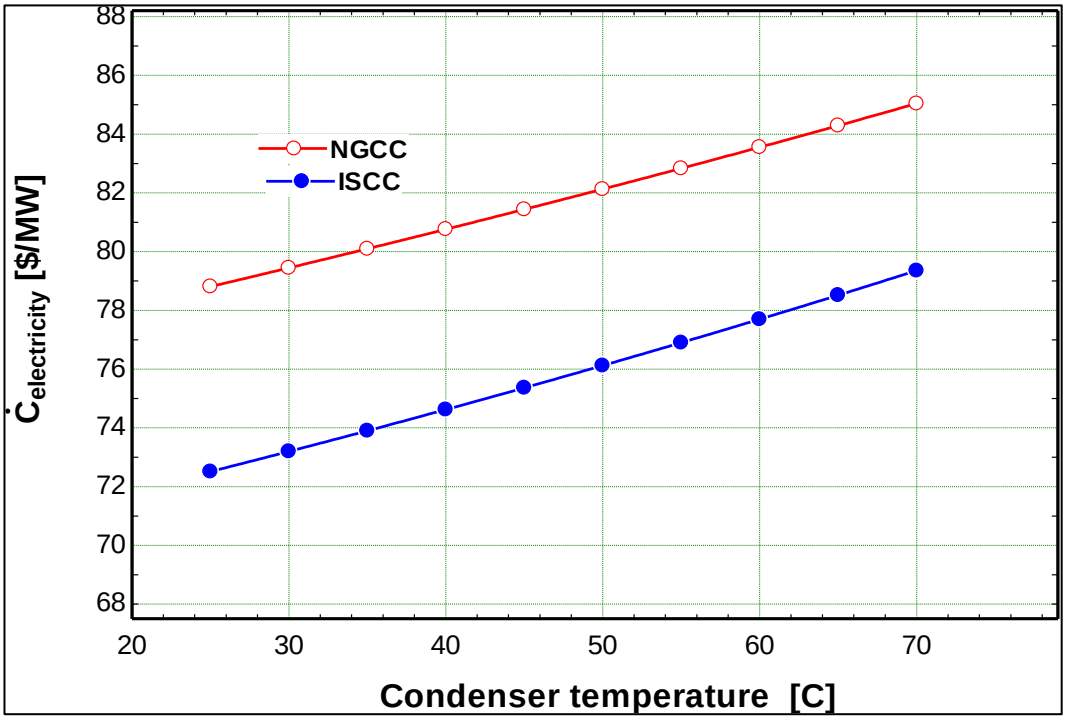

Figure 4.19. Effect of condenser temperature on the cost for systems.

The total CO_2 emissions for the ISCC system increase because increasing in Wnet from 387.6 to 406.9 $kgCO_2/MWh$ as the ambient temperature varies between 25 and 70°C. For the NGCC system, CO_2 emissions increase from 440.8 to 457 $kgCO_2/MWh$ over the same temperature range, as illustrated in Figure 4.20.

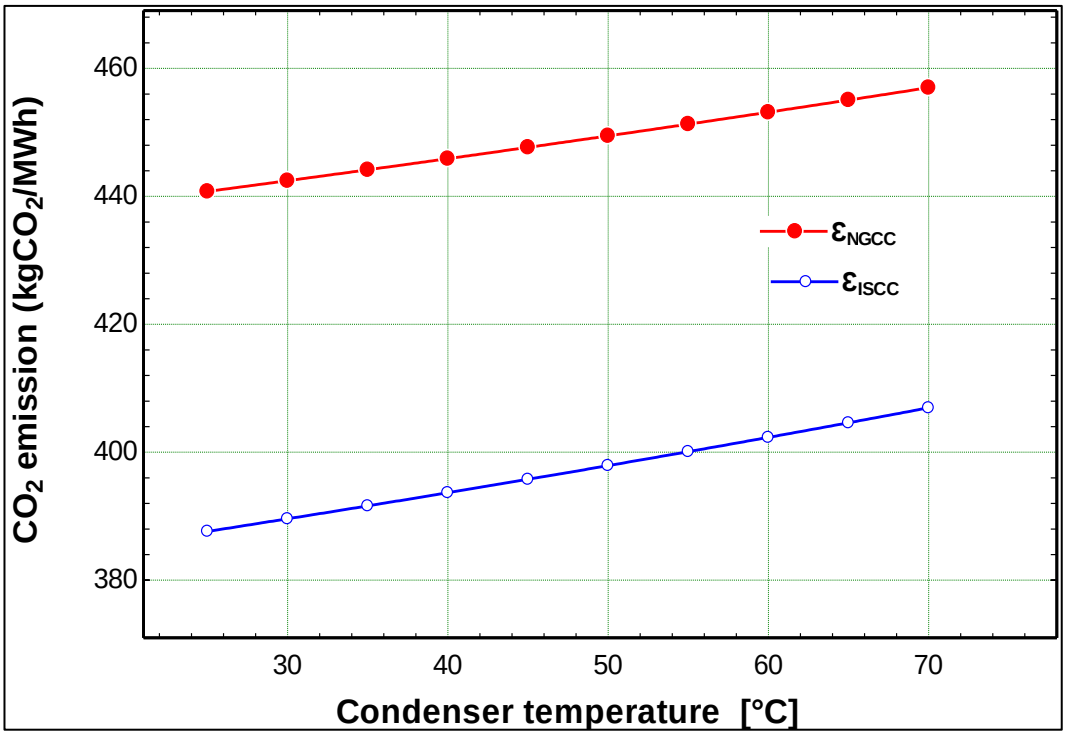

Figure 4.20. Effect of condenser temperature on the CO_2 for systems.

4.3.3 Environmental Analysis

The environmental investigation focuses on the system's CO_2 emissions, comparing the Brayton cycle, NGCC, and ISCC over a year. The Brayton cycle emits between 581.7 and 583.2 $kgCO_2/MWh$, indicating a relatively consistent trend with minor fluctuations. In comparison, the NGCC emits slightly higher amounts, ranging from 439.2 to 449.3 kg CO_2/MWh, gradually increasing towards the end of the year. The ISCC system has the lowest emissions, ranging from 405 to 375.6 kg CO_2/MWh, with a general declining trend and occasional variations, as illustrated in Figure 4.21. The comparison reveals that the ISCC has the lowest annual CO_2 emissions, followed by the NGCC and then the Brayton cycle. This highlights the environmental benefits of integrating solar energy into power generation systems.

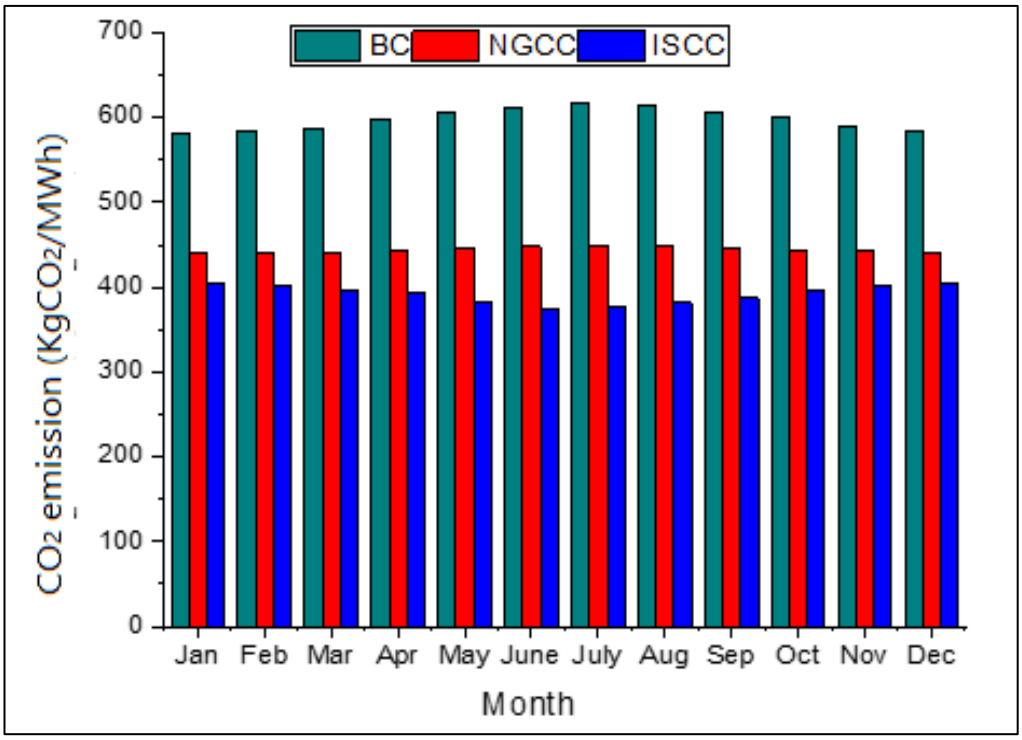

Figure 4.21. Annual CO_2 emission for the three systems

4.3.4 Annual Demonstration Power Output and Entire Cost of Energy for ISCC

Figure 4.22 displays the percentage of monthly power production by each cycle. The results indicate that BC energy generation increases as the outside temperature drops during the cooler months, enhancing the compressor's operating conditions. In January, the NGCC achieved its highest output at 514.4 MW; in July, it reached its lowest level at 465.5 MW. Additionally, the ISCC system produced the most energy in June (562.6 MW) due to optimal compressor conditions and high DNI (approximately 5.52 kWh/m²/day). In contrast, October saw the lowest energy production at about 547.8 MW.

Figure 4.23 illustrates the monthly variations in the total cost of energy for BC, NGCC, and ISCC under optimal operating conditions. The figure clearly shows that the thermo-economic performance of these systems is not significantly affected by changes in environmental conditions. For the ISCC system, the specific cost of energy fluctuates between 70.08 and 76.79 $//MWh, while for the NGCC system, it ranges from 79.4 to 80.05 $//MWh.

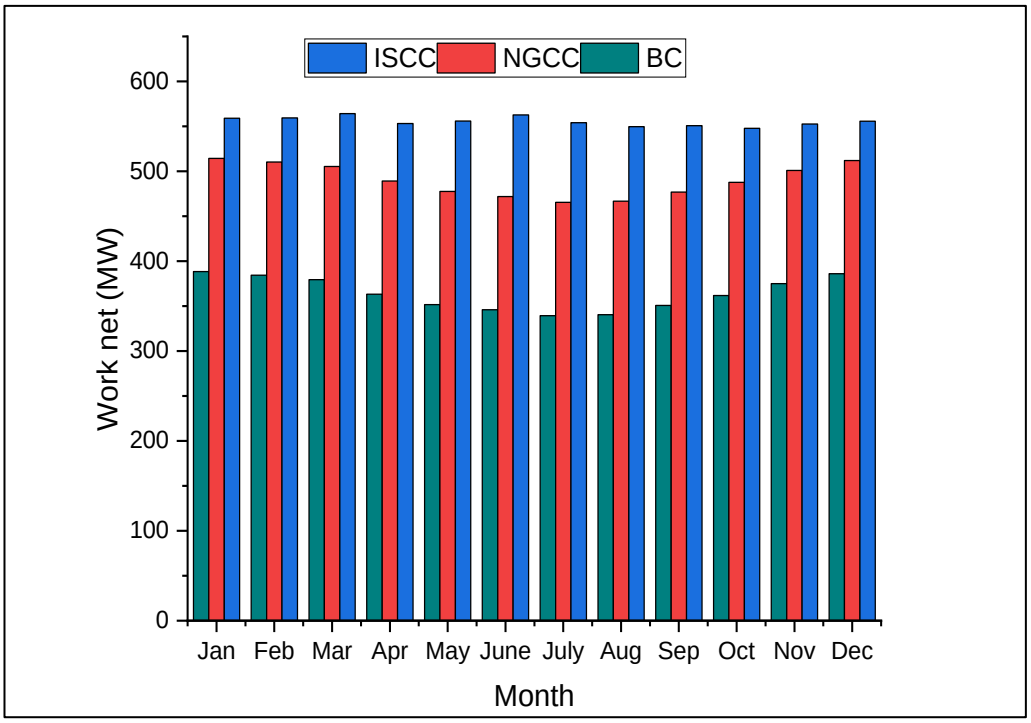

Figure 4.22. Annual power production across the three systems

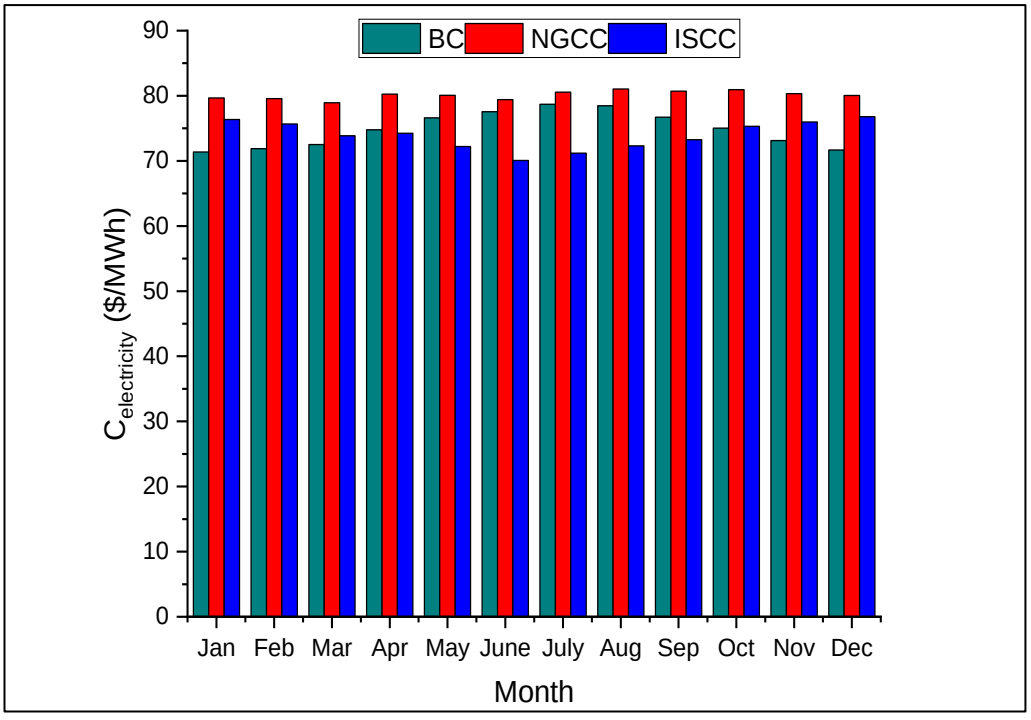

Figure 4.23. Annual specific cost of energy across the three systems

4.4 POLYGENERATION SYSTEM FOR ISCC WITH AND WITHOUT ARC.

4.4.1 Energy, Exergy, and Economy Analysis for the ISCC-ARC System

Table 4.6 showcases the thermodynamic properties of the existing condition in the ISCC-ARC system design, which are essential for calculating power and exergy within this system.

Table 4.6. characteristics for every step of ISCC-ARC with optimal conditions.

Steps	Mass (kg/s)	Pressure (kPa)	Temperature (K)	Enthalpy (kJ/kg)	Entropy (kJ/kg K)	Exergy (MW)
1	418.5	101	283	261.3	5.679	-
2	418.5	1,276	632.7	621.8	5.774	138.8
3	7.573	101	288	−4,672	11.53	392.6
4	425.6	1,213	1,360	235.4	8.036	406.8
5	425.6	104.5	822.9	−419.2	8.144	114.4
6	425.6	101	402.9	−885.1	7.365	15.04
7	665.4	371.5	101.3	−922.3	7.322	6.135
8	150.4	121.6	373.1	548.8	1.65	16.76
9	150.4	10,133	406.4	566.8	1.659	19.07
10	150.4	9,829	794.9	3,433	6.681	296.7
11	150.4	2,007	581.8	3,044	6.802	232.8
12	150.4	1,946	774.9	3,473	7.452	268.2
13	135.4	31	352.5	2,645	7.81	114.8
14	15.04	121.6	463.4	2,855	7.702	16.4
15	135.4	31	343	292.4	0.9533	8.504
16	135.4	121.6	343	292.6	0.9534	8.517
17	520.5	1,000	665	780.6	1.675	146.5
18	520.5	1,000	566	539.3	1.283	81.68
19	7,038	101	283	41.39	0.1489	-
20	7,038	101	295	91.66	0.3228	7.301
1a	85.21	310	0.8634	81.92	0.238	3.291
2a	85.21	310.2	6.944	81.93	0.238	3.291
3a	85.21	342.9	6.944	151.5	0.451	3.807
4a	72.84	361	6.944	219.6	0.4816	7.554

5a	72.84	333	6.944	167.2	0.3305	7.019
6a	72.84	321.6	0.8634	167.2	0.3306	7.017
7a	12.37	361	6.944	2,656	7.506	3.291
8a	12.37	312	6.944	162.7	0.557	0.01654
9a	12.37	278	0.8634	162.7	0.586	−0.09024
10a	12.37	278	0.8634	2,510	9.029	−2.179
11a	650	323	298	323.6	5.777	0.9202
12a	1,845	298	308	104.3	0.3651	0.2987
13a	1,845	308	298	146.1	0.5031	1.33
14a	2,890	298	308	104.3	0.3651	0.4681
15a	2,890	308	298	146.1	0.5031	2.084

The data in Table 4.7 compares the output generated by two systems: ISCC and ISCC-ARC. The table shows the ISCC system provides slightly more energy to air compressors at 486.98 MW compared to 451.984 MW for the ISCC-ARC system. Both systems are almost identical in their energy production from GTs, with the ISCC at 836.63 MW and the ISCC-ARC at 835.832 M. HPST and LPST outputs are nearly identical in both systems. The ISCC-ARC system shows a higher work production at 581.1 MW compared to 554.6 MW for the ISCC system, suggesting enhanced efficiency or additional work generation capabilities with ARC technology. Both systems show slight differences in the thermal efficiency with the ISCC-ARC system marginally more efficient at 51.15% compared to 50.89% for the ISCC system. There is a slight increase in exergy efficiency in the ISCC-ARC system (49.4%) compared to the ISCC system (49.14%).

Overall, the ISCC-ARC system shows marginal improvements in efficiency metrics and work production, suggesting that the ARC technology might offer slight enhancements in performance, especially in terms of efficiency and additional work output. The ARC technology may provide minor performance gains, particularly regarding efficiency and extra work output since the ISCC-ARC system exhibits small increases in efficiency metrics and overall work production.

Table 4.7. The amounts of output generated by ISCC and ISCC-ARC systems.

Output generated	**ISCC**	**ISCC-ARC**
The energy provided to ACs (MW)	486.98	451.984
Energy production by GTs (MW)	836.63	835.832
Energy production by HPST (MW)	56.144	56.136
Energy production by LPST (MW)	143.544	143.516
The energy provided to P1 (kW)	1,881	1,881
The energy provided to P2 (kW)	18.96	18.96
The energy provided to P3 (kW)	-	0.08
Work production (MW)	554.6	581.1
Entire η_{energy} (%)	50.89	51.15
Entire η_{exergy} (%)	49.14	49.4

Table 4.8 displays the main exergy analysis results for various components of the ISCC-ARC, providing detailed data on fuel, product, and destruction exergies for each component. The table also includes details on $\dot{\mathbf{E}}_{\mathbf{d}}$ and Ψ percentages. the findings present components with the highest exergy destruction (Ed in MW), including the Combustion Chamber (373.8 MW), PTC (41.25 MW), and CONDENSER 1 (64.74 MW). This suggests substantial energy dissipation, particularly in high temperatures and pressure transformations. The Combustion Chamber again stands out with the highest percentage of exergy destruction at 53.51%, indicating a central area where efficiency improvements could yield significant gains. Conversely, elements like the Pumps and the Evaporators show negligible destruction percentages, suggesting very efficient operation in those areas.

The Heat Exchanger and Evaporators exhibit remarkably high efficiencies (above 96%), with the Heat Exchanger achieving nearly 96.58%, indicating optimal operation with minimal exergy losses. On the other hand, the Generator has notably low efficiency at 17.4%, suggesting that it could be a critical point for potential improvements to increase the overall system efficiency. The Air Compressor and Gas Turbine have moderate efficiencies at 92.16% and 95.3%, respectively.

Table 4.8. ISCC-ARC Exergy assessment.

Element	$\dot{E}_F$ (MW)	$\dot{E}_P$ (MW)	$\dot{E}_d$ (MW)	$\dot{E}_d$ (%)	Ψ (%)
AC	525	416.5	35.42	5.071	92.16
CC	1,594	1,220	373.8	53.51	76.55
GT	877.1	835.8	41.25	5.905	95.3
HRSG	363	305.2	57.83	8.278	84.07
HPST	61.35	56.14	5.209	0.7457	91.51
LPST	163.6	143.5	20.06	2.871	87.74
Condenser 1	71.56	6.828	64.74	9.267	9.541
OFWH	22.34	12.08	10.27	1.47	54.05
Pump 1	1.881	1.581	0.3001	0.04296	84.04
Pump 2	0.01896	0.01529	0.003669	0.0005253	80.64
PTC	139.4	64.79	74.64	10.68	46.47
Generator	9.926	1.727	8.199	1.181	17.4
Condenser 2	0.8035	0.3105	0.493	0.07105	38.64
Absorber	1.449	0.4865	0.9625	0.13873	33.58
Heat exchanger	0.1311	0.1266	0.004481	0.00064587	96.58
Pump3	0.00008	0.00008	0.00000029	0.000000041	100
Evaporator	0.5125	0.167	0.3456	0.0498134	32.58
Evaporator 1	0.004058	0.02214	0.262	0.0377636	84.51
Evaporator 2	1.722	1.722	0.0005273	0.000076	99.97

Table 4.9 provides an exergoeconomic analysis of the ISCC-ARC system, breaking down the costs associated with capital investment ($\dot{Z}_K$), exergy destruction ($\dot{C}_D$), total cost ($\dot{Z}_K + \dot{C}_D$), and the exergoeconomic factor (f) for each component. The data reveal significant costs due to exergy destruction in key elements such as the combustion chamber (1,551 $/h), the GT (2,236 $/h), and the HRSG (914.4 $/h), which highlight substantial exergy losses in these areas. The ($\dot{Z}_K + \dot{C}_D$), column integrates the exergy destruction costs with capital investment costs, pinpointing areas with major financial implications. Notably, the gas turbine and combustion chamber incur costs of 1,000.5 $/h and 1,556.04 $/h, respectively. Additionally, the table indicates that the total combined cost of capital and exergy losses for the entire system is 6,944.323 $/h, with an exergoeconomic factor for the entire system of 58.9%.

Table 4.9. ISCC-ARC Exergoeconomic for each element.

Element	$\dot{C}_D$ **(\$/h)**	$\dot{Z}_K$ **(\$/h)**	$\dot{Z}_K + \dot{C}_D$ **(\$/h)**	**f (%)**
AC	210.7	1,107.4	1,318	84.01
CC	1,551	5.04	1,556.04	0.03263
GT	223.6	781.2	1,005	77.76
HRSG	294.4	506.9	801.3	63.26
HPST	31.63	197.1	228.73	86.17
LPST	118	380.16	489.16	76.32
Condenser 1	380.7	3.98	384.7	1.036
OFWH	60.41	116.892	177.3	65.92
Pump 1	2.073	11.64	13.71	84.88
Pump 2	0.02534	0.445	0.473	94.61
PTC	0	1,000.44	1,000.44	100
Generator	0.2431	5.152	5.395	95.49
Absorber	0.06612	0.9432	1.009	93.45
Heat exchanger	0.00074	0.1	0.10074	99.24
Pump3	0	0.009	0.009	100
Evaporator	2.71	1.2456	3.956	31.49
Evaporator 1	0.00006	0.0054	0.00547	98.9
Evaporator 2	0.000087	0.03	0.03	99.73
Total System	2,875.56	4,118.763	6,944.323	58.9

4.4.2 Effect of The Operation Conditions On The Performance, Cost, And Environmental Impact of The ISCC And ISCC-ARC Systems

Figure 4.24 depicts the effect of the pressure ratio (Pr) on the total work output ($\dot{W}_{net}$) for both the ISCC and ISCC-ARC systems, illustrating how an increase in Pr adversely impacts the net work output of each cycle component. As Pr increases, the power consumption of the compressors also escalates, leading to reduced power generation across all components. Specifically, when Pr is raised from 6 to 18 bars, the $\dot{W}_{net}$ for the ISCC-ARC system declines from 614.4 MW to 530.9 MW. Similarly, the $\dot{W}_{net}$ for the ISCC system decreases from 602.1 MW to 505 MW. Additionally, the data indicate that integrating an absorption refrigeration system into the ISCC improves its power output by reducing the energy consumed by air compressors. This enhancement

allows the ISCC with an absorption cooling system to generate more power than the standard ISCC system.

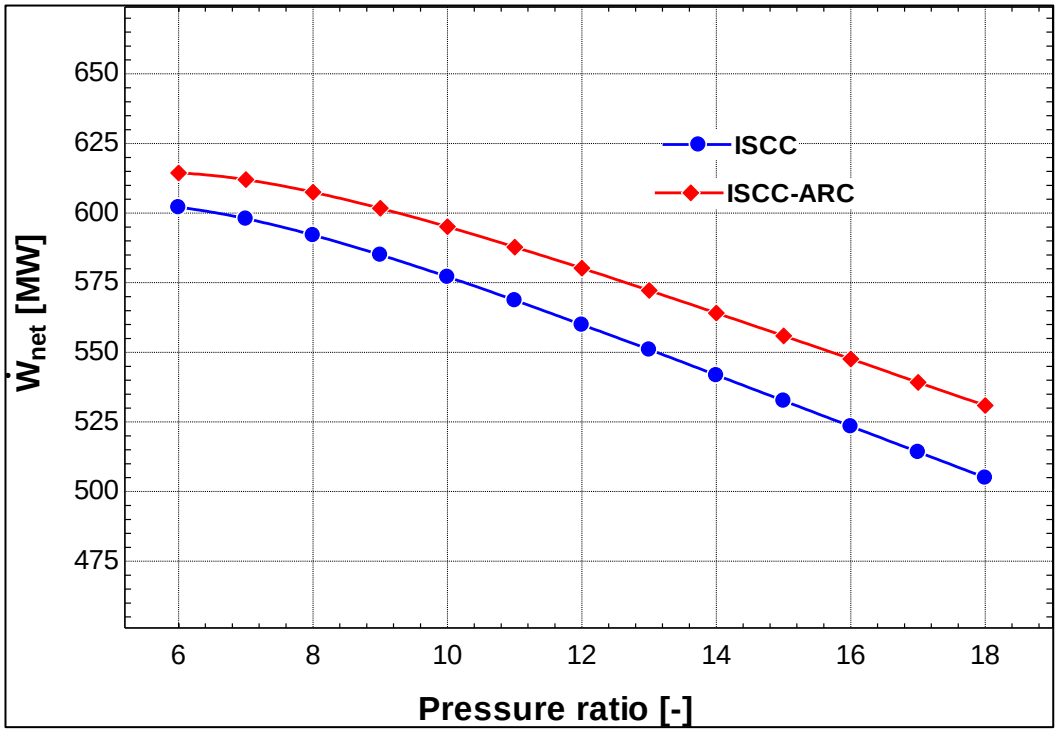

Figure 4.24. The pressure ratio effect on the $\dot{W}_{net}$ for the two systems.

The specific energy cost for both systems decreased as the pressure ratio (Pr) increased, peaked at a certain point, and then rose again with further increases in Pr, as shown in Figure 4.25. The graph also highlights why a Pr of 12 is the optimal pressure ratio. At Pr=12, the specific cost for the ISCC-ARC system ranged between $75.85 and $68.26 per MWh, compared to the ISCC system, which varied between $79.16 and $77.84 per MWh. Additionally, the energy consumption by compressors and the economic investment required for the Brayton cycle (BC) components increase alongside a rise in Pr. Reaching a Pr of 12 enhances the economic efficiency of the system.

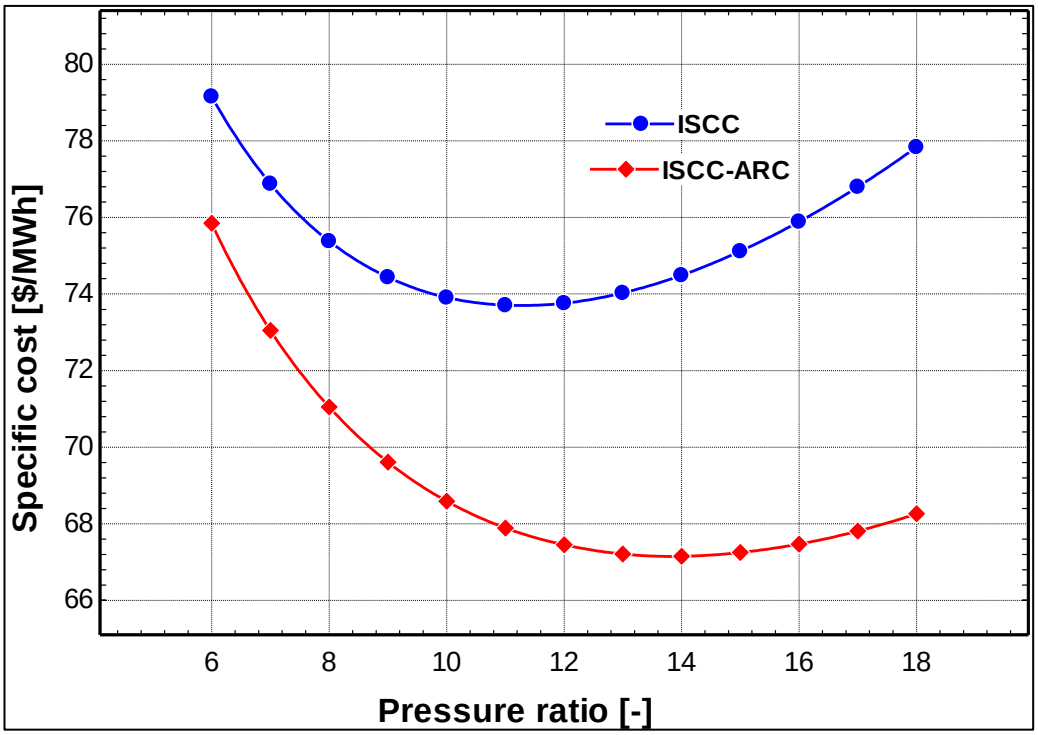

Figure 4.25. The pressure ratio affects the specific cost for the two systems.

Figures 4.26 and 4.27 demonstrate that the pressure ratio (Pr) significantly impacts the overall efficiency of both strategies. The graphs show that as Pr increases, the overall efficiency of both technologies also improves. According to the outcomes, the ISCC-ARC technique's $\eta_{thermal}$ and η_{exergy} improve from 46.39% and 44.8% to 51.55% and 49.78%, respectively, as Pr increases from 6 bar to 18 bar. Similarly, the ISCC technology shows gains, with $\eta_{thermal}$ increasing from 46.42% to 51.1% and η_{exergy} rising from 44.83% to 49.34%.

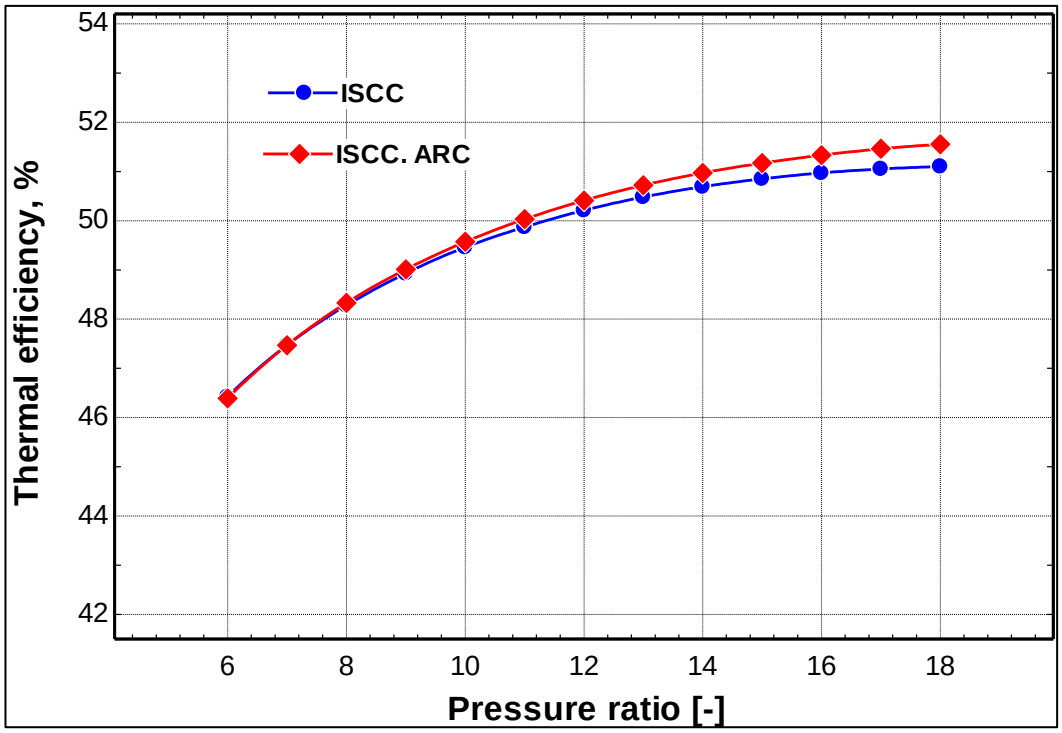

Figure 4.26. The pressure ratio affects the thermal efficiency of the two systems.

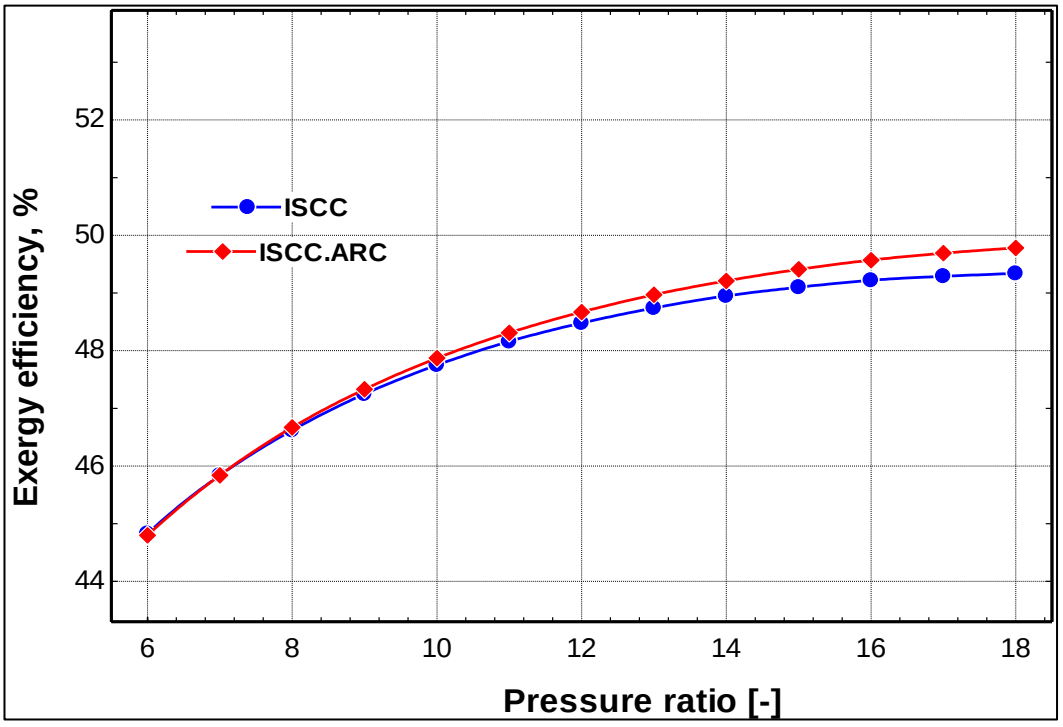

Figure 4.27. The pressure ratio affects the exergy efficiency of the two systems.

According to the data in Figure 4.28, when the pressure ratio (Pr) is increased from 6 bars to 18 bars, CO_2 emissions in the ISCC-ARC system decrease from 425.3 kg CO_2/MWh to 382.7 kg CO_2/MWh. Similarly, CO_2 emissions in the ISCC system decreased from 425 kgCO_2/MWh to 386.1 kgCO_2/MWh.

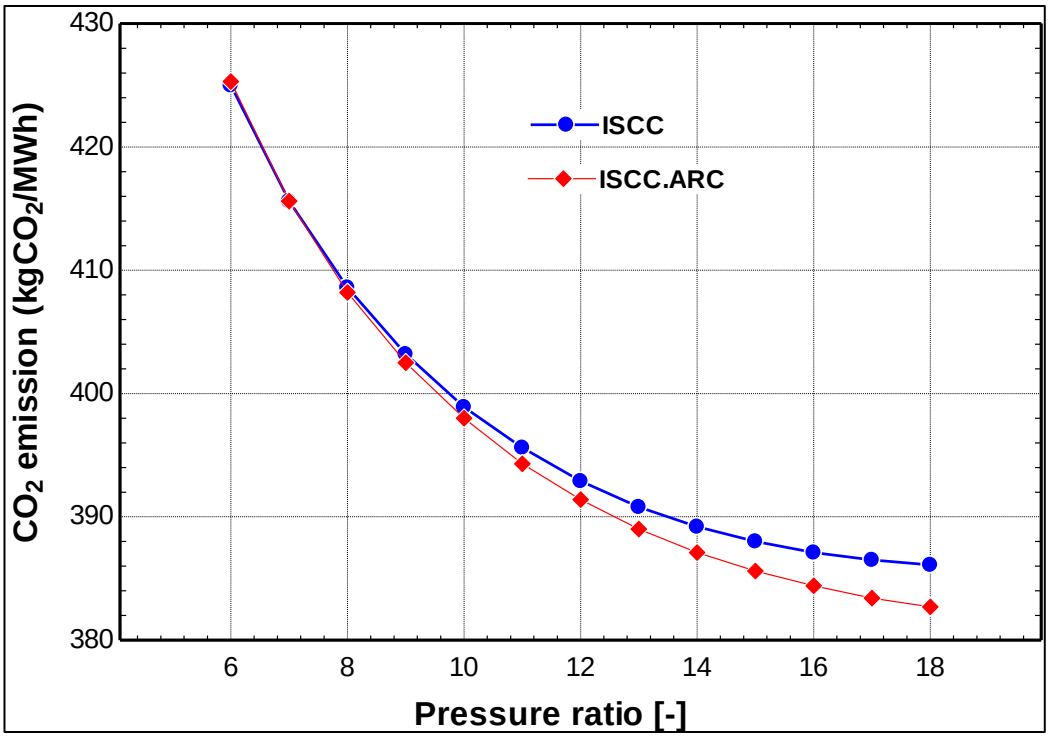

Figure 4.28. The pressure ratio affects the CO_2 emission for the two systems.

Figure 4.29 presents the relationship between gas turbine inlet temperature (GTIT) and the network output (Wnet) for ISCC and ISCC-ARC systems. Both ISCC and ISCC-ARC systems show an increase in Wnet as the GTIT increases from 1250 K to 1550 K. This indicates that higher inlet temperatures lead to greater network output for both systems. The figure demonstrates the clear advantage of the ISCC-ARC system over the standard ISCC system in terms of network output at various gas turbine inlet temperatures.

The ISCC-ARC system consistently outperforms the ISCC system across the range of inlet temperatures. At 1250 K, the ISCC-ARC system produces approximately 466.9 MW of network, while the ISCC system produces slightly less, around 446.1 MW. As

GTIT increases to 1550 K, the ISCC-ARC system's network output rises to about 774 MW, whereas the ISCC system reaches around 753.1 MW.

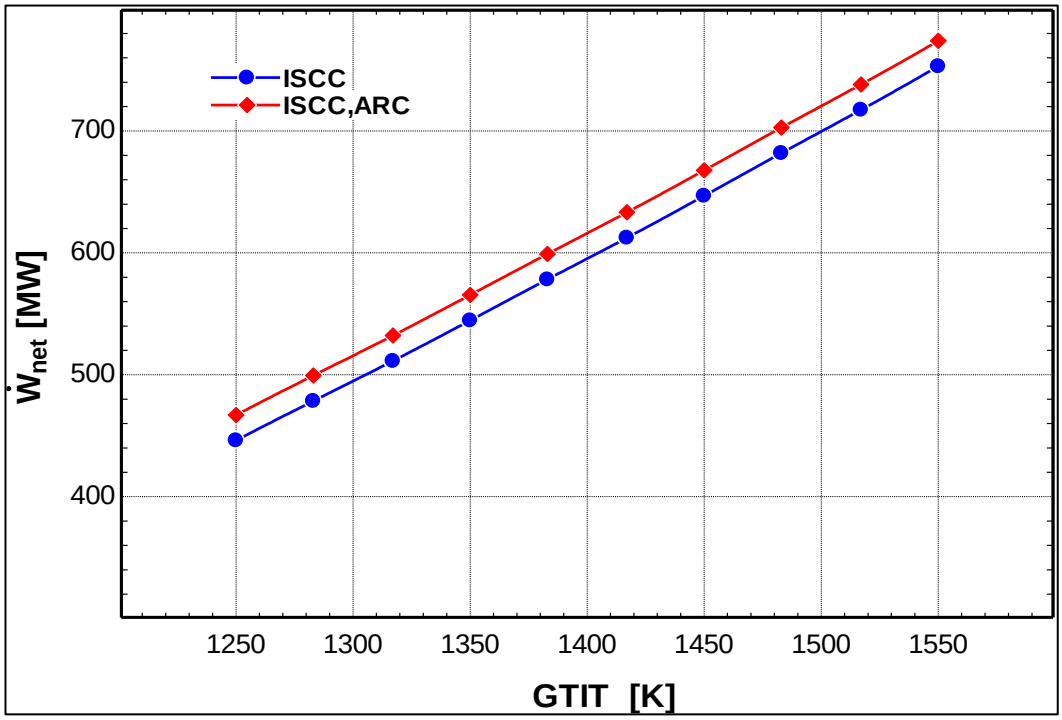

Figure 4.29. GTIT effect on the $\dot{W}_{net}$ for the two systems.

Figure 4.30 illustrates the effect of GTIT on the specific cost of energy ($/MW) for two systems: ISCC and ISCC-ARC. The findings present the ISCC-ARC system consistently shows lower specific costs compared to the ISCC system across the range of GTIT values. For both ISCC and ISCC-ARC systems, the specific cost decreases as GTIT increases from 1250 K to around 1517 K. Beyond this point, the specific cost starts to increase again. This indicates a U-shaped curve where the specific cost initially declines with rising GTIT but then begins to rise after reaching an optimal temperature. The lowest specific cost for the ISCC system is about 67.71 $/MWh at GTIT, around 1517 K, whereas for the ISCC-ARC system, it is approximately 63.04 $/MWh at the same temperature.

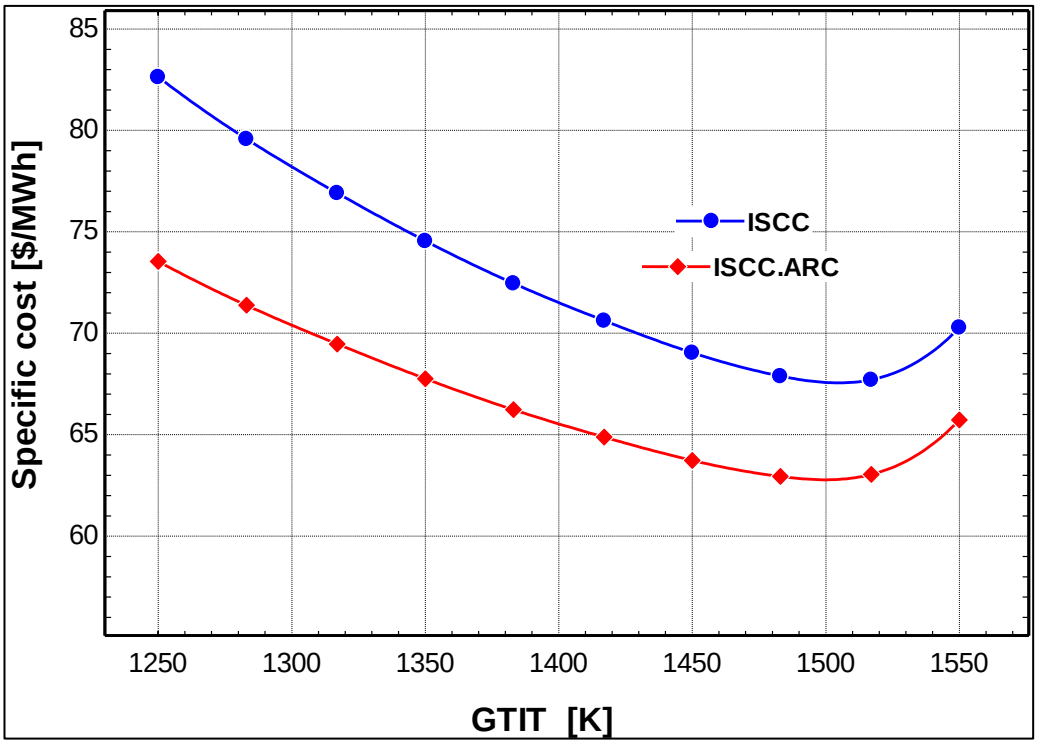

Figure 4.30. GTIT effect on the specific cost for the two systems.

Figures 4.31 and 4.32 illustrate the impact of GTIT on thermal efficiency and exergy efficiency for the ISCC and ISCC-ARC systems. These figures demonstrate that higher Gas Turbine Inlet Temperatures positively influence both thermal and exergy efficiencies for ISCC and ISCC-ARC systems. Increasing GTIT is beneficial for both thermal and exergy efficiencies, indicating that optimizing GTIT can lead to better overall performance for both systems. Both ISCC and ISCC-ARC systems exhibit an increase in thermal efficiency as GTIT rises from 1250 K to 1550 K.

The ISCC-ARC system maintains higher overall efficiencies than the ISCC system across the entire range of GTIT. At 1250 K, the thermal efficiency of the ISCC system is around 42.7%, while the ISCC-ARC system starts at approximately 49.02%. By 1550 K, the ISCC system reaches a thermal efficiency of about 47.45%, whereas the ISCC-ARC system improves to around 52.04%. At 1250 K, the exergy efficiency of the ISCC system is around 47.33%, while the ISCC-ARC system starts at about 47.64%. By 1550 K, the exergy efficiency of the ISCC system reaches approximately 50.02%, while the ISCC-ARC system achieves around 50.37%.

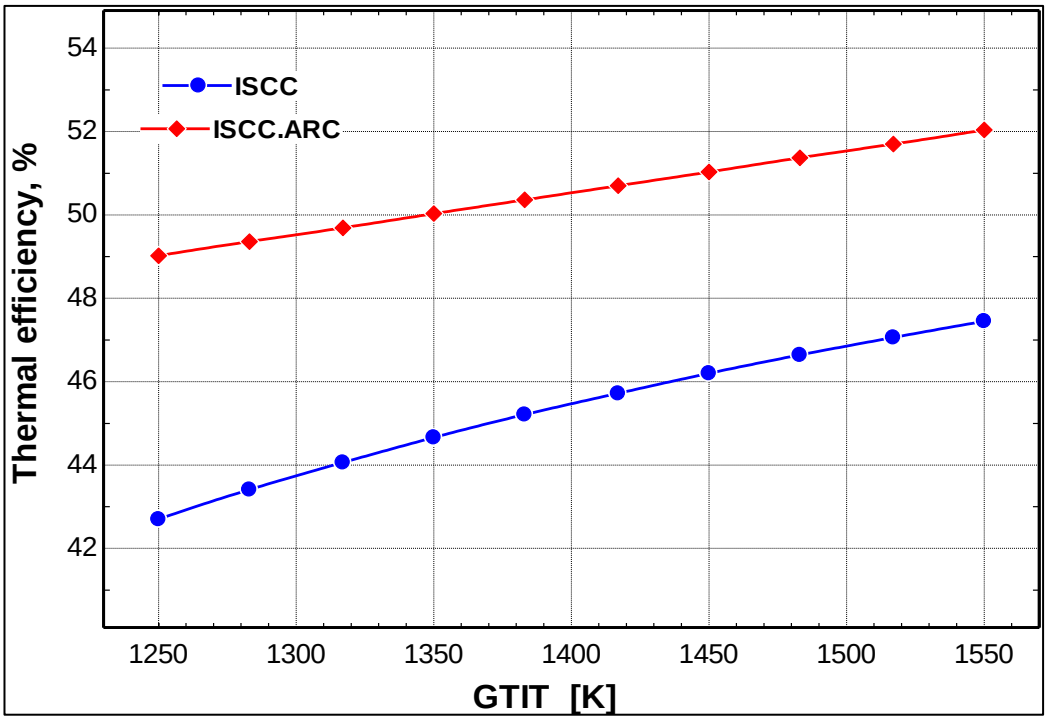

Figure 4.31. GTIT effect on the thermal efficiency for the two systems.

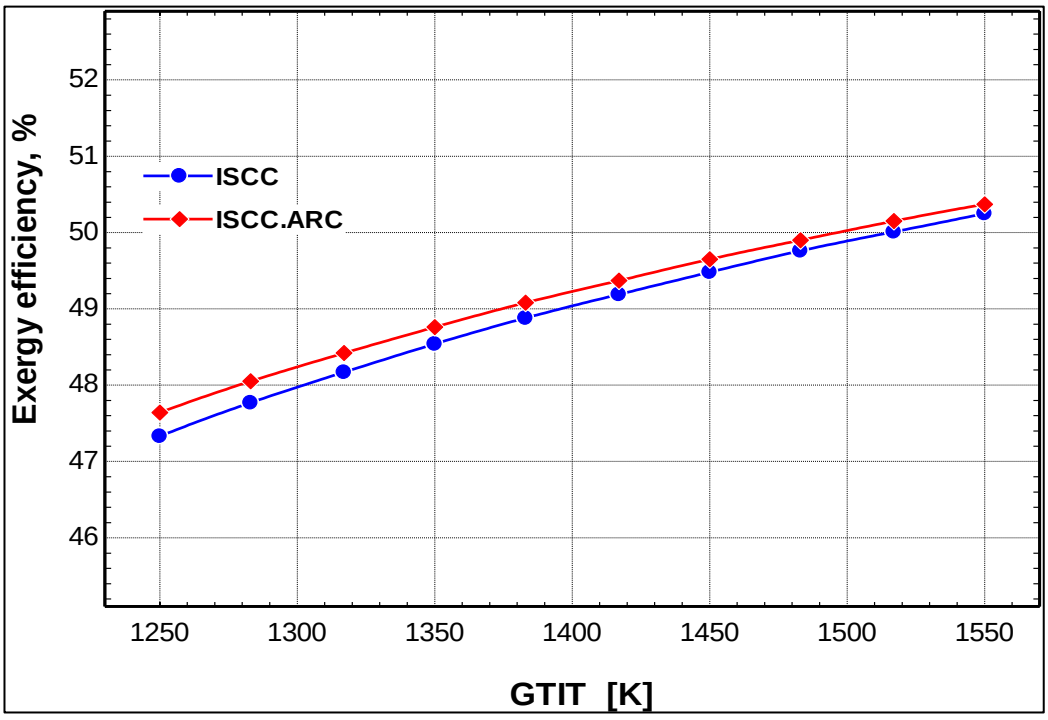

Figure 4.32. GTIT effect on the exergy efficiency for the two systems.

Figure 4.33 illustrates the impact of GTIT on CO_2 emissions (measured in kg CO2/MWh) for two different systems. The findings demonstrate that higher GTIT leads to reduced CO_2 emissions for both ISCC and ISCC-ARC systems, with the

ISCC-ARC system showing a slight advantage. For both ISCC and ISCC-ARC systems, CO_2 emissions decrease as GTIT increases from 1250 K to 1550 K. Higher inlet temperatures lead to lower CO_2 emissions per unit of energy produced for both systems. The CO_2 emissions for the ISCC system are 402.5 kg CO_2 /MWh at 1,250 K and 379.1 kg CO_2 /MWh at 1,550 K. For the ISCC-ARC system, the CO_2 emissions are 399.9 kg CO_2 /MWh at 1,250 K and 378.2 kg CO_2 /MWh at 1,550 K.

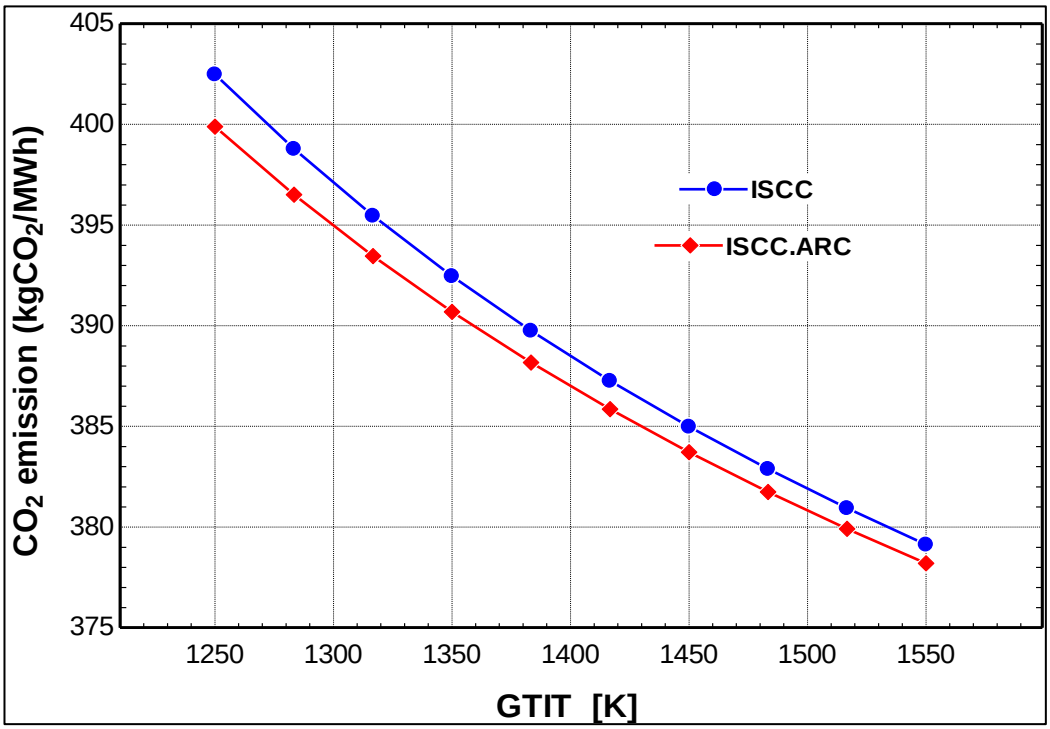

Figure 4.33. GTIT effect on the CO_2 emission for the two systems.

Figure 4.34 illustrates the effect of inlet pressure at the high-pressure steam turbine ($P_{HPST.in}$) on the network output ($\dot{W}_{net}$) for two different systems: ISCC and ISCC-ARC. For both ISCC and ISCC-ARC systems, $\dot{W}_{net}$ increases as $P_{HPST.in}$ rises from 80 to 120 bar. This indicates that higher $P_{HPST.in}$lead to greater network output for both systems.

The ISCC-ARC system consistently shows higher $\dot{W}_{net}$ than the ISCC system across the entire range of inlet pressures. At 80 bar, the ISCC system has a work net output of approximately 551.2 MW, while the ISCC-ARC system starts at around 572.1 MW. At 120 bar, the ISCC system's network output increases to about 557.3 MW, whereas the ISCC-ARC system reaches around 578.2 MW.

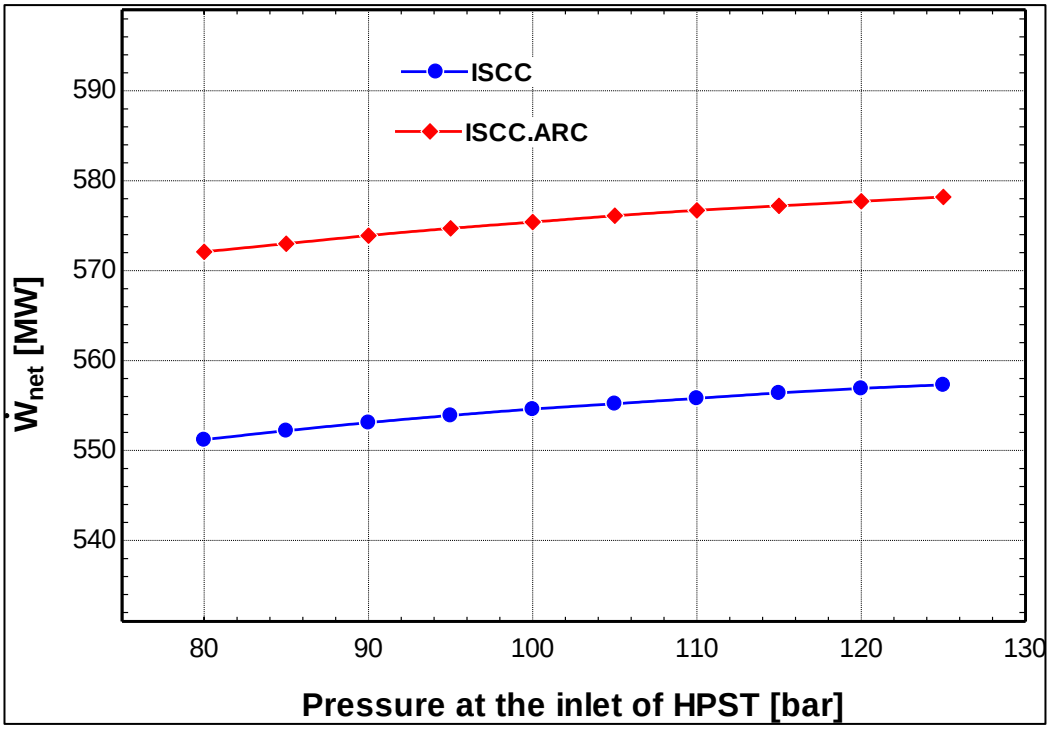

Figure 4.34. $P_{HPST.in}$ effect on the $\dot{W}_{net}$ for two systems.

Figure 4.35 illustrates the impact of $P_{HPST.in}$ on the specific cost ($/MW) for two different systems. The results demonstrate that increasing the $P_{HPST.in}$ leads to decreased specific costs for both ISCC and ISCC-ARC systems, with the ISCC-ARC system showing consistently lower specific costs. For both ISCC and ISCC-ARC systems, the specific cost decreases as $P_{HPST.in}$ increases from 80 bar to 120 bar.

The ISCC-ARC system consistently shows lower specific costs than the ISCC system across the entire range of inlet pressures. At 80 bar, the specific cost for the ISCC system is around 74.91 $/MW, while for the ISCC-ARC system, it is approximately 68.21 $/MW. At 120 bar, the specific cost for the ISCC system decreases to about 73.09 $/MW, whereas for the ISCC-ARC system, it drops to around 66.54 $/MW.

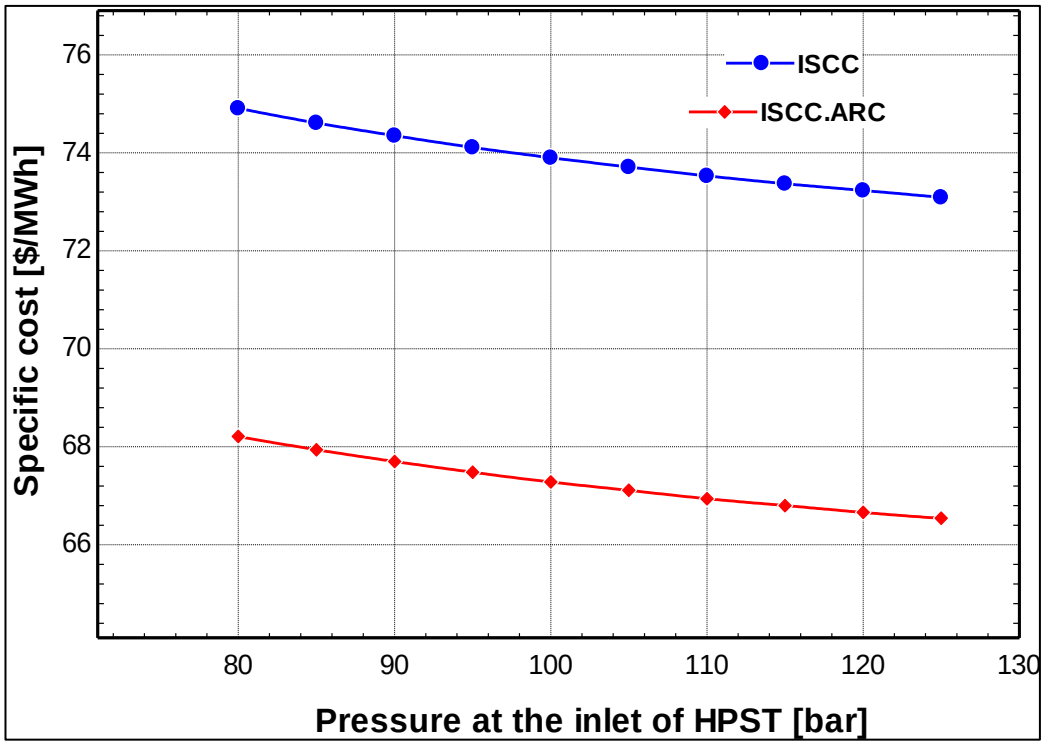

Figure 4.35. $P_{HPST.in}$ effect on the specific costs for the two systems.

Figure 4.36 and Figure 4.37 illustrate the impact of $P_{HPST.in}$ on the thermal efficiency and exergy efficiency for two different systems. The findings demonstrate that increasing the $P_{HPST.in}$ enhances overall efficiencies for ISCC and ISCC-ARC systems. Both overall efficiencies for the ISCC and ISCC-ARC systems increase as $P_{HPST.in}$ rises from 80 bar to 120 bar. This indicates that higher $P_{HPST.in}$ improves the work net and the overall efficiencies of both systems.

The ISCC-ARC system consistently shows slightly higher efficiencies compared to the ISCC system across the entire range of $P_{HPST.in}$. At an inlet pressure of 80 bar, the thermal efficiency of the ISCC system is about 50.07%, while the ISCC-ARC system achieves approximately 50.31%. When the $P_{HPST.in}$ increases to 120 bar, the thermal efficiency of the ISCC system rises to around 50.63%, with the ISCC-ARC system reaching approximately 50.84%. For exergy efficiency, at 80 bar, the ISCC system is around 48.35%, and the ISCC-ARC system is about 48.58%. As the $P_{HPST.in}$ increases to 120 bar, the exergy efficiency of the ISCC system improves to around 48.89%, whereas the ISCC-ARC system increases to approximately 49.09%.

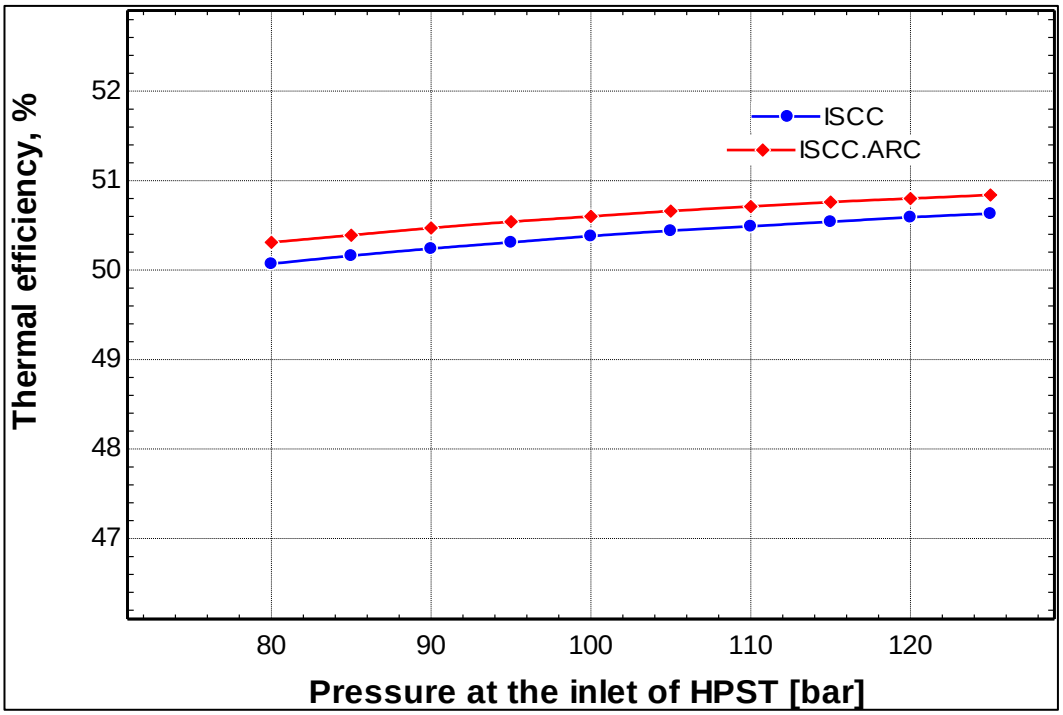

Figure 4.36. $P_{HPST.in}$ effect on the thermal efficiency of the two systems.

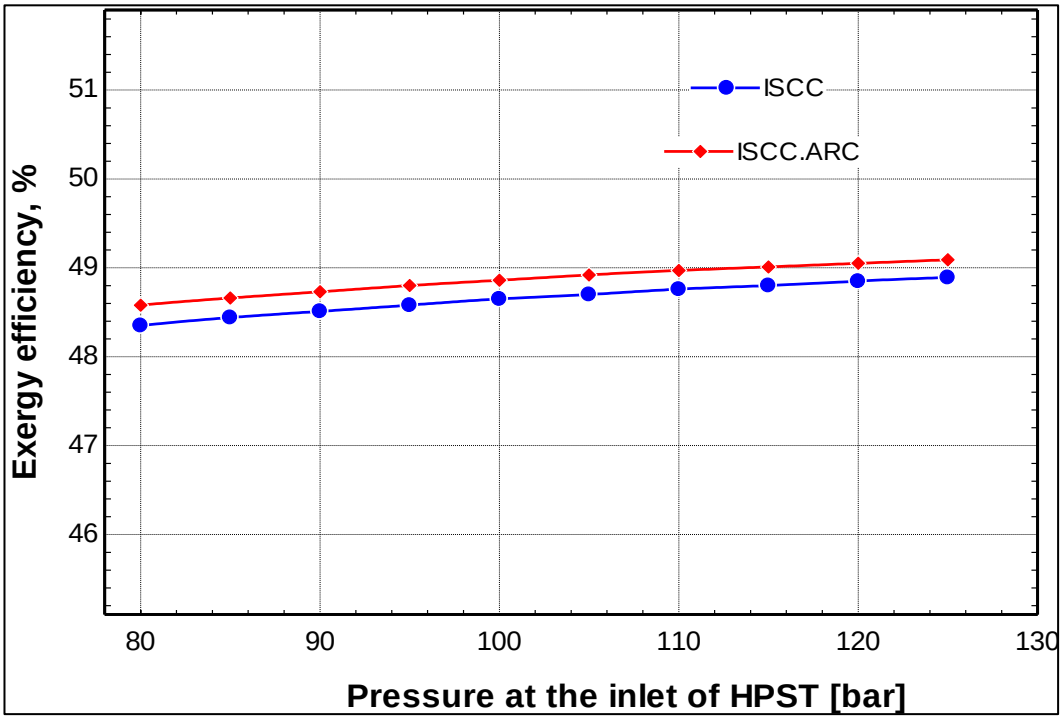

Figure 4.37. $P_{HPST.in}$ effect on the exergy efficiency of the two systems.

Figure 4.38 illustrates the impact of $P_{HPST.in}$ on CO_2 emissions for two different systems. CO_2 emissions drop when the pressure $P_{HPST.in}$ climbs from 80 bar to 120 bar in both the ISCC and ISCC-ARC systems. This suggests that increasing the $P_{HPST.in}$

results in reduced carbon dioxide (CO_2) emissions per unit of energy generated for both systems. The ISCC-ARC system consistently exhibits lower levels of CO_2 emissions than the ISCC system. At a pressure of 80 bar, the ISCC system emits roughly 394 $kgCO_2$ /MWh, while the ISCC-ARC system begins at around 392.2 $kgCO_2$ per MWh. At a pressure of 120 bar, the carbon dioxide (CO_2) emissions decrease to around 389.7 $kgCO_2$/MWh for the ISCC system and roughly 388.1 $kgCO_2$/MWh for the ISCC-ARC system.

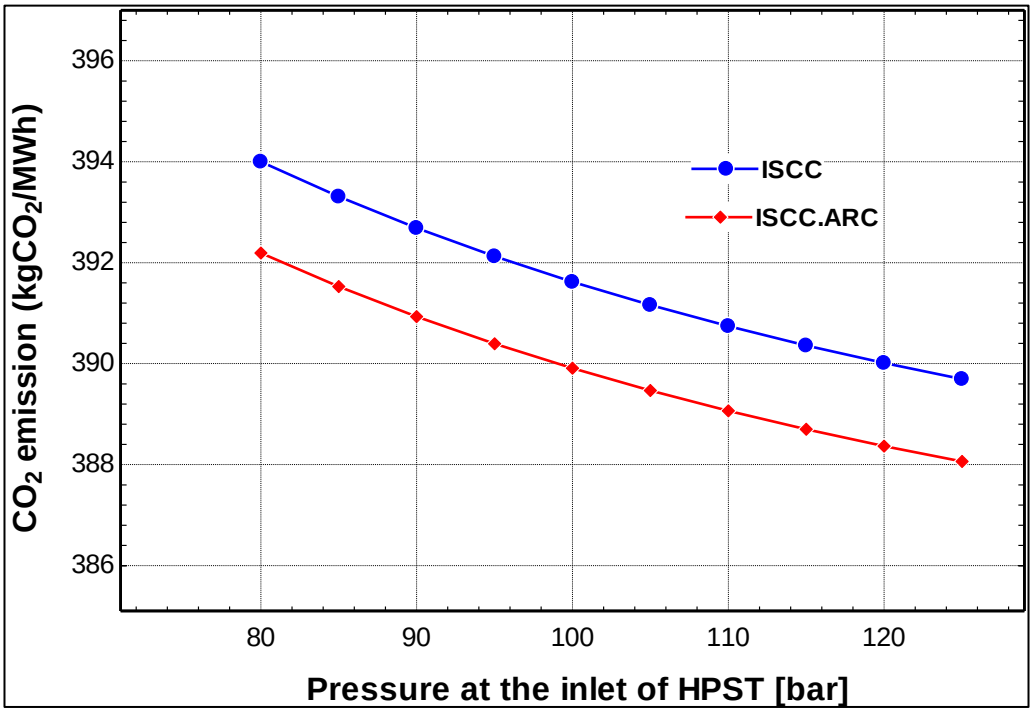

Figure 4.38. $P_{HPST.in}$ effect on the CO_2 emission for the two systems.

Figure 4.39 illustrates the impact of condenser temperature (T_{cond}) on the network output for two different systems. The figure demonstrates that increasing the T_{cond} decreases network output for both ISCC and ISCC-ARC systems. As the T_{cond} rises, the pressure at which the steam is condensed likewise rises. Consequently, there is a decrease in the expansion ratio inside the turbine, resulting in a decline in the steam's work production. In addition, the steam entering the condenser experiences a loss in quality, leading to increased energy needed for condensation.

The ISCC-ARC system consistently shows higher than the ISCC system across the entire range of T_{cond}. At 25°C, the network output for the ISCC system is approximately 554.6 MW, while the ISCC-ARC system starts at around 581.1 MW. At 70°C, the network output for the ISCC system decreases to about 533.7 MW, whereas for the ISCC-ARC system, it drops to around 554.5 MW.

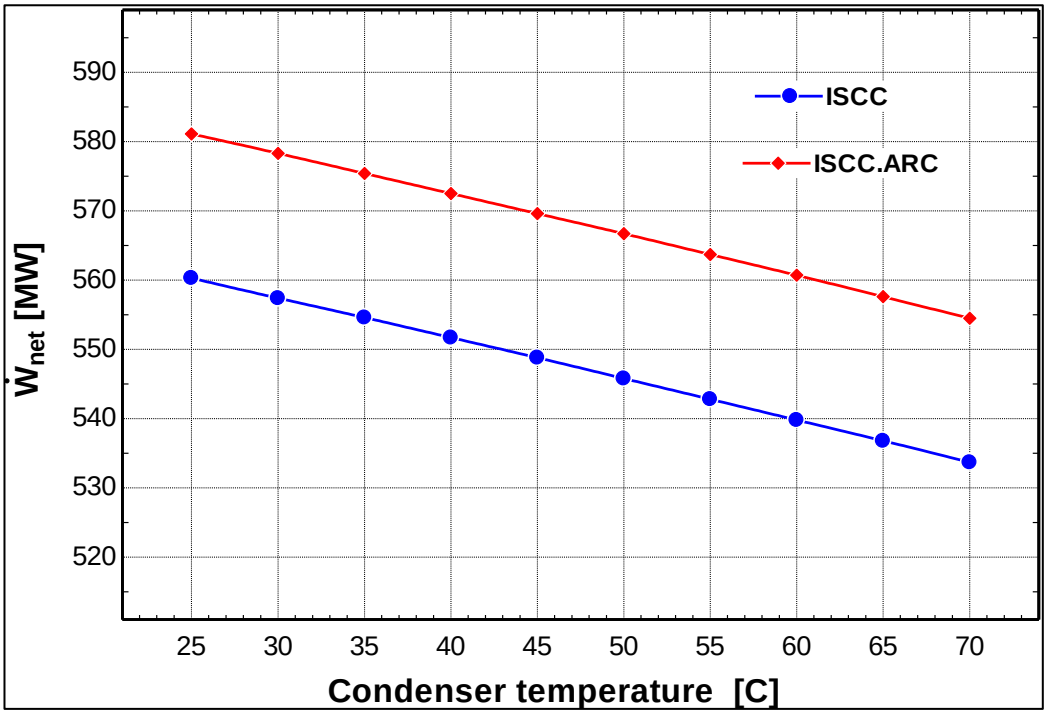

Figure 4.39. T_{cond} effect on the $\dot{W}_{net}$ for the two systems.

Figure 4.40 depicts the influence of condenser temperature on the specific cost, measured in dollars per megawatt, for two different systems. For both the ISCC and ISCC-ARC systems, the cost per unit increases as the T_{cond} climbs from 25°C to 70°C. These findings suggest that expanding the condenser temperatures increases both systems' costs.

The ISCC-ARC system consistently exhibits lower specific costs than the ISCC system at all condenser temperatures. The cost for the ISCC system at a temperature of 25°C is roughly 72.51 $/MWh, but for the ISCC-ARC system, it is around 66.01 $/MWh. At a temperature of 70°C, the specific cost for the ISCC system experiences an increase to around 79.36 $/MWh. In contrast, the ISCC-ARC system climbs to roughly 72.28 $/MWh.

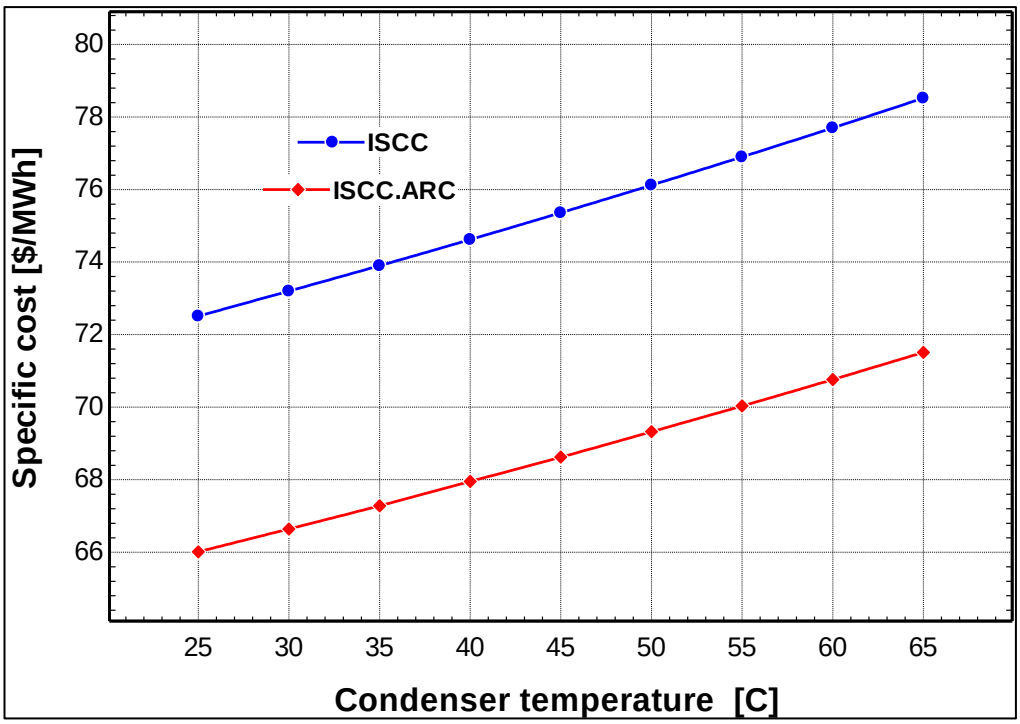

Figure 4.40. T_{cond} effect on the specific costs for the two systems.

Figures 4.41 and 4.42 depict the condenser temperature's influence on the two systems' thermal and exergy efficiency. The results indicate that raising the T_{cond} causes a loss in both thermal and exergy efficiencies for both ISCC and ISCC-ARC Systems. This is due to the decrease in power output for both systems. The ISCC-ARC system has marginally superior thermal efficiency compared to the ISCC system across all T_{cond} levels.

The thermal efficiency of the ISCC system at a temperature of 25°C is roughly 51.1% and η_{exergy} drops from 49.35 % to 47.09 %, but for the ISCC-ARC system, it is around 50.9%. At a temperature of 70°C, the thermal efficiency of the ISCC system falls to around 48.76%, whereas for the ISCC-ARC system, it declines to roughly 48.48% and η_{exergy} from 49.15 percent to 46.81 percent.

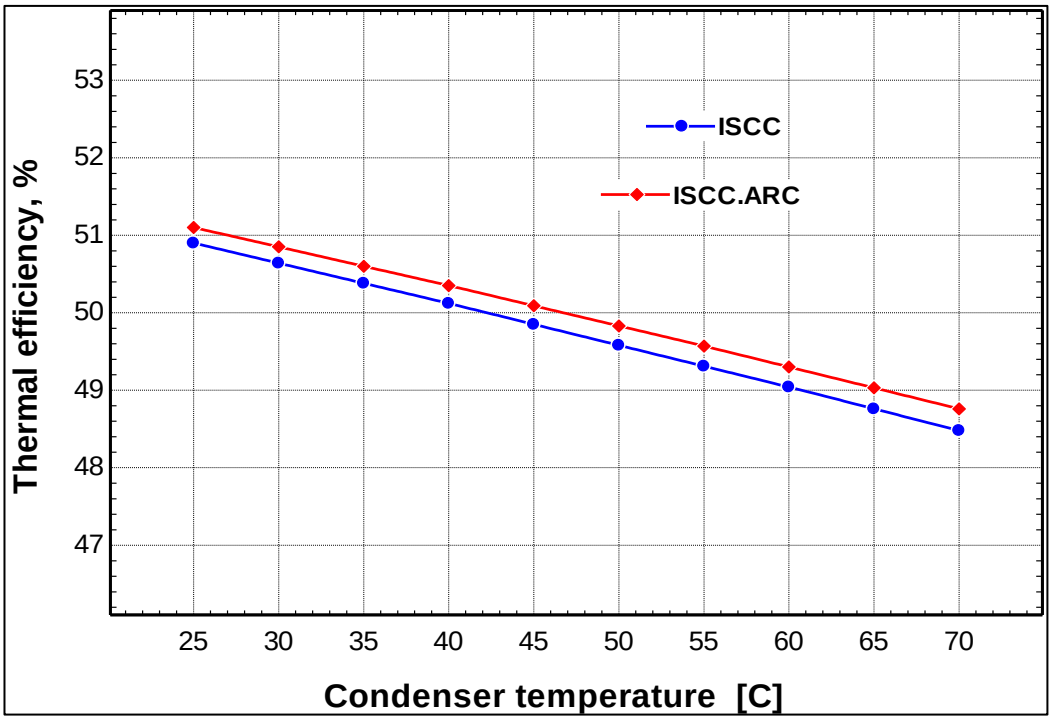

Figure 4.41. T_{cond} effect on the thermal efficiency of the two systems.

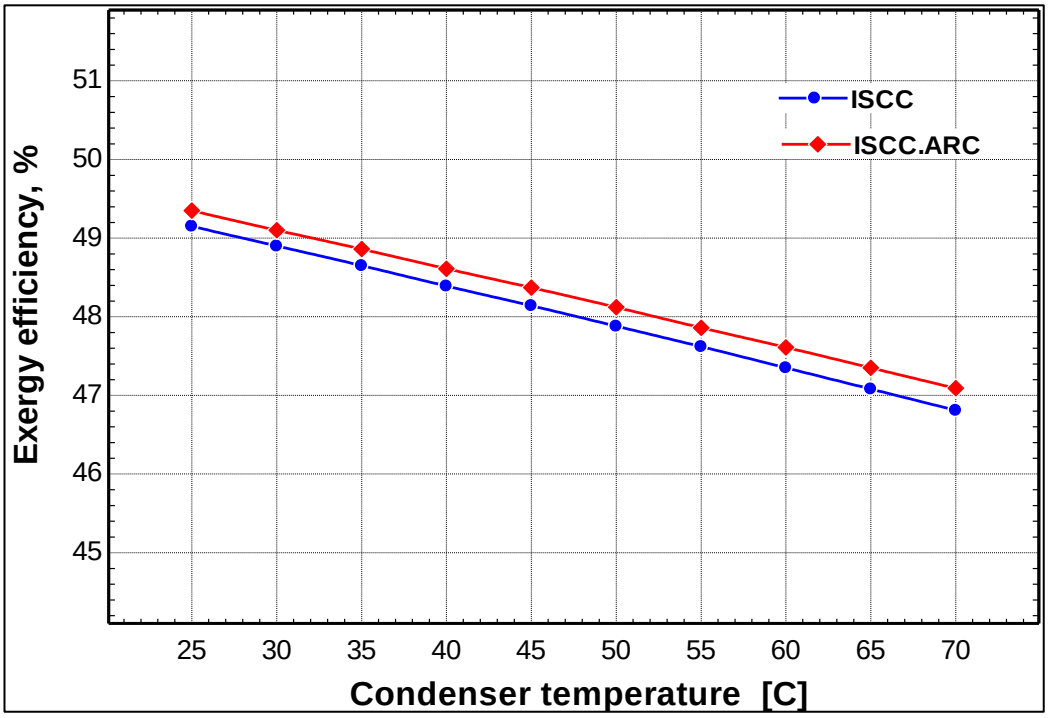

Figure 4.42. T_{cond} effect on the exergy efficiency of the two systems.

Figure 4.43 demonstrates the correlation between condenser temperature and CO_2 emissions for two distinct systems. The findings indicate that raising the T_{cond} leads to higher levels of CO_2 emissions in both ISCC and ISCC-ARC systems. The ISCC-ARC system consistently exhibits lower levels of CO_2 emissions compared to the ISCC system, regardless of the T_{cond} being considered. At a temperature of 25°C, the carbon dioxide (CO_2) emissions for the ISCC system are roughly 388 $kgCO_2/MWh$, while for the ISCC-ARC system, they are around 386 $kgCO_2/MWh$. At a temperature of 70°C, the CO_2 emissions for the ISCC system's experience increase to around 407 $kgCO_2/MWh$. In contrast, for the ISCC-ARC system, the emissions climb to roughly 404 $kgCO_2/MWh$.

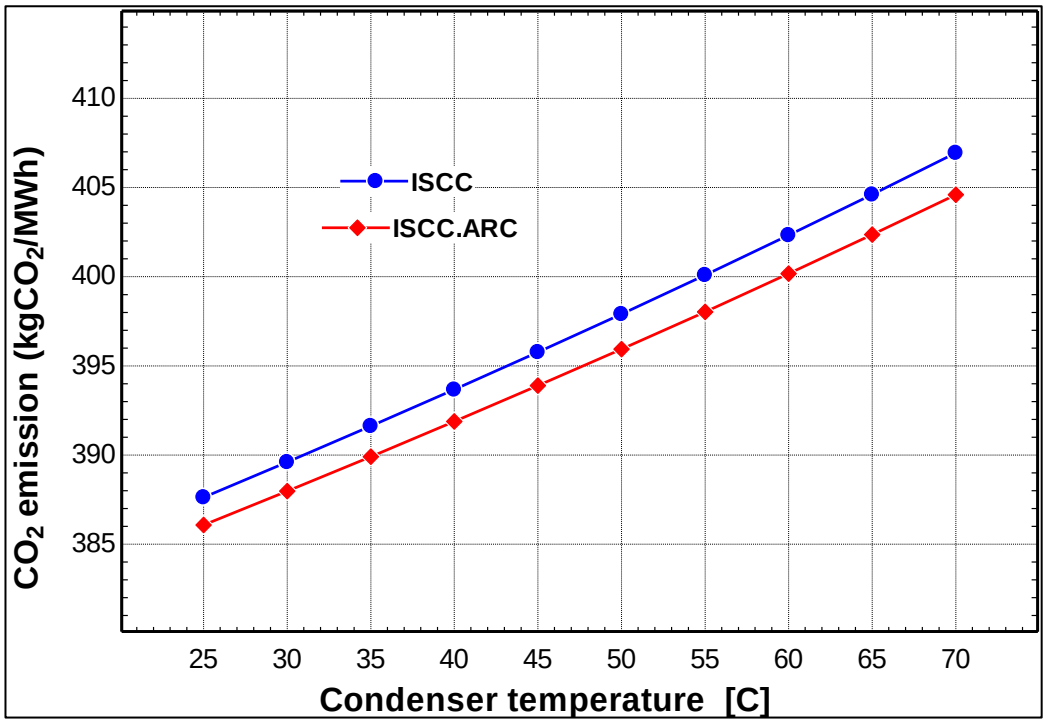

Figure 4.43. T_{cond} effect on the CO_2 emission for the two systems.

4.4.3 Environmental Analysis

The environmental analysis focuses on the system's CO_2 emissions, comparing the ISCC and ISCC-ARC systems over a year. The ISCC-ARC system consistently demonstrates lower CO_2 emissions compared to the ISCC system. Notably, the emissions for the ISCC-ARC system show a steady decline with infrequent fluctuations throughout the year, ranging from 405.3 $kgCO_2/MWh$ in December to

373.5 kgCO_2/MWh in June. In comparison, the ISCC system's CO_2 emissions range from 405 kgCO_2/MWh in December to 375.6 kgCO_2/MWh in June. Overall, the comparison indicates that the ISCC-ARC system has the lowest annual CO_2 emissions, followed by the ISCC system.

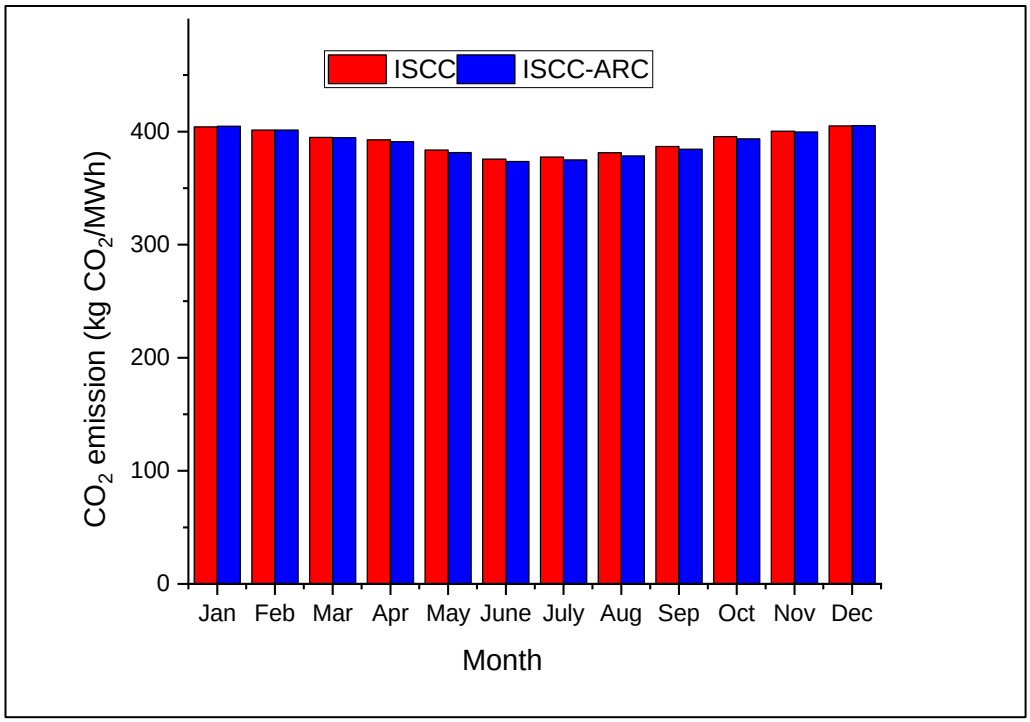

Figure 4.44. The annual entire CO_2 emission for the ISCC, and ISCC-ARC systems.

4.4.4 Annual Demonstration Energy Generation and Entire Cost for ISCC-ARC

The percentage of monthly energy generated by each system is displayed in Figure 4.45. The results show that during the winter season, the energy generation for both systems is comparable due to the drop in ambient temperature and the reduced significance of the absorption cooling system. The ISCC system produces additional electricity in the colder months because of the lower ambient temperature, allowing the gas turbine to operate more efficiently. Studies indicate that the ISCC technology becomes more efficient in winter as the lower outside temperature enhances gas turbine cycles, resulting in the maximum network output. In June, the ISCC system achieved a maximum production of 562.6 MW. Conversely, during the summer, the ISCC-ARC system generates more energy due to the extremely high Direct Normal

Irradiance (DNI) and the ARC technology's capability to reduce the air compressor's inlet temperature to match the outside temperature. These parameters maximize the system's production in the summer. The ISCC-ARC system reached its peak net generation of 591.4 MW in June.

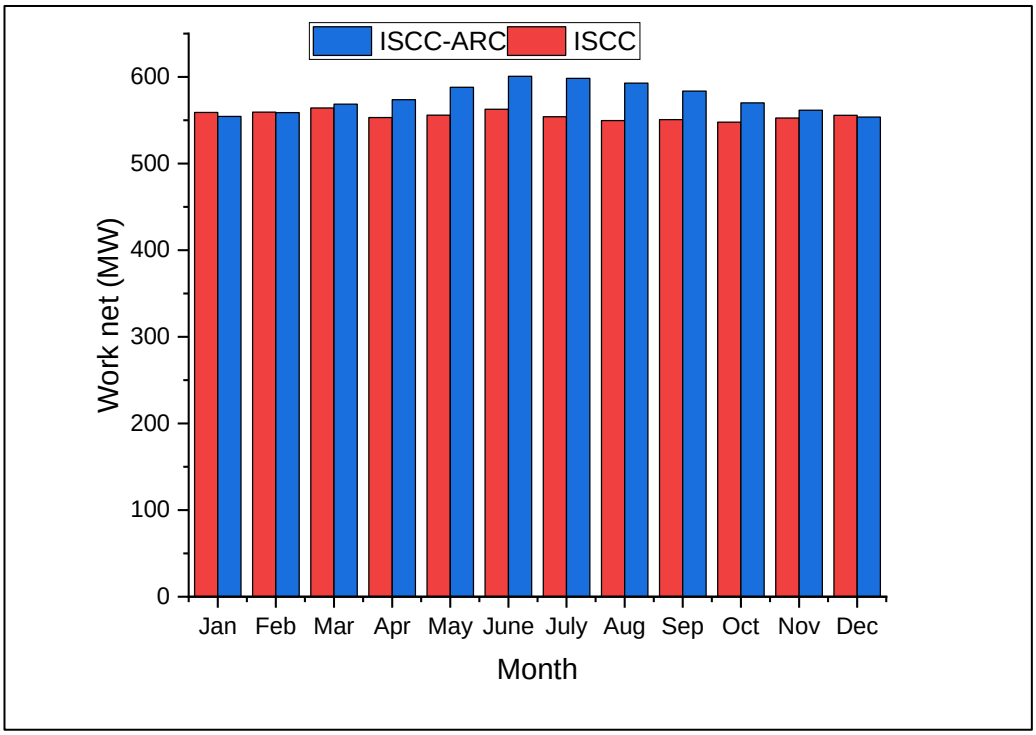

Figure 4.45. The annual entire power generation for the ISCC, and ISCC-ARC systems.

The monthly exact costs for each technology are shown in Figure 4.46. The graph indicates that atmospheric variations significantly impact the thermodynamic performance of these technologies. According to the investigation's results, the total specific costs for the ISCC-ARC system range from 62.33 $/MWh in June to 72.18 $/MWh in December. Similarly, the total costs for the ISCC system fluctuate between 70.08 $/MWh in June and 76.79 $/MWh in December.

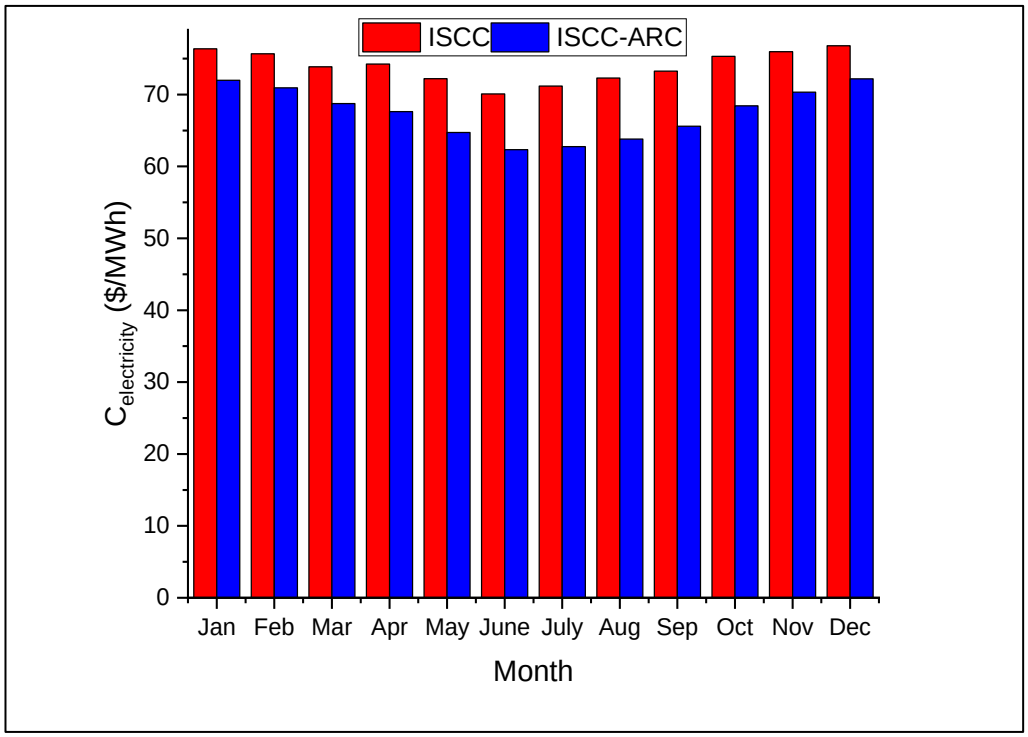

Figure 4.46. The annual cost for the ISCC and ISCC-ARC systems.

4.5. SUMMARY OF THE RESULTS

Table 4.10 summarizes the output values for four models: BC Model, NGCC Model, ISCC Model, and ISCC-ARS Model. The findings show that the ISCC-ARS Model stands out with the highest net power output, highest efficiencies (both thermal and exergy), and lowest CO2 emissions. The BC Model has the lowest efficiency and highest CO2 emissions but also the lowest total cost. The ISCC-ARS Model provides the highest net power output at 581.1 MW.

ISCC-ARS Model has the highest efficiencies at 51.1% and 49.39%, respectively. ISCC-ARS Model has the lowest CO2 emissions at 386.1 kg/MWh. ISCC-ARS Model has the lowest capital investment cost at 66.01 $/hr and the lowest specific energy unit cost at $58.47/MWh.

Table 4.10. Summary of the output values in the current study.

Calculated Parameters	**BC Model**	**NGCC Model**	**ISCC Model**	**ISCC-ARS Model**
Fuel mass flow rate. $\dot{\mathbf{m}}_{\mathbf{fuel}}$ (kg/s)	7.33	7.33	7.33	7.635
Steam mass flow rate, $\dot{\mathbf{m}}_{steam}$ (kg/s)	-	81	147.1	147.2
BC power, $\dot{\mathbf{W}}_{\mathbf{BC}}$ (MW)	363.1	363.1	363.1	389.2
RC power, $\dot{\mathbf{W}}_{RC}$ (MW)	-	125.9	191.5	191.6
Net power, $\dot{\mathbf{W}}_{\mathbf{net}}$ (MW)	363.1	489	554.6	581.1
Thermal efficiency, $\boldsymbol{\eta}_{\mathbf{I}}$ (%)	32.98	44.42	50.38	51.1
Exergy efficiency, $\boldsymbol{\eta}_{\mathbf{II}}$ (%)	31.85	43.89	48.65	49.39
COP for ARC	-	-	-	08077
Exergy destruction,$\dot{\mathbf{E}}_{\mathbf{D,Total}}$ (MW)	550.4	620.7	665.5	683.3
Specific energy unit cost ($/MWh)	74.81	80.1	73.9	58.47
$\mathbf{CO_2}$ mass flow rate, $\dot{\mathbf{m}}_{\mathbf{CO_2}}$ (kg/s)	60.33	60.33	60.33	61.24
$C0_2$ emission, $\boldsymbol{\varepsilon}_{\mathbf{CO2}}$ ($\mathbf{kg}_{\mathbf{CO_2}}$/MWh)	598.2	440.8	387.6	386.1

PART 5

CONCLUSIONS

Pursuing sustainable and efficient energy solutions has become paramount in addressing the global challenges of climate change, resource depletion, and energy security. In this context, integrating renewable energy sources into traditional power generation systems presents a viable pathway toward achieving these goals. This thesis explores the innovative integration of solar energy and an absorption refrigeration cycle (ARC) into the Al-Qayara gas turbine power plant in Iraq, transforming it into an Integrated Solar Combined Cycle (ISCC-ARC) system. Iraq, a country with substantial solar irradiance and significant energy needs, offers a unique opportunity to harness solar power to enhance its energy infrastructure.

The Al-Qayara power plant, located in a region with over 3,300 hours of sunshine annually and solar radiation exceeding 2000 kWh/m², is an ideal candidate for such an integration. This study addresses the critical need for upgrading Iraq's power infrastructure, which has suffered from frequent wars and insufficient maintenance. This research seeks to improve the power plant's overall efficiency, economic viability, and environmental sustainability by incorporating solar energy and waste heat recovery into the existing gas turbine framework. The ISCC-ARC configuration utilizes exhaust gases from the Al-Qayara plant and a parabolic trough collector (PTC) field to generate steam through a high-recovery steam generation process. This steam is then employed in an absorption refrigeration cycle that supplies low-temperature air to the Brayton cycle, significantly enhancing the plant's performance.

The thermoeconomic analysis conducted in this study demonstrates that the ISCC-ARC system increases power output and reduces specific energy costs and carbon dioxide emissions, thereby providing a more economical and environmentally friendly solution than conventional systems. The key objectives of this research include

optimizing energy efficiency and performance under various climatic conditions, incorporating clean energy sources to minimize the environmental footprint, and evaluating the financial viability of the integrated system based on operational data. Through a comprehensive analysis of energy, exergy, exergoeconomic, and ecological aspects, this thesis contributes to the growing body of knowledge on renewable energy integration. It offers practical insights for developing advanced power generation systems.

The findings underscore the potential of ISCC-ARC systems to play a crucial role in addressing energy deficits, improving power generation capacity, and supporting sustainable development in regions with high solar potential. This research provides a strategic approach to enhancing Iraq's energy infrastructure. It aligns with global trends towards more sustainable and resilient energy systems, paving the way for future advancements in renewable energy and power generation. The key findings and implications of this study are as follows:

- The ISCC-ARC system demonstrated a significant improvement in power output and efficiency compared to traditional systems. The net power output increased from 554.6 MW in the ISCC system to 581.1 MW in the ISCC-ARC system. This configuration also achieved higher thermal and exergy efficiencies of 51.15% and 49.4%, respectively, compared to 50.89% and 49.14% for the ISCC system.
- The thermoeconomic analysis revealed that the ISCC-ARC system is cost-effective. The specific costs for the ISCC-ARC system ranged from 62.33$/MWh in June to 72.18 $/MWh in December, which is more favorable than the ISCC and NGCC systems.
- The use of solar energy and ARC resulted in a decrease in carbon dioxide emissions. The ISCC-ARC system continuously exhibited lower levels of CO2 emissions throughout the year, with values ranging from 373.5 kgCO2/MWh in June to 405.3 kgCO2/MWh in December. In comparison, the ISCC system's emissions varied from 375.6 kgCO2/MWh to 405 kgCO2/MWh over the same periods.

- Increasing the pressure ratio has an initial positive impact on performance, followed by a fall. It also lowers energy expenditures until reaching an ideal position and decreases CO2 emissions for both ISCC and ISCC-ARC systems.
- Increasing the GTIT improves network production, decreases specific energy costs to an ideal level, and reduces CO2 emissions for both ISCC and ISCC-ARC systems.
- Increasing the temperature at the HPST inlet improves the work output for both ISCC and ISCC-ARC systems, with costs remaining stable and CO2 emissions showing minimal variation, indicating that higher HPST inlet temperatures have a minor impact on overall environmental performance.
- Higher condenser temperatures decrease the work output, increase the specific cost of energy, and lead to higher CO2 emissions for both ISCC and ISCC-ARC systems, negatively impacting both economic and environmental performance.
- The findings indicate that using the ISCC-ARC arrangement in power plants is beneficial, particularly in regions with ample solar radiation, such as Mosul, Iraq. This plan aligns with global trends toward sustainable energy solutions and has the potential to have a substantial impact in addressing energy shortages and environmental concerns. Further research is necessary to improve the system's performance in different climatic conditions and explore the potential of using other renewable energy sources.

REFERENCES

1. "Al Qayyarah Power Station", https://www.gem.wiki/Al_Qayyarah_power_station#cite_ref-autoref_2_4-2 .

2. "Power Generation and Power Transmission", https://web.archive.org/web/20221224190056/https://www.ge.com/power/en/middle-east/iraq-ge (2022).

3. Zohuri, B., "Navigating the Global Energy Landscape Balancing Growth, Demand, and Sustainability", *J Mat Sci Apl Eng*, 2 (4): 1–07 (2023).

4. Dawood, T. A., Raphael, R., Barwari, I., and Akroot, A., "Solar Energy and Factors Affecting the Efficiency and Performance of Panels in Erbil / Kurdistan", *International Journal Of Heat And Technology*, 41 (2): 304–312 (2023).

5. Zhang, Z., Duan, L., Wang, Z., and Ren, Y., "Integration Optimization of Integrated Solar Combined Cycle (ISCC) System Based on System/Solar Photoelectric Efficiency", *Energies*, 16 (8): (2023).

6. ERBAŞ, O., "Evaluation of the Structure and Energy Generation of a Integrated Solar Combined Cycle Power Plant", *Kırklareli Üniversitesi Mühendislik Ve Fen Bilimleri Dergisi*, 8 (1): 136–147 (2022).

7. Ning, L., Yuan, T., and Wu, H., "New Power System Based on Renewable Energy in the Context of Dual Carbon", *International Transactions On Electrical Energy Systems*, 2022: (2022).

8. Ononogbo, C., Nwosu, E. C., Nwakuba, N. R., Nwaji, G. N., Nwufo, O. C., Chukwuezie, O. C., Chukwu, M. M., and Anyanwu, E. E., "Opportunities of waste heat recovery from various sources: Review of technologies and implementation", *Heliyon*, 9 (2): e13590 (2023).

9. Jana, K., Ray, A., Majoumerd, M. M., Assadi, M., and De, S., "Polygeneration as a future sustainable energy solution – A comprehensive review", *Applied Energy*, 202: 88–111 (2017).

10. Saleem, M. S. and Abas, N., "Optimizing renewable polygeneration: A synergetic approach harnessing solar and wind energy systems", *Results In Engineering*, 21: (2024).

11. Kasaeian, A., Bellos, E., Shamaeizadeh, A., and Tzivanidis, C., .

12. Di Fraia, S., Shah, M., and Vanoli, L., "Biomass Polygeneration Systems Integrated with Buildings: A Review", *Sustainability (Switzerland)*, 16 (4): (2024).

13. Ying, Y. and Hu, E. J., "Thermodynamic advantages of using solar energy in the regenerative Rankine power plant", *Applied Thermal Engineering*, 19 (11): 1173–1180 (1999).

14. Bdaiwi, M., Akroot, A., Wahhab, H. A. A., and Mahariq, I., "Numerical analysis of the steam turbine performance in power station with a low power cycle", (2023).

15. Nawaf, M. Y., Akroot, A., and Wahhab, H. A. A., "Numerical simulation of a porous media solar collector integrated with thermal energy storage system", (2023).

16. Cirocco, L. R., Belusko, M., Bruno, F., Boland, J., and Pudney, P., "Controlling stored energy in a concentrating solar thermal power plant to maximise revenue", *IET Renewable Power Generation*, 9 (4): 379–388 (2015).

17. Sen, O., Faruk Guler, O., Yilmaz, C., and Kanoglu, M., "Thermodynamic modeling and analysis of a solar and geothermal assisted multi-generation energy system", *Energy Conversion And Management*, 239: 114186 (2021).

18. Ying, Y. and Hu, E. J., "Thermodynamic advantages of using solar energy in the regenerative Rankine power plant", *Applied Thermal Engineering*, 19 (11): 1173–1180 (1999).

19. Hasan, M. M., Hossain, S., Mofijur, M., Kabir, Z., Badruddin, I. A., Yunus Khan, T. M., and Jassim, E., .

20. Maka, A. O. M. and Alabid, J. M., "Solar energy technology and its roles in sustainable development", *Clean Energy*, 6 (3): 476–483 (2022).

21. Kurkute, N. and Priyam, A., .

22. Al-Yasiri, Q., Szabó, M., and Arıcı, M., "A review on solar-powered cooling and air-conditioning systems for building applications", *Energy Reports*, 8: 2888–2907 (2022).

23. Internet: SolarPACES, "Solar Radiation in Iraq", https://www.solarpaces.org/csp-technologies/csp-potential-solar-thermal-energy-by-member-nation (2024).

24. AlKassem, A., "A performance evaluation of an integrated solar combined cycle power plant with solar tower in Saudi Arabia", *Renewable Energy Focus*, 39 (December): 123–138 (2021).

25. Siddiqui, O. and Dincer, I., "Analysis and performance assessment of a new solar-based multigeneration system integrated with ammonia fuel cell and solid oxide fuel cell-gas turbine combined cycle", *Journal Of Power Sources*, 370: 138–154 (2017).

26. Martins, F., Felgueiras, C., Smitkova, M., and Caetano, N., "Analysis of fossil fuel energy consumption and environmental impacts in european countries", *Energies*, 12 (6): 1–11 (2019).

27. Golneshan, A. A. and Nemati, H., "Comparison of six gas turbine power cycle, a key to improve power plants", *Mechanics And Industry*, 22: (2021).

28. Hamouda, M. A., Shaaban, M. F., Sharaf Eldean, M. A., Fath, H. E. S., and Al Bardan, M., "Technoeconomic assessment of a concentrated solar tower-gas turbine co-generation system", *Applied Thermal Engineering*, 212 (August 2021): 118593 (2022).

29. Ni, M., Yang, T., Xiao, G., Ni, D., Zhou, X., Liu, H., Sultan, U., Chen, J., Luo, Z., and Cen, K., "Thermodynamic analysis of a gas turbine cycle combined with fuel reforming for solar thermal power generation", *Energy*, 137: 20–30 (2017).

30. Al-Kouz, W., Almuhtady, A., Nayfeh, J., Abu-Libdeh, N., and Boretti, A., "A 140 MW solar thermal plant with storage in Ma'an, Jordan", *E3S Web Of Conferences*, 181: 1–5 (2020).

31. Temraz, A., Rashad, A., Elweteedy, A., and Elshazly, K., "Thermal Analysis of the Iscc Power Plant in Kuraymat, Egypt", *The International Conference On Applied Mechanics And Mechanical Engineering*, 18 (18): 1–15 (2018).

32. Manente, G., Rech, S., and Lazzaretto, A., "Optimum choice and placement of concentrating solar power technologies in integrated solar combined cycle systems", *Renewable Energy*, 96: 172–189 (2016).

33. Wang, S., Fu, Z., Sajid, S., Zhang, T., and Zhang, G., "Thermodynamic and economic analysis of an Integrated Solar Combined Cycle System", *Entropy*, 20 (5): (2018).

34. Kannaiyan, S., Bokde, N. D., and Geem, Z. W., "Solar collectors modeling and controller design for solar thermal power plant", *IEEE Access*, 8: 81425–81446 (2020).

35. Adnan, M., Zaman, M., Ullah, A., Gungor, A., Rizwan, M., and Raza Naqvi, S., "Thermo-economic analysis of integrated gasification combined cycle co-generation system hybridized with concentrated solar power tower", *Renewable Energy*, 198 (August): 654–666 (2022).

36. Alqahtani, B. J. and Patiño-Echeverri, D., "Integrated Solar Combined Cycle Power Plants: Paving the way for thermal solar", *Applied Energy*, 169: 927–936 (2016).

37. Saeed, I. M., Ramli, A. T., and Saleh, M. A., "Assessment of sustainability in energy of Iraq, and achievable opportunities in the long run", *Renewable And Sustainable Energy Reviews*, 58 (2016): 1207–1215 (2016).

38. Hassan, Q., Hafedh, S. A., Hasan, A., and Jaszczur, M., "Evaluation of energy generation in Iraqi territory by solar photovoltaic power plants with a capacity of 20 MW", *Energy Harvesting And Systems*, 9 (1): 97–111 (2022).

39. Kazem, H. A. and Chaichan, M. T., "Status and future prospects of renewable energy in Iraq", *Renewable And Sustainable Energy Reviews*, 16 (8): 6007–6012 (2012).

40. M. AMANI*, A. SMAILI**, A. G., .

41. Wang, G., Wang, S., Lin, J., and Chen, Z., "Exergic Analysis of an ISCC System for Power Generation and Refrigeration", *International Journal Of Thermophysics*, 42 (7): 1–23 (2021).

42. Faisal, S. H., Naeem, N. K., and Jassim, A. A., "Energy and exergy study of Shatt Al-Basra gas turbine power plant", *Journal Of Physics: Conference Series*, 1773 (1): (2021).

43. Pirzadi, M. and Asghar Ghadimi, A., "AUT Journal of Electrical Engineering Performance evaluation of the first Iranian large-scale photovoltaic power plant", 52 (1): 19–30 (2020).

44. Salah, S. A., Abbas, E. F., Ali, O. M., Alwan, N. T., Yaqoob, S. J., and Alayi, R., "Evaluation of the gas turbine unit in the Kirkuk gas power plant to analyse the energy and exergy using ChemCad simulation", *International Journal Of Low-Carbon Technologies*, 17 (June): 603–610 (2022).

45. Ahmed, A. H., Ahmed, A. M., and Hamid, Q. Y., "Exergy and energy analysis of 150 MW gas turbine unit: A case study", *Journal Of Advanced Research In Fluid Mechanics And Thermal Sciences*, 67 (1): 186–192 (2020).

46. Kareem, A. F., Akroot, A., Wahhab, H. A. A., Talal, W., Ghazal, R. M., and Alfaris, A., "Exergo – Economic and Parametric Analysis of Waste Heat Recovery from Taji Gas Turbines Power Plant Using Rankine Cycle and Organic Rankine Cycle", (2023).

47. Li, Y. and Yang, Y., "Thermodynamic analysis of a novel integrated solar combined cycle", *Applied Energy*, 122: 133–142 (2014).

48. Zhang, Z., Duan, L., Wang, Z., and Ren, Y., "General performance evaluation method of integrated solar combined cycle (ISCC) system", *Energy*, 240: 122472 (2022).

49. Enciso Contreras, E., Saldaña, J. G. B., Alejo, J. de la C., Torres, C. D. C. G., Bernal, J. A. J., and Vazquez, M. B. A., "A Feasibility Analysis of a Solar Power Plant with Direct Steam Generation System in Sonora, Mexico", *Energies*, 16 (11): 1–14 (2023).

50. Ameri, M. and Mohammadzadeh, M., "Thermodynamic, thermoeconomic and life cycle assessment of a novel integrated solar combined cycle (ISCC) power plant", *Sustainable Energy Technologies And Assessments*, 27 (January): 192–205 (2018).

51. Adibhatla, S. and Kaushik, S. C., "Energy, exergy and economic (3E) analysis of integrated solar direct steam generation combined cycle power plant", *Sustainable Energy Technologies And Assessments*, 20: 88–97 (2017).

52. Migla, L., Bogdanovics, R., and Lebedeva, K., "Performance Improvement of a Solar-Assisted Absorption Cooling System Integrated with Latent Heat Thermal Energy Storage", *Energies*, 16 (14): (2023).

53. Kwon, H. M., Kim, T. S., Sohn, J. L., and Kang, D. W., "Performance improvement of gas turbine combined cycle power plant by dual cooling of the

inlet air and turbine coolant using an absorption chiller", *Energy*, 163: 1050–1061 (2018).

54. Nezammahalleh, H., Farhadi, F., and Tanhaemami, M., "Conceptual design and techno-economic assessment of integrated solar combined cycle system with DSG technology", *Solar Energy*, 84 (9): 1696–1705 (2010).

55. Aqachmar, Z., Allouhi, A., Jamil, A., Gagouch, B., and Kousksou, T., "Parabolic trough solar thermal power plant Noor I in Morocco", *Energy*, 178: 572–584 (2019).

56. Rovira, A., Abbas, R., Sánchez, C., and Muñoz, M., "Proposal and analysis of an integrated solar combined cycle with partial recuperation", *Energy*, 198: (2020).

57. Sachdeva, J. and Singh, O., "Thermodynamic analysis of solar powered triple combined Brayton, Rankine and organic Rankine cycle for carbon free power", *Renewable Energy*, 139 (2019): 765–780 (2019).

58. Temraz, A., Rashad, A., Elweteedy, A., Alobaid, F., and Epple, B., "Energy and exergy analyses of an existing solar-assisted combined cycle power plant", *Applied Sciences (Switzerland)*, 10 (14): (2020).

59. Roshanzadeh, B., Asadi, A., and Mohan, G., "Technical and Economic Feasibility Analysis of Solar Inlet Air Cooling Systems for Combined Cycle Power Plants", *Energies*, 16 (14): (2023).

60. Baghernejad, A. and Yaghoubi, M., "Exergoeconomic analysis and optimization of an Integrated Solar Combined Cycle System (ISCCS) using genetic algorithm", *Energy Conversion And Management*, 52 (5): 2193–2203 (2011).

61. Rahman, S. M., Al-Ismail, F. S. M., Haque, M. E., Shafiullah, M., Islam, M. R., Chowdhury, M. T., Alam, M. S., Razzak, S. A., Ali, A., and Khan, Z. A., "Electricity Generation in Saudi Arabia: Tracing Opportunities and Challenges

to Reducing Greenhouse Gas Emissions", *IEEE Access*, 9: 116163–116182 (2021).

62. Nourpour, M. and Khoshgoftar Manesh, M. H., "Evaluation of novel integrated combined cycle based on gas turbine-SOFC-geothermal-steam and organic Rankine cycles for gas turbo compressor station", *Energy Conversion And Management*, 252 (August 2021): 115050 (2022).

63. Abdelhay, A. O., Fath, H. E. S., and Nada, S. A., "Case Studies in Thermal Engineering Enviro-exergo-economic analysis and optimization of a nanofiltration-multi effect desalination , power generation and cooling in an innovative trigeneration plant", *Case Studies In Thermal Engineering*, 31 (February): 101857 (2022).

64. Abubaker, A. M., Darwish Ahmad, A., Salaimeh, A. A., Akafuah, N. K., and Saito, K., "A novel solar combined cycle integration: An exergy-based optimization using artificial neural network", *Renewable Energy*, 181: 914–932 (2022).

65. Wang, S., Zhang, L., Liu, C., Liu, Z., Lan, S., Li, Q., and Wang, X., "Techno-economic-environmental evaluation of a combined cooling heating and power system for gas turbine waste heat recovery", *Energy*, 231: 120956 (2021).

66. Bellos, E. and Tzivanidis, C., "Parametric analysis of a solar-driven trigeneration system with an organic Rankine cycle and a vapor compression cycle", *Energy And Built Environment*, 2 (3): 278–289 (2021).

67. Duan, L. and Wang, Z., "Performance study of a novel integrated solar combined cycle system", *Energies*, 11 (12): (2018).

68. Cavalcanti, E. J. C., .

69. Settino, J., Ferraro, V., and Morrone, P., "Energy analysis of novel hybrid solar and natural gas combined cycle plants", *Applied Thermal Engineering*, 230 (PA): 120673 (2023).

70. Manesh, M. H. K., Ghadikolaei, R. S., Modabber, H. V., and Onishi, V. C., "Integration of a combined cycle power plant with med-ro desalination based on conventional and advanced exergy, exergoeconomic, and exergoenvironmental analyses", *Processes*, 9 (1): 1–29 (2021).

71. Ahamad, T., Parvez, M., Lal, S., Khan, O., and Idrisi, M. J., "4-E analysis and multiple objective optimizations of a novel solar-powered cogeneration energy system for the simultaneous production of electrical power and heating", *Scientific Reports*, 13 (1): 1–22 (2023).

72. Bonforte, G., Buchgeister, J., Manfrida, G., and Petela, K., "Exergoeconomic and exergoenvironmental analysis of an integrated solar gas turbine/combined cycle power plant", *Energy*, 156: 352–359 (2018).

73. Elmorsy, L., Morosuk, T., and Tsatsaronis, G., "Comparative exergoeconomic evaluation of integrated solar combined-cycle (ISCC) configurations", *Renewable Energy*, 185: 680–691 (2022).

74. Benabdellah, H. M. and Ghenaiet, A., "Energy, exergy, and economic analysis of an integrated solar combined cycle power plant", *Engineering Reports*, 3 (11): 1–25 (2021).

75. Tiwari, A. K., Hasan, M. M., and Islam, M., "Exergy analysis of combined cycle power plant: NTPC Dadri, India", *International Journal Of Thermodynamics*, 16 (1): 36–42 (2013).

76. Khandelwal, N., Sharma, M., Singh, O., and Shukla, A. K., "Comparative evaluation of Integrated Solar combined cycle plant with cascade thermal storage system for different heat transfer fluids", *Journal Of Cleaner Production*, 353 (March): 131519 (2022).

77. Besevli, B., Kayabasi, E., Akroot, A., Talal, W., Alfaris, A., Assaf, Y. H., Nawaf, M. Y., Bdaiwi, M., and Khudhur, J., "Technoeconomic Analysis of Oxygen-Supported Combined Systems for Recovering Waste Heat in an Iron-Steel Facility", *Applied Sciences*, 14 (6): 2563 (2024).

78. Temraz, A., Rashad, A., Elweteedy, A., and Elshazly, K., "Thermal Analysis of the Iscc Power Plant in Kuraymat, Egypt", *The International Conference On Applied Mechanics And Mechanical Engineering*, 18 (18): 1–15 (2018).

79. Alqahtani, B. J. and Patiño-Echeverri, D., "Integrated Solar Combined Cycle Power Plants: Paving the way for thermal solar", *Applied Energy*, 169: 927–936 (2016).

80. M. AMANI*, A. SMAILI**, A. G., .

81. Pirzadi, M. and Asghar Ghadimi, A., "AUT Journal of Electrical Engineering Performance evaluation of the first Iranian large-scale photovoltaic power plant", 52 (1): 19–30 (2020).

82. Enciso Contreras, E., Saldaña, J. G. B., Alejo, J. de la C., Torres, C. D. C. G., Bernal, J. A. J., and Vazquez, M. B. A., "A Feasibility Analysis of a Solar Power Plant with Direct Steam Generation System in Sonora, Mexico", *Energies*, 16 (11): 1–14 (2023).

83. Aqachmar, Z., Allouhi, A., Jamil, A., Gagouch, B., and Kousksou, T., "Parabolic trough solar thermal power plant Noor I in Morocco", *Energy*, 178: 572–584 (2019).

84. Rahman, S. M., Al-Ismail, F. S. M., Haque, M. E., Shafiullah, M., Islam, M. R., Chowdhury, M. T., Alam, M. S., Razzak, S. A., Ali, A., and Khan, Z. A., "Electricity Generation in Saudi Arabia: Tracing Opportunities and Challenges to Reducing Greenhouse Gas Emissions", *IEEE Access*, 9: 116163–116182 (2021).

85. Tiwari, A. K., Hasan, M. M., and Islam, M., "Exergy analysis of combined cycle power plant: NTPC Dadri, India", *International Journal Of Thermodynamics*, 16 (1): 36–42 (2013).

86. Polyzakis, A. L., Koroneos, C., and Xydis, G., "Optimum gas turbine cycle for combined cycle power plant", *Energy Conversion And Management*, 49 (4): 551–563 (2008).

87. Lee, J. J., Kang, D. W., and Kim, T. S., "Development of a gas turbine performance analysis program and its application", *Energy*, 36 (8): 5274–5285 (2011).

88. Li, D., Hu, Y., Li, D., and Wang, J., "Combined-cycle gas turbine power plant integration with cascaded latent heat thermal storage for fast dynamic responses", *Energy Conversion And Management*, 183 (January): 1–13 (2019).

89. Li, D., Hu, Y., Li, D., and Wang, J., "Combined-cycle gas turbine power plant integration with cascaded latent heat thermal storage for fast dynamic responses", *Energy Conversion And Management*, 183 (January): 1–13 (2019).

90. Hu, Y., Gao, Y., Lv, H., Xu, G., and Dong, S., "A new integration system for natural gas combined cycle power plants with CO_2 capture and heat supply", *Energies*, 11 (11): (2018).

91. Al-Rawy, A. and Sulaiman, E., "Integrated combined cycle system with parabolic trough technology: A comprehensive review", *SVU-International Journal Of Engineering Sciences And Applications*, 4 (2): 194–208 (2023).

92. Rovira, A., Abbas, R., Muñoz, M., and Sebastián, A., "Analysis of an integrated solar combined cycle with recuperative gas turbine and double recuperative and double expansion propane cycle", *Entropy*, 22 (4): (2020).

93. Rovira, A., Abbas, R., Muñoz, M., and Sebastián, A., "Analysis of an integrated solar combined cycle with recuperative gas turbine and double recuperative and double expansion propane cycle", *Entropy*, 22 (4): (2020).

94. Ahmed, A., Esmaeil, K. K., Irfan, M. A., and Al-Mufadi, F. A., "Design methodology of heat recovery steam generator in electric utility for waste heat recovery", *International Journal Of Low-Carbon Technologies*, 13 (4): 369–379 (2018).

95. Khudhur, J., Akroot, A., and Al-Samari, A., "Experimental Investigation of Direct Solar Photovoltaics that Drives Absorption Refrigeration System",

Journal Of Advanced Research In Fluid Mechanics And Thermal Sciences, 106 (1): 116–135 (2023).

96. Elberry, M. F., Elsayed, A. A., Teamah, M. A., Abdel-Rahman, A. A., and Elsafty, A. F., "Performance improvement of power plants using absorption cooling system", *Alexandria Engineering Journal*, 57 (4): 2679–2686 (2018).

97. "Turkey, Syria and Iraq / the London Geographical Institute", https://collections.lib.uwm.edu/digital/collection/agdm/id/17473/ .

98. Talal, W. and Akroot, A., "Exergoeconomic Analysis of an Integrated Solar Combined Cycle in the Al-Qayara Power Plant in Iraq", *Processes*, 11 (3): (2023).

99. Talal, W. and Akroot, A., "An Exergoeconomic Evaluation of an Innovative Polygeneration System Using a Solar-Driven Rankine Cycle Integrated with the Al-Qayyara Gas Turbine Power Plant and the Absorption Refrigeration Cycle", *Machines*, 12 (2): 133 (2024).

100. Akroot, A. and Namli, L., "Performance assessment of an electrolyte-supported and anode-supported planar solid oxide fuel cells hybrid system", *J Ther Eng*, 7 (7): 1921–1935 (2021).

101. Akroot, A., "Effect of Operating Temperatures on the Performance of a SOFCGT Hybrid System", *International Journal Of Trend In Scientific Research And Development*, Volume-3 (Issue-3): 1512–1515 (2019).

102. Rahman, M. M., Ibrahim, T. K., and Abdalla, A. N., "Thermodynamic performance analysis of gas-turbine power-plant", *International Journal Of Physical Sciences*, 6 (14): 3539–3550 (2011).

103. Alam, K. and Dubey, M. K. K., "PERFORMANCE ANALYSIS OF COMBINED GAS TURBINE-STEAM TURBINE POWER GENERATION CYCLE BACHELOR OF TECHNOLOGY IN MECHANICAL ENGINEERING", (1614).

104. Dubey*, K. K. and Mishra, R. S., "Statistical Analysis for Parametric Optimization of Gas Turbine-Steam Turbine Combined Power Cycle with Different Natural Gas Combustion", *International Journal Of Recent Technology And Engineering (IJRTE)*, 8 (4): 4563–4570 (2019).

105. Elmorsy, L., Morosuk, T., and Tsatsaronis, G., "Exergy-based analysis and optimization of an integrated solar combined-cycle power plant", *Entropy*, 22 (6): 1–20 (2020).

106. Wang, J., Lu, Z., Li, M., Lior, N., and Li, W., "Energy, exergy, exergoeconomic and environmental (4E) analysis of a distributed generation solar-assisted CCHP (combined cooling, heating and power) gas turbine system", *Energy*, 175: 1246–1258 (2019).

107. Zahedi, R., Ahmadi, A., and Dashti, R., "Energy, exergy, exergoeconomic and exergoenvironmental analysis and optimization of quadruple combined solar, biogas, SRC and ORC cycles with methane system", *Renewable And Sustainable Energy Reviews*, 150 (June): 111420 (2021).

108. Akroot, A. and Nadeesh, A., "Performance Analysis of Hybrid Solid Oxide Fuel Cell-Gas Turbine Power System", (2021).

109. Wang, S., Zhang, L., Liu, C., Liu, Z., Lan, S., Li, Q., and Wang, X., "Techno-economic-environmental evaluation of a combined cooling heating and power system for gas turbine waste heat recovery", *Energy*, 231: 120956 (2021).

110. Yüksel, Y. E., "Thermodynamic assessment of modified Organic Rankine Cycle integrated with parabolic trough collector for hydrogen production", *International Journal Of Hydrogen Energy*, 43 (11): 5832–5841 (2018).

111. Bakhshmand, S. K., Saray, R. K., Bahlouli, K., Eftekhari, H., and Ebrahimi, A., "Exergoeconomic analysis and optimization of a triple-pressure combined cycle plant using evolutionary algorithm", *Energy*, 93: 555–567 (2015).

112. Köse, Ö., Koç, Y., and Yağlı, H., "Energy, exergy, economy and environmental (4E) analysis and optimization of single, dual and triple configurations of the

power systems: Rankine Cycle/Kalina Cycle, driven by a gas turbine", *Energy Conversion And Management*, 227 (August 2020): (2021).

113. Cavalcanti, E. J. C., "Exergoeconomic and exergoenvironmental analyses of an integrated solar combined cycle system", *Renewable And Sustainable Energy Reviews*, 67: 507–519 (2017).

114. Musharavati, F., Khanmohammadi, S., and Pakseresht, A., "A novel multi-generation energy system based on geothermal energy source: Thermo-economic evaluation and optimization", *Energy Conversion And Management*, 230 (October 2020): 113829 (2021).

115. Nami, H., Mahmoudi, S. M. S., and Nemati, A., "Exergy, economic and environmental impact assessment and optimization of a novel cogeneration system including a gas turbine, a supercritical CO_2 and an organic Rankine cycle (GT-HRSG/SCO_2)", *Applied Thermal Engineering*, 110: 1315–1330 (2017).

116. Bakhshmand, S. K., Saray, R. K., Bahlouli, K., Eftekhari, H., and Ebrahimi, A., "Exergoeconomic analysis and optimization of a triple-pressure combined cycle plant using evolutionary algorithm", *Energy*, 93: 555–567 (2015).

117. A Bejan, G Tsatsaronis, M. M., "Thermal Design and Optimization", Energy, 433–434 (1996).

118. Pierobon, L., Nguyen, T. Van, Larsen, U., Haglind, F., and Elmegaard, B., "Multi-objective optimization of organic Rankine cycles for waste heat recovery: Application in an offshore platform", *Energy*, 58: 538–549 (2013).

119. Cavalcanti, E. J. C., "Exergoeconomic and exergoenvironmental analyses of an integrated solar combined cycle system", *Renewable And Sustainable Energy Reviews*, 67: 507–519 (2017).

120. Akroot, A. and Al Shammre, A. S., "Techno-Economic and Environmental Impact Analysis of a 50 MW Solar-Powered Rankine Cycle System", *Processes*, 12 (6): 1059 (2024).

121. Tian, H., Li, R., Salah, B., and Thinh, P. H., "Bi-objective optimization and environmental assessment of SOFC-based cogeneration system: performance evaluation with various organic fluids", *Process Safety And Environmental Protection*, 178 (April): 311–330 (2023).

122. Sachdeva, J. and Singh, O., "Thermodynamic analysis of solar powered triple combined Brayton, Rankine and organic Rankine cycle for carbon free power", *Renewable Energy*, 139 (2019): 765–780 (2019).

123. Lugand, P. and Parietti, C., "Combined cycle plants with frame 9F gas turbines", *Proceedings Of The ASME Turbo Expo*, 4: 1–8 (1990).

RESUME

Wadah Talal Taha AL TEKREETY, a mechanical engineer, earned a Bachelor of Mechanical Engineering degree from Mosul University in Iraq in 2000. In 2010, he earned a Master of Engineering Management degree from UPM University Putra Malaysia. He is now pursuing his Ph.D. degree in Mechanical Engineering at Karabuk University.